Establishment of a bipartite ciliary signaling compartment in a *C. elegans* thermosensory neuron

by

Thi Phuong Anh Nguyen

M.Sc. (Biology), McGill University, 2006
B.Sc. (Biology), McGill University, 2004

Thesis Submitted in Partial Fulfillment of the
Requirements for the Degree of
Doctor of Philosophy

in the
Department of Molecular Biology and Biochemistry
Faculty of Science

SIMON FRASER UNIVERSITY

Spring 2014

Approval

Name: **Thi Phuong Anh Nguyen**

Degree: **Doctor of Philosophy (Molecular Biology and Biochemistry)**

Title of Thesis: ***Establishment of a bipartite ciliary signaling compartment in a* C. elegans *thermosensory neuron***

Examining Committee: **Chair:** David Baillie
Professor

Michel Leroux
Senior Supervisor
Professor

Harald Hutter
Supervisor
Professor

Edgar Young
Supervisor
Associate Professor

Catharine Rankin
Supervisor
Professor
University of British Columbia

Lynne Quarmby
Internal Examiner
Professor
SFU/Department of Molecular Biology and Biochemistry

Kirk Mykytyn
External Examiner
Associate Professor
Department of Pharmacology
The Ohio State University

Date Defended/Approved: April 17, 2014

Partial Copyright Licence

Abstract

Signaling proteins are often sequestered into cellular domains, where different modulator proteins, and potentially lipid environments, ensure efficient signal transduction. How such domains form represents an important, largely unexplored question. Known as the antennae of the cell, cilia are organelles required for many signaling pathways, presenting an unique opportunity to explore how signal transduction is arranged spatially and regulated dynamically in the cells. Using the AFD thermosensory neurons of *C. elegans* as the model system, my research investigated the roles of ciliary proteins in regulating a signaling cascade closely associated with the cilium – the cGMP signaling pathway. I showed that different functional categories of ciliary proteins help establish two contiguous, yet distinct cGMP signaling compartments in the sensory end of AFD neurons. One compartment, a *bona fide* cilium, is delineated by Bardet-Biedl syndrome (BBS), Meckel syndrome (MKS) and nephronophthisis (NPHP) associated proteins at its base, and requires Inversin/NPHP-2 to anchor a cGMP-gated ion channel within the proximal ciliary region. The other, a subcompartment characterized by profuse microvilli and different lipid environment, is separated from the dendrite by a cellular junction and requires BBS-8 and DAF-25/Ankmy2 for correct localization of guanylyl cyclases needed for thermosensation. Consistent with a requirement for a membrane diffusion barrier at the subcompartment base, my data revealed the unexpected presence of ciliary transition zone proteins where no canonical transition zone ultrastructure (Y-links) is observed. My results also showed that the ciliary mutants have a reduced ability in moving toward favorable temperatures, a behavior known as thermotaxis. Finally, using a novel conditional knockout method developed during this research, I showed that the cilium acts cell-autonomously for the function of AFD neurons in thermotaxis. Based on the similarities with mammalian photoreceptors, my research suggests that differential compartmentalization of signal transduction components using different classes of ciliary proteins is important for the functions of ciliated sensory neurons.

Keywords: cilia; cGMP signaling; signaling compartment; transition zone; thermotaxis; sensory neurons.

To Mom

Acknowledgements

I would like to thank my senior supervisor, Dr. Michel Leroux, for his guidance and support, my committee members, Dr. Harald Hutter, Dr. Edgar Young, and Dr. Catharine Rankin, for their feedbacks and guidance throughout the course of this study. I would also like to thank my examiners, Dr. Kirk Mykytyn and Dr. Lynne Quarmby, for their comments on the thesis.

I would like to acknowledge our collaborators, Dr. David Hall (Albert Einstein College of Medicine), Dr. Willisa Liou (Chang Gung University, Taiwan) for sharing their unpublished data and providing electron microscopy training, Dr. Piali Sengupta and Dr. Matthew Beverly (Brandeis University) for their help collecting data. I would like to thank Maïté Carre-Pierrat (CNRS) for isolating the *daf-19* strain with *Mos1* insertion, the *Caenorhabditis* Genetics Center (CGC) for strains, and the VanWorm community for various reagents.

I would like to thank my colleagues at the Leroux lab, for their help and discussions with lab works, especially Dr. Melissa Frederic, Chunmei Li, and Dr. Jacque-Lynne Johnson, Dr. Michael Healey, Dr. Victor Jensen, Dr. Tiffany Timbers, and Catrina Loucks. I would also like to thank many researchers whom I have talked to at meetings and conferences for their discussions of my work. I would like to thank Canadian Institutes of Health Research (CIHR) and SFU for their financial support.

Lastly, I would like to thank my friends and family for their love, support, and inspiration for me to finish this work.

Table of Contents

List of Tables

List of Figures

List of Acronyms

AC	Adenylyl cyclase
BBS	Bardet-Biedl syndrome
CaM	Calmodulin
cGMP	Cyclic guanosine monophosphate
CLS	Ciliary localization signal
CNG	Cylic nucleotide-gated
DBD	DNA binding domain
FLP	Flippases
FRT	Flippase recognition target
GC	Guanylyl cyclase
GEF	guanine exchange factor
GFP	Green fluorescent protein
GPCR	G protein-coupled receptor
GRK	G protein-coupled receptor kinase
IF	Intermediate filament
IFT	Intraflagellar transport
MKS	Meckel syndrome
NCS	Neuronal calcium sensor
NPHP	Nephronophthisis
PCMC	Periciliary membrane compartment
PCP	Planar cell polarity
PCR	Polumerase chain reaction
PDE	Phosphodiesterase
PKG	cGMP-dependent protein kinase
SHH	Sonic hedgehog
SMO	Smoothened
TEM	Transmission electron microscopy
TRP	Transient receptor potential
TTX	Thermotaxis
TZ	Transition zone

Preface

One way of describing a cell is to use the 'water bag of stuff' analogy. This gives the impression of cellular components floating around, interacting with each other by random collisions. While at the most basic level, everything is by random chances, the cell expenses a lot of its energy in organizing itself so that components that have evolved to interact with each other are also close together at some point in time. This is true for events to happen inside of the cell, and especially so for events on its surface, for that is the cell's interface with the outside world, where things are even more chaotic and less controllable than the surrounded space in the cell. So by organizing signal transduction machineries into complexes and, more broadly, into signaling centers at the cell surface, cells can maximize the chance of getting the information needed from their external environment for their homeostasis. The organizing of these signaling centers in turn requires a sophisticated machinery of trafficking to target the components to where they are needed, when they are needed.

The cilium is an example of such signaling centers. Being the most visible organelle of the eukaryotic cell, it is incorporated into many signaling pathways and used ubiquitously by many cell types to sense and response to their environment. As such, the organization of signaling components inside the cilium, how those components get to where they are, and how their function can be regulated dynamically for the fine-tuning of signaling processes are important topics in the study of ciliary biology. In this dissertation, I will describe how these topics can be explored in the context of a signaling pathway used in the temperature sensing process of a ciliated cell.

Chapter 1. Introduction

The goal of my thesis is to explore the function of the cilium in the AFD thermosensory neurons of the nematode *Caenorhabditis elegans*. Through this, I hope to gain understandings about the function of ciliary proteins in the organization and regulation of signaling transduction in the cell.

1.1. The cilium as a signaling center

1.1.1. General structure of cilia

Cilia are broadly divided into two categories, motile and non-motile. Motile cilia have a whip-like shape, they are present in large numbers on cells such as those lining the respiratory track, the oviducts, or the brain ventricles in mammals. These cilia beat in coordination to move fluid across cell surface. Another type of motile cilia is flagella, they are seen in fewer numbers or as solitary organelles, such as those of protists or animal sperm. These flagella are used for cellular motility, but they are distinct from bacterial flagella. Non-motile cilia (sometimes called primary cilia) are generally present as singular organelles on the surface of eukaryotic cells. These cilia function as a sensory device, being able to recognize and relay into the cell different signals from the extracellular environment. Adapted to optimize their function as cellular antennae, non-motile cilia are of diverse shapes and sizes, ranging from the rod-like cilia that sense fluid flow in the kidney duct, to the elaborated photoreceptor outer segment that function in vertebrate vision. The strict division of motile cilia with motility functions and non-motile cilia with sensory functions is getting blurred, however, as more is learnt about the sensory ability of most cilia. For example, the motile cilia of respiratory epithelia have been shown to use their chemosensory ability to regulate ciliary beat frequency (Shah et al., 2009), while it is suggested that the mechanosensory cilia of the chordotonal

neurons in Drosophila have a motile portion that helps increase their sensitivity (Göpfert et al., 2005). In this thesis, I will focus on the sensing and not the motility aspects of cilia.

The basic structure of cilia can be described as a microtubule-based axoneme covered with the ciliary membrane that is continuous but distinct from the plasma membrane (Figure 1.1A). This membrane is not only enriched with proteins important for signaling, but also have a lipid composition different from that of the plasma membrane. Work on the motile cilia of protists as well as mammalian olfactory cilia showed that they are rich in sterols and saturated fatty acids (reviewed in Kaneshiro, 1990; Jenkins et al., 2009). Because these lipids are normally associated with lipid-rafts, it has been suggested that this membrane lipid composition not only helps increase physical strength of the cilium, but also contains discrete domains for specialized functions, such as signaling (Tyler et al., 2009; Emmer et al., 2010). Ciliary membranes may also be enriched in phosphorylated phosphatidylinositols because the inositol 5-phosphatase INPP5E has been found in cilia, and mutations in this protein lead to ciliary phenotypes (Bielas et al., 2009; Jacoby et al., 2009).

Underneath the membrane, originated from the centriole, the basal body resides at the base of the cilium and contains a ring of nine microtubule triplets (with A, B, and C tubules), which also contain γ tubulins (reviewed in Dutcher, 2001). From there, nine doublets of α and β tubulins grow from A and B tubules to give rise to the ciliary axoneme, with the microtubule plus end pointing to the distal end of the cilium. In some cilia, the axoneme ends with singlets of A tubules, as B tubules do not continue past certain length. Whereas non-motile cilia have this 9+0 microtubule pattern, motile cilia have an additional pair of tubules in the center (central pair), giving rise to the so called 9+2 configuration. They also have axonemal dynein arms between microtubules, which mediate the sliding of these tubules during motility. There are exceptions to this rule of ciliary microtubule patterns, however, as the 9+0 cilia of the embryonic node are motile due to the retention of dynein arms, and the 9+2 cilia of the olfactory and auditory systems are considered non-motile. Post-translational modifications of tubulin, such as acetylation, detyrosination, glutamylation have been shown for ciliary microtubules, and are thought to be important for the interaction with motors and other microtubule interacting proteins (reviewed in Gaertig and Wloga, 2008).

The work force in the building and maintenance of ciliary structure and function is the intraflagellar transport (IFT) machinery. IFT was first discovered as the bidirectional movement of particles along the flagella of Chlamydomonas using differential interference contrast imaging (Kozminski et al., 1993), and has since been observed with fluorescent markers in other systems, including living *C. elegans* neurons (Orozco et al., 1999). During IFT, the plus end motor kinesin-2 carries cargoes toward the tip of the cilium in the anterograde movement, while the cytoplasmic dynein complex brings them back to the ciliary base in the retrograde direction. Associated with these motors are IFT complexes A and B, first purified in biochemical studies using Chlamydomonas flagella (Cole et al., 1998). Subsequent studies have identified other components, with the total of 20 proteins discovered so far (reviewed in Bhogaraju et al., 2013). Together with the motors and cargoes, these protein complexes are thought to form the IFT trains that can be observed between the axoneme and the membrane within the cilium. Defects in IFT A complex lead to protein accumulations at the ciliary tip, so it is suggested to function in retrograde transport. Meanwhile, because of the defects in cilia formation of some IFT B mutants, it has been proposed that this complex is involved in anterograde transport.

Most IFT proteins are evolutionarily conserved and share similarities with components of coat protein I (COPI) and clathrin-coated vesicles (Jékely and Arendt, 2006). Therefore, they could function in coated-vesicle transport, and form protein-protein interaction platforms needed for binding between motors and their cargoes on ciliary membrane patches. The exact mechanism of how each IFT protein functions is under active investigation, but *in vitro* studies suggest that only a subset are required for complex formation, indicating that numerous sites are available for binding motors and cargoes (Taschner et al., 2011). However, only a limited number of IFT cargoes have been identified so far, with fewer interactions directly demonstrated (reviewed in Bhogaraju et al., 2013). Nevertheless, the nature of these cargoes indicates that IFT transports both structural components needed to build and maintain the cilium, such as tubulin and motors, as well as signaling components needed for its function, such as receptors and signaling enzymes. Also important for the operation of IFT are Bardet-Biedl syndrome (BBS) associated proteins. Some BBS proteins are thought to function in holding IFT A and B complexes together, as the absence of BBS proteins inside *C.*

elegans cilia causes dissociation of IFT A and B movement (Ou et al., 2005). BBS proteins are also part of a highly conserved protein complex important in ciliary protein transport, the BBSome (Nachury et al., 2007).

Besides the IFT trains, there are more static connections between the microtubules and membrane of cilia. At the distal tip, microtubules of primary cilia end with an electron-dense material connecting the tubules with the membrane, whereas those of motile cilia have more elaborated capping structures, which could provide mechanical strength during motility (reviewed in Fisch and Dupuis-Williams, 2011). Little is known about the function of ciliary caps, and even less is known about their composition; but it is noteworthy that the ciliary tip is where the axoneme grows and resorbs, and where IFT is remodeled from anterograde to retrograde transport. Also, the plus-end microtubule-binding protein EB1 has been found to localize to the ciliary tip (Pedersen et al., 2003; Sloboda and Howard, 2007), suggesting a role for the caps in microtubule dynamics.

At the base of the cilium, transition fibers are wing-shaped structures emanating from the basal body, connecting the C tubules with the membrane. The composition of transition fibers is largely unknown, but it has been shown to be the docking site for IFT particles (Deane et al., 2001). More distal to the basal body is a region called the transition zone. It is characterized by the so-called Y-links connecting the microtubule doublets with the membrane at the ciliary necklace, where arrays of membrane particles can be observed through freeze-fracture (Gilula and Satir, 1972). Even though the Y-links composition is largely unknown, there is a growing list of proteins associated with the transition zones (reviewed in Szymanska and Johnson, 2012). Together, the transition fibers and transition zone form what is hypothesized as the ‘ciliary gate’, separating the ciliary lumen from the cytoplasm (Rosenbaum and Witman, 2002; Reiter et al., 2012).

Just outside of the cilium, the membrane region around the base of the cilium has distinct features that differentiate it from the rest of the plasma membrane. This region is generally called the periciliary membrane, but has specific names in some cases. In photoreceptor cells, the periciliary ridge complex (PRC) consists of nine symmetric arrays of ridges and grooves, where vesicles fusion has been observed

(Papermaster et al., 1985). Similarly, *C. elegans* cilia is surrounded by the periciliary membrane compartment (PCMC) where endocytic proteins are found to function in regulating membrane content (Kaplan et al., 2012). In both cases, signaling proteins such as G- protein-coupled receptors (GPCRs) have been found at the periciliary membrane region. In other cells, it is likely that this special membrane compartment also exists but is less obvious. In the ciliated MDCK cells, a region exists around the base of the cilium that seems to have a special lipid composition, visible only by the use of lipid-anchored fluorescent proteins (Vieira et al., 2006). The periciliary membranes are thought to be important for protein trafficking to cilia.

1.1.2. Functions of cilia

Cilia are organelles uniquely designed for the capture and relay of signals from their extra-milieu. To maximize their chance of interacting with the stimuli, cilia are located on the apical surface of the cell, often pointing toward the direction where the signal comes from. To increase the sensitivity, receptor molecules are concentrated on the ciliary membrane, and in some cases they are not found anywhere else on the cell membrane. Signaling molecules are compartmentalized into the ciliary space, away from the rest of the cytoplasm, creating micro-domains with high concentrations in a relatively small space. Sensory tissues also have cilia with elaborated membrane structures to maximize the receptor surface while keeping the volume small. This small space helps the amplification step in signal transduction, as high concentrations of effector molecules can be reached within a short period of time and with a small quantity of stimuli. Not only having high sensitivity, cilia also provide means for the cell to control the signaling process. Regulator molecules can be shuttled in and out of the cilium or between ciliary sub-compartments in a controlled fashion, providing an effective way to spatially adjust the signal strength in accordance with other processes in the rest of the cell. Below are specific examples of how cilia are used as a sensory device.

Cilia in sensory cells

Examples below are taken from vertebrate and insect sensory organs, whereas ciliated sensory neurons of *C. elegans* are described in Section 1.2.

Chemosensation

Chemosensation is fundamental to all living cells as every cell is able to sense and react to different molecules in their extracellular space. Beyond this basic function, chemoreceptor cells also employ specialized structures like cilia to increase their sensitivity to various chemicals in the environment of the organism in an organized way. In vertebrates, the receptor cells of the olfactory epithelium are bipolar neurons with a dendritic knob at one end. From this knob, dozens of long, whip-like cilia extend from multiple basal bodies into the nasal cavity, where they sense odorants dissolved in the mucus. Each cilium can be divided into two parts, a short and thick proximal segment, and a long, thin distal segment. Although the proximal axoneme has a 9+2 microtubule configuration, cilia in most olfactory organs are non-motile as they lack dynein arms. The distal segment of the cilium is much longer than the proximal part, and only has a few singlet microtubules (Menco, 1984).

All components of the chemosensation signaling cascade are found in the cilia (reviewed in Menco, 1997).The large family of GPCRs act as the odorant receptors. Upon binding to specific odorants, GPCRs activate adenylyl cyclase III (ACIII) through $G\alpha_{olf}$ of the heterotrimeric G proteins to produce cyclic AMP (cAMP). This second messenger binds and opens a cyclic nucleotide-gated (CNG) channel, creating a cation influx and depolarizing the cell, resulting in action potentials. The influx of Ca^{2+} through CNG channels also activates Ca^{2+}-gated Cl^- channels and leads to further depolarization of the cell due to a Cl^- efflux (reviewed in Kaupp, 2010). A subset of mammalian olfactory sensory neurons use cGMP-based signaling instead of cAMP (Meyer et al., 2000). These cells are not known to express odorant receptors of the GPCR family, but are thought to use a receptor-type guanylyl cyclase (GC-D) to bind natriuretic peptides to sense cues related to hunger and satiety (Leinders-Zufall et al., 2007). The signaling machinery is also localized at the ciliary end in these cells (Meyer et al., 2000). Since all these signaling components have been found in the olfactory cilia, normal ciliary formation and trafficking are needed for olfactory functions. Indeed, animals with short cilia due to mutations in *bbs* genes have reduced odorant responses (Kulaga et al., 2004; Tadenev et al., 2011). Moreover, mislocalization of signaling components in ciliary mutants can also lead to olfactory defects without the loss of cilia. For example, hypomorphic mutations of CEP290, a transition zone protein, cause anosmia in mice

and humans through the specific loss of G proteins without defects in other signaling protein localizations or general ciliary structure (McEwen et al., 2007; Craige et al., 2010).

Olfactory sensory neurons show adaptation to prolonged exposure to odorants, as unlike in photoreceptors, which are optimized to maximize the capture of stimuli (see below), the main function of olfactory neurons is to be able to differentiate small differences in odor concentrations, which in turns can provide useful spatial information (Elsaesser and Paysan, 2007). (Adaptation is used in this thesis to mean changes in neuronal activities in response to constant stimuli). Adaptation in olfactory neurons is produced by phosphorylation of the receptors through a G protein-coupled receptor kinase (GRK) or Ca^{2+}-mediated modulation of downstream signaling components (reviewed in Kaupp, 2010). For example, Ca^{2+} binds to calmodulin, and together they bind to CNG channel, decreasing the channel opening probability (Chen and Yau, 1994). CNG channels in olfactory neurons are made up of 3 subunits, with the CNGA2 being the main functional subunit, but the CNGA4 and CNGB1b subunits seem to mediate calmodulin effects on adaptation (Bradley et al., 2001). Ca^{2+}-calmodulin also activates CaM kinase II - which phosphorylates ACIII and reduces its activity, as well as the ciliary phosphodiesterase PDE 1C - which breaks down cAMP; the activation of these proteins can facilitate adaptation (Wei et al., 1998; Cygnar and Zhao, 2009). Since all the signaling components important for adaptation are enriched in the cilia, ciliary proteins can potentially play an important part in olfactory adaptation. For example, phosphorylation and β-arrestin binding can remove odorant receptors out of the cilium with the help of ciliary proteins, leading to desensitization (Mashukova et al., 2006). The CNGB1b channel subunit, which is required for CNG enrichment in the cilium and mediates calmodulin-dependent adaptation, needs the ciliary kinesin-2 motor KIF17 for proper localization in the olfactory cilia (Bradley et al., 2001; Jenkins et al., 2006).

Insects also have ciliated olfactory sensory neurons, and in Drosophila, they are located in the bristle sensilla at the third antennal segment as well as the maxillary palp, a separate structure near the mouth piece. Arising from a short connecting cilium of 9+0 doublet configurations, the cilia are either branched or unbranched with various numbers of microtubule singlets (Shanbhag et al., 1999). Odors enter through pores in the bristle wall and dissolve in the sensillum lymph before binding to the receptors on the cilia. The

signaling pathway is not very well understood. It is suggested that the odorant receptors are ligand-gated ion channels (Sato et al., 2008; Wicher et al., 2008). The ciliary localization of these receptors requires the co-receptor OR83b, and probably the general ciliary trafficking pathway as no other olfactory-specific factors are needed for the ectopic expression of these olfactory receptors to the mechanosensory cilia (Larsson et al., 2004; Benton et al., 2006).

Photoreception

Perhaps the most prominent ciliary structure modified for the sensory function is that of vertebrate photoreceptor cells (reviewed in Insinna and Besharse, 2008)). It is composed of a basal body that gives rise to the connecting cilium and an extensive membrane structure called the outer segment. The connecting cilium is in fact equivalent to the transition zone, having numerous Y-links connecting the 9+0 microtubules with the membrane, and is easily recognized as a small constriction between the inner and outer segments of the cell. There are singlet microtubules at one side of the outer segment, but they are not well organized and of various lengths. The outer segment of rod photoreceptors comprises about 1000 membrane stacks that detach from the cell membrane as disks, whereas cone photoreceptors often have fewer stacks, which are still connected with the cell membrane at one side. At the proximal end of the stacks, near the connecting cilium, there are new evaginations that are formed continually to replace the more distal stacks gradually. Indeed, about 100 discs are shed everyday by rod photoreceptors, which are engulfed by nearby retinal pigment epithelial cells for the recycling of photopigments. This high turnover rate of photoreceptor membrane therefore demands a high rate of trafficking of material through the narrow connecting cilium.

Similar to the olfactory neurons, vertebrate photoreceptors also use a cyclic nucleotide-based signaling cascade for phototransduction but activation results from hyperpolarization rather than depolarization of the membrane (reviewed in Ebrey and Koutalos, 2001). When the GPCR rhodopsin absorbs photons, its chromophore 11-cis retinal is converted into all-trans retinal and allows rhodopsin to bind to the G protein transducin. This protein is a Go/Gi family member, and can activate PDE to hydrolyze cyclic GMP (cGMP). The reduced level of cGMP leads to decreased probability of the

CNG channel being open, resulting in hyperpolarization of the membrane and changes in synaptic transmission. In the absence of light, cations enter the cell through the opened CNG channel, creating the so-called dark current. All components of the signaling cascade are found in the outer segment. Rhodopsins are packed densely on the disk membrane, maximizing the probability of photon capture. The guanylyl cyclase (GC) needed for cGMP production is also found in the disk membrane. Interestingly, the CNG channel and the Na^+/K^+-Ca^{2+} exchanger needed for the removal of Ca^{2+} are localized together on the cell membrane adjacent to the disk rim. The beta subunit of CNG channel has a large cytoplasmic glutamic-acid-rich part (GARP) domain that is also expressed as soluble forms. These GARP proteins bind the channel-exchanger complex, and possibly other membrane proteins to form a disk rim complex through the Peripherin-2/Rom-1 complex (Körschen et al., 1999; Poetsch et al., 2001). The complex of signaling proteins at the rim is thought to facilitate adaptation (Körschen et al., 1999), and the Peripherin-2/Rom-1 complex has been implicated in disk morphogenesis and photoreceptor degeneration (Clarke et al., 2000; Loewen and Molday, 2000). Because of the tight packing in the outer segment membrane, rhodopsin also has a structural role because rhodopsin knockout mice fail to develop photoreceptor outer segments (Humphries et al., 1997; Lem et al., 1999).

Phototransduction needs a fast recovery rate to allow a better temporal resolution of the visual system. Conversely, photoreceptors also show adaptation to constant light in a similar manner as olfactory adaptation described above. Moreover, in the case of phototransduction, there is a light-induced translocation of proteins in and out of the outer segment believed to be important for photoreceptor sensitivity (reviewed in Calvert et al., 2006), as well as protection of the structure from over/understimulation (Fain, 2006). In particular, bright illumination causes the rhodopsin regulator arrestin to move into the outer segment, while there is a movement out of this compartment of the G protein transducin as well as recoverin, an inhibitor of the rhodopsin kinase (a GRK). As mentioned above, the high turnover rate of photoreceptor disks requires a large movement of proteins through the connecting cilium to maintain the extensive elaboration of the disk membrane. Photoreceptors are also sensitive to abnormal changes in phototransduction, and such anomalies often result in cell death (Fain, 2006). As such, defects in the general ciliary machinery as well as specific factors

involved in the transport of photoreceptor signaling components are expected to severely interfere with the development, function and maintenance of photoreceptors (reviewed in Wheway et al., 2013). Ciliary function could also play a role in adaptation of the photoresponse; however light-induced translocation is thought to be based on diffusion and not active transport (Calvert et al., 2006), so the role of ciliary proteins in this process is currently unknown.

Mechanosensation

Cells capable of sensing mechanical stimuli have cilia with a range of morphologies, from the single primary cilia of the kidney epithelia that detect fluid flow, to the modified cilia of mechanoreceptors in insects that detect forces on their exoskeleton, and the kinocilia in vertebrate hair cells important for detecting sound and movement. Unlike chemosensation and photosensation, changes in membrane potential during mechanosensation happen fast for signal transduction using second messenger cascades (μs range), so instead it is believed to involve direct gating of ion channels by mechanical forces in the so-called gating-spring model (Gillespie and Walker, 2001).

Hair cells are present in the vestibular system and the cochlea of the vertebrate ear, as well as the lateral line organs of fish. At the apical surface, numerous microvilli arrange in an increasing order of height to create the hair bundles. These microvilli are called stereocilia, even though they are actin-based structures and thus are not true cilia. At one end of the hair bundle is often found a true cilium, called the kinocilium. The stereocilia are linked by filaments, especially at the tips of the shorter projection to the lateral wall of the neighboring taller one (Pickles et al., 1984). When the hair bundle is pushed by air or fluid flow, these tip links can stretch or slacken, and the ion influx has been shown to be greatest at the stereociliary tips (Denk et al., 1995; Lumpkin and Hudspeth, 1995). It is therefore hypothesized that the mechanical force that moves the hair bundle changes the tension of the tip links, which opens or closes an ion channel, affecting the membrane potential. TRP channels have been proposed to be the mechanical-gated channel in the hair cells (Sidi et al., 2003; Corey et al., 2004). The kinocilium is also connected to the tallest stereocilium through fibrous links, but its function in hair cell is not known. It may not be involved in the transduction of mechanical force per se, as it atrophies during the development of cochlea hair cells. It

is noteworthy that the kinocilium develops before the stereocilia, so it may provide structural support for the developing microvilli. The kinocilium also dictates the arrangement of stereocilia in increasing height during development (Tilney et al., 1992). This directionality of the hair bundle is important because its movement in one direction causes depolarization, and in the other direction hyperpolarization (Hudspeth, 1989). Since planar cell polarity (PCP) is important for bundle orientation (Dabdoub and Kelley, 2005), and primary cilia may function in the non-canonical Wnt/PCP signaling, it is possible that the kinocilium is playing the role of a primary cilium, and not of a sensory cilium, in hair cells by setting up the planar polarity through Wnt signaling. It is not known whether the kinocilium plays a role in adaptation of hair cells. This adaptation is thought to involve the effect of Ca^{2+}-calmodulin on the mechanoreceptor channel (fast adaptation), and on the actin-based motor myosin-1c (slow adaptation), and probably the cAMP-dependent phosphorylation of the channel and motor molecules (Fettiplace and Ricci, 2003). Since all these components are present in the stereocilia, adaptation is more likely to happen in the stereocilia than in the kinocilium.

The mechanosensory organs of insects are the external sensilla and the chordotonal organs, sensing forces associated with touch, air flow, cuticle deformation, gravity and sound (Jarman, 2002; Yack, 2004). Mechanosensory cells of the sensilla have a single cilium of 9+0 arrangement with a dense structure at the distal tip called the tubular body. The sensory cells of the chordotonal organs have a more complex structure. They contain a proximal basal body with root processes, and a distal basal body linked to transition fibers and the transition zone. The axoneme has a 9+0 configuration, with the proximal part believed to be motile as there are dynein arms between microtubules. Between the proximal and distal segments, the axoneme swells into the ciliary dilation where the microtubules bend and an electron-dense material is seen in the middle. The electron-dense material in both structures, the tubular body and the ciliary dilation, is believed to be microtubule-based, where the doublecortin microtubule-associated protein (DCX-EMAP) is located (Bechstedt et al., 2010). Flies lacking DCX-EMAP have empty ciliary dilations and missing tubular bodies, resulting in uncoordination and deafness. This leads the authors to hypothesize that mechanical forces cause compression or expansion of the electron-dense materials (Bechstedt et al., 2010), which can open nearby ion channels such as the TRP channel NompC and

activate the cell (Walker et al., 2000). Therefore, the formation and maintenance of the cilium, as well as the proper channel localization by the ciliary machinery, are required for normal mechanosensation (Newton et al., 2012).

Thermosensation

Temperature changes can affect all cellular processes and can be considered as a ubiquitous stimulus, as thermal energy changes the state of biological molecules such as lipids, proteins, and nucleic acids (Digel, 2011). Therefore, organisms need to have specific way of sensing and regulating their cellular processes and/or behaviors to adapt to temperature changes. In mammals, outside temperature is sensed by thermoreceptor cells with their sensory end terminating in free nerve endings in the skin (Schepers and Ringkamp, 2010). These sensory termini are similar to those of mechanoreceptor and nociceptor cells, and are not thought to be ciliary (Iggo and Andres, 1982). Similarly, the thermoreceptor cells, AC and HC neurons, in Drosophila are not ciliated (Hamada et al., 2008; Gallio et al., 2011). The thermosensor molecules in both cases belong to the TRP channel family (McKemy, 2007; Hamada et al., 2008). There are also evidences for the involvement of GPCRs in temperature sensing in Drosophila (Gallio et al., 2011; Shen et al., 2011; Ni et al., 2013). The mechanism of temperature sensing by TRP channels and GPCRs is currently unknown, but it is thought to resemble mechanosensation but result in numerous uncoordinated events instead of a net stretch (Digel, 2011). Similarly, temperature sensing is thought to also response to membrane tension as for mechanosensation. However, since the phase transition of lipids takes place over a wide temperature range compared to what the thermoreceptor cells can sense, it is unlikely that membrane lipids are the determinant of temperature sensitivity in these cells. So far, little is known about the involvement of ciliary proteins in thermosensation (Tan et al., 2007).

In summary, the cilia in sensory cells are highly modified appendages well adapted to detect specific stimuli (Figure 1.1B). Indeed, many cell-specific factors and variations of the ciliary machinery have been shown to contribute to this structural diversity of sensory ends (reviewed in Silverman and Leroux, 2009). The role of ciliary proteins in adaptation is less well understood, however. Nevertheless, many molecules crucial for both transduction and adaptation are enriched in the ciliary compartment, so

ciliary proteins have the potential to play an important role in the regulation of sensory transduction. As more tools are developed to investigate the regulatory aspects of signal transduction, there will be new insights into the function of ciliary proteins in sensory perception.

Cilia in developmental signaling

The discovery that the primary cilium is an important factor in vertebrate Hedgehog signaling has contributed to the renewed interest in this organelle (Corbit et al., 2005), with its gradually being recognized as a signaling center in the cell. Many other developmental pathways have later been linked to primary cilia, including Wnt (Simons et al., 2005), PDGFα (platelet-derived growth factor receptor alpha) (Schneider et al., 2005), fibroblast growth factor (Neugebauer et al., 2009) , Notch (Ezratty et al., 2011), TGF-β (transforming growth factor beta) (Clement et al., 2013), IGF (insulin growth factor) (Zhu et al., 2009), mTOR (mammalian target of rapamycin) (Boehlke et al., 2010), and NFκB (nuclear factor kappa-light-chain-enhancer of activated B cells) (Wann et al., 2014). Unlike the cilia of sensory receptor cells, the cilia that participate in these developmental pathways are primary cilia with the basic structure as depicted in Figure 1.1A. In this case, the underlying signaling pathways are complex with many players identified, and the role of ciliary proteins in the regulation of the signaling cascades are better studied than in the case of sensory cilia. The following sections will describe the roles of primary cilia in two major pathways, Sonic hedgehog and Wnt, to demonstrate how cilia can participate in signaling transduction at the regulatory level.

Sonic hedgehog signaling

Sonic hedgehog (SHH) acts as the morphogen in the development of the limb bud and the neural tube, as well as bone and cartilage development. A simplified view of SHH signaling in the cilia is as followed: In the absence of the ligand SHH, the ciliary receptor protein Patched (PTC) can inhibit the action of the GPCR Smoothened (SMO). The transcription factor precursors GLI2/3 in a complex with SUFU (Suppressor of Fu) are phosphorylated by kinases at the basal body. GLI2/3 are then processed and translocated into the nucleus as transcriptional repressors (GLI2/3R). Upon SHH binding, PTC exits the cilium, and SMO can now be phosphorylated and localized in the

cilium. GLI2/3 accumulate at the ciliary tip and dissociate from SUFU, their full-length forms are then moved into the nucleus as an activator.

The link between SHH and cilia was first discovered when genes coding for proteins involved in IFT were isolated in mutagenesis screens looking at SHH phenotypes in mice (Huangfu et al., 2003). Subsequent studies found other ciliary associated proteins that are required for the complex orchestration of SHH signaling within and near the cilium. Together, these studies suggest that the cilium is required for the repression as well as the transduction of the signals. This is because different tissues have different requirements for GLI proteins (Huangfu and Anderson, 2005). GLI repressors play a major role the limb bud development, so the lack of cilia results in the opposite phenotype to that of SMO mutations. In contrast, in the neural tube, where GLI activators are needed for cell type specification, mutants of IFT and SMO both display phenotypes of a loss of SHH signaling. Other specific ciliary proteins that have been shown to be required for SHH signaling include the IFT motor KIF3A needed for SMO ciliary localization (Kovacs et al., 2008), and TULP3 (Tubby-related protein 3) needed for ciliary localization of proteins involved in GLI phosphorylation(Norman et al., 2009). Kinases required for GLI phosphorylation are also associated with the basal body. However, it is not clear how PTC can affect SMO localization, and how the cilium promotes the regulation of GLI processing by SMO.

Wnt signaling

Another important developmental pathway linked to cilia is Wnt signaling, however the link is much less defined compared to the case of SHH. Ciliary proteins have been shown to affect both the canonical Wnt pathway that involves β-catenin, and the PCP (planar cell polarity) branch of non-canonical Wnt signaling. The basic steps of Wnt/β-catenin signaling are binding of Wnt ligands to their Frizzled (Fz) receptor, the recruitment of the cytoplasmic protein Disshelved (Dvl), the breakdown of the destruction complex, and the translocation of β-catenin into the nucleus to regulate gene expression. The Wnt/PCP signaling also involves the activation of Dvl, and this affects the cytoskeleton through the small G proteins Rho and Rac, regulating cell shape and patterning along the plane of the tissue (planar polarity). Both pathways have multiple

feedback mechanisms, and the cilium is an attractive candidate for concentrating and regulating these signaling efforts.

One of the first and important insights into the function of cilia in Wnt signaling is the role of the ciliary protein Inversin/Nephrocystin2 (Inv/NPHP2) in regulating Dvl function. Overexpression of Inv inhibits the effects of Dvl on β-catenin-mediated transcription, suggesting that cilia negatively regulate canonical Wnt signaling (Simons et al., 2005). Manipulations of Inv levels also have effects on Wnt/PCP readouts (Simons et al., 2005). Likewise, disruptions of other ciliary proteins, such as the kinesin-II KIF3a, IFT or BBS proteins lead to hyperactive canonical Wnt responses in mice and cultured cells, and show defects in planar cell polarity (Corbit et al., 2005; Gerdes et al., 2007). Subsequent studies also pointed to the constraint of canonical Wnt and regulation of PCP pathways by ciliary proteins in various systems; however, there are also studies showing the opposite effects, i.e. an upregulation of canonical Wnt signaling by ciliary proteins in some (Lancaster et al., 2009), and a lack of Wnt phenotypes in others (Huang and Schier, 2009; Ocbina et al., 2009).

This discrepancy in the link between cilia and Wnt signaling is far from being solved, but several explanations have been suggested, including ciliary proteins playing different functions in Wnt signaling, the different effects of short cilia vs. no cilia, tissue-specific regulation of Wnt signaling by cilia (Lienkamp et al., 2012; Oh and Katsanis, 2013). In particular, some phenotypes used as readouts of Wnt/PCP are complex, involving the integration of different autonomous processes, such that the genetic interactions observed between cilia and PCP may be an indirect effect (Wallingford and Mitchell, 2011). Indeed, there have been few physical interactions found between ciliary and PCP proteins, and it is not clear what is the mechanistic basis of ciliary function in Wnt/PCP signaling. It has been shown that mutations in *ift88* affect planar polarization without disturbing the asymmetric distribution of Wnt/PCP proteins (Jones et al., 2008), which may suggest that ciliary proteins function downstream or in parallel to the Wnt/PCP pathway. The second possibility is likely since Wnt/PCP and some proteins associated with cilia also involve in centrosome positioning, an important process in cell polarization. One more complication is the dependence of ciliogenesis on PCP signaling proteins themselves. Mutations in Dvl and its PCP effector proteins often affect ciliogenesis through failures in basal body docking, or targeted trafficking. Again, it is

unclear if there is a direct cause of failures in ciliogenesis by PCP signaling defects, or this instead reflects the role of some PCP proteins in the apical positioning of both PCP machinery and ciliary basal bodies (Wallingford and Mitchell, 2011).

Given the role of cilia in important sensory and developmental processes, mutations in ciliary genes often result in various disorders, collectively known as ciliopathies. Indeed, the findings that ciliary dysfunction can lead to diseases in humans is the major reason for the great interest in recent years for this once considered vestigial structure. The combination of proteomics, comparative genomics, and transcription analyses in various models has resulted in a large collection of predicted genes required for the formation and function of cilia (Arnaiz et al., 2009). With next generation sequencing techniques becoming more common, the list of ciliopathies is growing as mutations in known ciliary genes are found among patients of certain conditions previously not connected to cilia. At the same time, genotyping patients with known ciliopathies also facilitate discoveries of new ciliary genes. Because of the ubiquitous presence of cilia on human cells, defects in ciliary components often have a pleiotropic effect, and ciliopathies often have overlapping symptoms. Common symptoms include renal cystic diseases, sensory deficits, laterality defects, polydactyly, cognitive impairment, skeletal defects, and obesity. Interestingly, the fact that not all organs are affected equally within each disorder and among different disorders suggests the importance of particular ciliary proteins in the affected organs. The studies of variability in ciliopathies also pointed toward a tendency for ciliary proteins to have context-dependent functions, similarly to what was described for Wnt signaling above (Davis and Katsanis, 2012). Although each individual ciliopathy remains rare, collectively they approach a frequency comparable to that of common disorders, such as Down syndrome (Davis and Katsanis, 2012). Therefore, studying the functions of ciliary proteins can have broad implications to important human diseases.

1.1.3. Mechanisms of protein transport

Protein transport is an important aspect for ciliary function. One basic reason is that cilia do not contain the translational machinery, so proteins need to be made elsewhere and delivered to the cilium. It is also thought that only a subset of proteins have access to this compartment, as it has a distinct protein content compared to the

rest of the cell (Inglis et al., 2006). Beyond this, the function of cilia requires the ability to accumulate specific signaling proteins within the ciliary compartment and/or sequester them away from the rest of the cell, so there needs to be methods of retaining proteins, membrane-bound as well as soluble, within the ciliary membrane and lumen, respectively. Furthermore, as made evident from the examples described above, the ability to dynamically control their protein content, directly or indirectly, allows cilia to initiate, fine tune, and terminate the signaling process. Within the cilium, proteins are also localized into sub-compartments as seen in the olfactory cilia and photoreceptor outer segment, and the sub-compartment localization could also be used as a way to regulate protein interactions during signaling. As such, once proteins are docked outside, how they can get into the cilium, and where they are localized within it, are both important for the function of cilia. Below I will summarize the current models for these following steps: how signaling proteins get to the cilium; how they gain entry and are retained in this compartment; how they are transported within the cilium and localized to different sub-compartments; and how they are removed from the cilium.

From the Golgi to the ciliary base

Membrane proteins are thought to be brought from the cell body to the cilium through the conventional vesicular transport system. In this way, proteins destined to function at the cilium are selectively packed into special vesicles heading toward the ciliary base, and the contents are released to the cilium when the vesicles fuse with the acceptor membrane. During the common vesicular transport process, the selective incorporation of cargoes into vesicles at the trans-Golgi requires the small GTPases of the Arf family. These proteins can recruit effector molecules important for membrane-membrane and membrane-cytoskeleton interactions. The cargo proteins often contain targeting sequences that are recognized by the GTPases themselves, or by the protein complex that they help form. This seems to be the case for some ciliary proteins, as in photoreceptors, the GTPase Arf4 binds to the VxPx sequence of rhodopsin for its transport to the outer segment (Mazelova et al., 2009a). This binding promotes the formation of a protein complex containing the GTPase Rab11 and its effector FIP3, as well as the guanine activating protein (GAP) ASAP1, and this complex triggers the budding of vesicles at the trans-Golgi site (Inoue et al., 2008; Mazelova et al., 2009a). Another effector of Arf4, the clathrin coat adaptor AP-1, has also been shown to mediate

the transport of ciliary membrane proteins in *C. elegans* neurons, including the olfactory receptor ODR-10, the TRP channel OSM-9, and the guanylyl cyclase ODR-1 (Dwyer et al., 2001). Thus, Arf4-mediated complex may act to mark vesicles out of the Golgi network to be transported to cilia. Another way in which proteins can get to the cilium is through their interaction with other ciliary proteins such as IFT20. In addition to its ciliary localization, IFT20 has also been found in the Golgi, and its depletion only at the Golgi pool led to the defective transport of a ciliary membrane protein, polycystin-2 (Follit et al., 2006). The same group also found that IFT20 binds the Golgi protein GMAP210, which can then interact with Arf GTPases (Follit et al., 2008). Thus IFT20 can function at the Golgi during sorting of ciliary proteins.

Interestingly, the VxPx motif has also been found in other ciliary proteins, including in the ciliary localization signal (CLS) of polycystin-2, a TRP channel in kidney epithelial cilia (Geng et al., 2006), and is needed for the proper localization of the CNG channel β1 subunit in the olfactory cilia (Jenkins et al., 2006). Another CLS, the Ax(S/A)xQ motif, is also found in the third intracellular loop of ciliary GPCRs such as the stomatotatin receptor SSTR3, the serotonin receptor 5-HTR6, the melanocortin-concentrating hormone receptor MCHR1, and the dopamine receptor D1. This CLS was shown to be necessary and sufficient for ciliary targeting, as it can confer the ciliary localization to a non-ciliary GPCR (Berbari et al., 2008a). The third intracellular loop of another ciliary GPCR, Gpr161 of Shh signaling, also contains a CLS, but it is of a different motif, (I/V)KARK (Mukhopadhyay et al., 2013). In fact, there is no clear concensus among CLS identified so far, which could mean that they bind to different partners to promote ciliary localization, and that there might be more than one way to get to the cilium. This is probably not too surprising, considering that there are many different proteins that need to get into the cilium at different times and in different manners during the signaling processes.

Leaving the Golgi, vesicles can be targeted toward cilia with the help of the exocyst complex. The exocyst complex was originally identified for their role in the exocytosis process of yeast cells. In this process, some exocyst proteins are localized on the vesicle membrane, others are on the target membrane, and their interaction helps guide the tethering of vesicles to the target membrane. Exocyst components have been found at the ciliary base (Rogers et al., 2004), and knockdown of one component,

Sec10, resulted in defective ciliogenesis in MDCK cells (Zuo et al., 2009). Interestingly, the exocyst is an effector of Rab11, a protein found in Arf4-containing vesicles of rhodopsin transport as mentioned above. Another effector of Rab11 is Rabin8, which is a GEF (guanine exchange factor) protein. Rabin8 can activate another small GTPase, Rab8, which mediates the exocyst function. The activation of Rab8 by Rab11 through Rabin8 is thought to be important for ciliogenesis (Yoshimura et al., 2007; Nachury et al., 2007), as well as ciliary protein transport, as disrupting Rab8 caused rhodopsin-containing vesicles to accumulate at the base of photoreceptor outer segment (Deretic et al., 1995; Moritz et al., 2001). Therefore, similar to other polarized trafficking systems, the Rab GTPase family is important for the arriving of vesicles at the ciliary base.

Besides Arf and Rab proteins, the transport of ciliary proteins also involves members of another small GTPase family, the Arl proteins. One member, Arl6/BBS3, can mediate membrane recruitment of the BBSome complex (Jin et al., 2010). Members of the BBSome contain structural elements common to COPI, COPII, and clathrin coat, and the recruitment of BBSome to synthetic membranes produces distinct patches of polymerized coat (Jin et al 2010). The BBSome can directly bind to the CLS of the GCPR SSTR3, and functions in the trafficking of this receptor to the ciliary membrane (Berbari et al., 2008b). The BBSome complex also binds to Rabin8 (Nachury et al., 2007), but the consequence of this interaction is not known. One possibility is Rab8 involves in bringing the BBSome to the ciliary base through the binding of BBSome with Rabin8, and vice versa, the BBSome functions together with Rab8, Rabin8, and the exocyst complex to recruit vesciles to the ciliary base (Figure 1.2).

At the ciliary base

Unlike vesicular transport to other destinations, there is no obvious acceptor membrane for the arriving vesicles to fuse with at the ciliary base. This is because direct entrance into the cilium through the base is blocked by cytoplasmic structures, including the transition fibers, the basal body, and the transition zone Y-links. This physical blockage is hypothesized to function as the ciliary gate, prevent the entry of vesicles and large molecules into the ciliary lumen (Rosenbaum and Witman, 2002). An option is for vesicles to fuse with the periciliary membrane surrounding the ciliary base, and this seems to be the case in photoreceptor cilia. Vesicles carrying ciliary proteins are fused

to the periciliary membrane through the action of SNARE (soluble *N*-ethylmaleimide-sensitive factor-attachment protein receptors) proteins. In photoreceptors, the t-SNARE (target-SNARE) protein syntaxin 3 is enriched at the base of the outer segment, and modulating the interaction of syntaxin 3 with its partner, SNAP-25, affected rhodopsin delivery to the ciliary membrane (Mazelova et al., 2009b). It is currently unknown which v-SNARE (vesicle-SNARE) binds to syntaxin 3/SNAP-25 to promote the fusion of vesicles at photoreceptor ciliary base.

Interestingly, the experiments with BBSome/Arl6 in the transport of SSTR3 described in the previous section also led to an intriguing observation. Disrupting the BBSome or Arl6 resulted in signaling proteins accumulated at the plasma membrane, which suggests that proteins can move from the plasma membrane to the ciliary membrane through the action of the BBSome at the ciliary base (Jin et al., 2010). An exchange between the plasma membrane and ciliary membrane pools upon mating signals in Chlamydomonas was also suggested for the glycoprotein agglutinin (Hunnicutt et al., 1990). This could be achieved through the lateral movement of proteins from the plasma membrane into the ciliary membrane, or by proteins being taken up from the plasma membrane through recycling endosomes and brought to the ciliary base through vesicular transport. Experiments with the SMO membrane proteins of Hedgehog signaling supported the first route - lateral movement (Milenkovic et al., 2009). Pulse-chase experiments show that upon SHH addition, there is an initial supply of ciliary SMO from the plasma membrane, before any intracellular source could be detected. In addition, disrupting endocytosis through the GTPase dynamin did not block SHH-induced SMO transport to cilia (Milenkovic et al., 2009). Therefore, signaling proteins can also move into cilia from an existing pool on the plasma membrane proteins upon signal induction.

Diffusion barriers

Regardless of how proteins get to the ciliary base, either by direct vesicular transport from Golgi, or by lateral movement from the plasma membrane, all membrane proteins need to get through the ciliary gate composed of the transition fibers and transition zone in order to access the ciliary membrane. How they do that is currently unclear, but a strong candidate is the active transport by the IFT machinery. Indeed, IFT

proteins have been found around the ciliary base, at the connection point of transition fibers to the membrane (Deane et al., 2001). The BBSome has recently been found to function in the assembly of IFT complexes at the ciliary base (Wei et al., 2012a). Given the functions of the BBSome in both IFT assembly and binding to receptor molecules, it is possible that membrane proteins are loaded onto the IFT train at the ciliary base through binding to the BBSome, and the IFT train then goes onto the microtubules and pushes its cargo through the ciliary gate. Another way in which proteins can be loaded onto IFT particles to get through the gate is through their interaction with IFT20 from the Golgi network as described earlier. Indeed, IFT proteins have been found on vesicles near the ciliary base, around the periciliary membrane area in photoreceptor cells (Sedmak and Wolfrum, 2011). It is not known what are the components of the transition fibers, but it is noteworthy that in *C. elegans*, the basal body degenerates after ciliogenesis has completed, but the transition fibers still persist, probably to function as a gate during ciliary function throughout life (Perkins et al., 1986).

The next component of the ciliary gate that needs to be overcome is the transition zone. Recent studies identified various components of the transition zone and ciliary gate, and grouped them into different protein modules that can interact with each other (Williams et al., 2011; Huang et al., 2011; Garcia-Gonzalo et al., 2011; Sang et al., 2011). These modules not only interact physically, they seem to function together at the ciliary gate. For example, genetic studies in *C. elegans* showed that disrupting individual transition zone proteins does not affect ciliogenesis, but disrupting different combinations of proteins from each module results in defects in ciliary formation (Williams et al., 2011). There are also components that seem to connect different modules together physically and functionally, such as the RPGRIP1L/MKS-5 protein connecting the NPHP and MKS modules in worms (Williams et al., 2011), and the INVS/inversin and AHI1/jouberin proteins bridging all modules in human cell lines (Sang et al., 2011). These proteins are thought to function as the gating components at the transition zone because their absence often results in altered ciliary composition, including protein accumulations in the cilium, absence of proteins normally localized at the transition zone, as well as abnormal ciliary entry of proteins normally found outside of the cilium (Williams et al., 2011; Garcia-Gonzalo et al., 2011; Chih et al., 2012). The transition zone often showed altered structures in these mutants, including missing Y-links or detachment of

membrane (Craige et al., 2010; Williams et al., 2011), so some are thought to be structural components of the gate such as the Y-link protein CEP290/NPHP6 (Craige et al., 2010). Indeed, a lot of these proteins have been shown to locate at the transition zone area (Williams et al., 2011). However, there are also proteins whose absence does not cause obvious structural defects and the precise mode of action for these components are currently unknown. One possibility is that they regulate the entry of loaded IFT train through the transition zone, as some transition zone proteins have been shown to interact with IFT components through biochemical and genetic studies (Jiang et al., 2009; Zhao and Malicki, 2011; Boldt et al., 2011).

Besides the ciliary gate described above, there is also an additional factor that helps prevent the mixing of ciliary and plasma membrane components, which is a membrane diffusion barrier just outside the base of the cilium. A strong evidence for the existence of such a diffusion barrier is the exclusion of a fluorescent protein with the lipid anchor glycosylphosphatidylinositol (GPI) from the cilium of MDCK cells (Vieira et al., 2006). Even though GPI proteins can be incorporated into lipid rafts, thereby limiting their diffusion without the use of a barrier, other lipid raft markers do not show this ciliary exclusion pattern. Moreover, GPI-anchored proteins can diffuse as rapidly as nonraft proteins in other membranes. Therefore, it is likely that the GPI-anchored protein cannot get incorporated into the ciliary membrane because of a diffusion barrier (Nachury et al., 2010).

It is thought that this diffusion barrier is made up of the septins. Septins are a group of GTPases first identified as components of the ring structure found at the bud neck of dividing yeast cells. At the membrane, septins form hetero-oligomers that are the building blocks of the septin filaments, and these filaments can assemble into a variety of shapes and sizes. One function of septin is to form a diffusion barrier by binding to the polybasic head of lipids and limit the diffusion of membrane-associated components. Septin barriers can be found in the bud neck of *S. cerevisiae*, at the sperm annulus, or at the base of the dendritic spines. Septin structure can also function as scaffolds to recruit proteins, such as the kinase cascade involved in the cytokinesis of *S. cerevisiae*, or the SNARES complexes (Beise and Trimble, 2011). In mouse kidney cells and Xenopus ciliated cells, septin 2 and septin 7 can be found as a ring structure at the base of the cilium (Hu et al., 2010). Knockdown of septin 2 caused ciliogenesis defects, and an

increased entry of membrane proteins into the cilia, and SMO is one of the transmembrane proteins shown to be affected by septin disruption. Thus the septin ring is a strong candidate for the diffusion barrier, and the septins there can also be involved in other processes happening at the base of the cilium, such as recruitment of proteins important for vesicle fusion and ubiquitination. How proteins such as SMO can cross this diffusion barrier during lateral movement from the plasma membrane is not known. One way is to use the binding of BBSome in a coated membrane patch such as in the case of SSTR3 (Jin et al., 2010). Again, the BBSome can be used to link its cargo to the IFT machinery so that motor proteins can drag the targeted proteins through the barrier. Lastly, the relationship between the septin barrier and the ciliary gate in regulating the ciliary entry is currently unclear.

For soluble molecules, anything smaller than the spacing of transition fiber blades and Y-links could in theory diffuse freely into the ciliary lumen. The transition fibers and the transition zone have been hypothesized to function as a ciliary pore complex, similarly to the nuclear pore complex, regulating entry and exit of protein through the pores in a size-dependent manner (Rosenbaum and Witman, 2002). There is evidence for a size-dependent diffusion barrier excluding protein larger than 40kDa from the epithelial cilium (Kee et al., 2012). Larger proteins are thought to be shuttled into the cilium with the use of the nuclear importing machinery, including importin-β2 and a gradient of Ran GTPase across the ciliary base. Indeed, the KIF17 motor protein carries a nuclear import signal that can bind to importin-β2 at the ciliary base in the presence of high level of Ran-GDP in the cytoplasm (Dishinger et al., 2010) The high level of Ran-GTP in the cilium can then help the release of proteins from importin-β2, effectively bringing them through the gate. It is unclear what is the mechanism of ciliary entry of importin-β2 itself at this point.

Diffusion of soluble proteins can also be driven by binding to specific retention sites available within the cilium, as hypothesized for the light-induced translocation of soluble phototransduction proteins described previously. Diffusion in this way is of comparable time scale compared to the measured rate of translocation in photoreceptors, and has the advantage of not being limited by the amount of the machinery during active transport (Calvert et al., 2006). Interestingly, for photoreceptors, some studies have found that diffusion through the connecting cilium (the equivalent of

the transition zone in photoreceptor) is not the rate-limiting step for cytoplasmic proteins up to 80kDa (Calvert et al., 2010; Najafi et al., 2012). Instead, the steric hindrance caused by the membrane disks with high protein density is the main cause for exclusion of proteins from the rod outer segment (Najafi et al., 2012). This is different from the results of the Kee et al., 2012 study described above. Photoreceptors might be a special case because of the limited space available in its ciliary lumen, but another study also showed that for a more canonical primary cilium, proteins as large as 650kDa could enter by diffusion, albeit over a long period of time (Lin et al., 2013). Thus, the slow diffusion rate can be considered as a barrier for the fast translocation of proteins needed during signaling processes.

Within the cilium

Inside the cilium, some signaling proteins have been shown to undergo IFT movement (the *C. elegans* TRP channels OSM-9, OCR-2 – Qin et al., 2005), and the Chlamydomonas TRP channel PKD2 – Huang et al., 2007), even though some others are largely immobile (the *C. elegans* TRP channel PKD-2 – Qin et al., 2005). In the photoreceptor membrane, rhodopsin is believed to diffuse freely (Poo and Cone, 1974), but opsins expressed in non-photoreceptor cells can undergo IFT (Trivedi et al., 2012). There is no clear evidence that IFT rate changes in response to signaling processes, which could be due to the averaging effect of IFT rate measurements. Another possibility is that the IFT rate stays relatively constant, but signaling proteins can attach and detach themselves from the IFT trains as a function of signaling processes, as seen for BBS particles in Chlamydomonas flagella (Lechtreck et al., 2009). The BBSome seems to be at a good position to mediate the interaction between the IFT train and its cargoes based on its interactions with both components and the ability to undergo IFT movement within the cilium (Blacque et al., 2004; Lechtreck et al., 2009). There are also other adaptors, such as the TUPL3 link between IFT A complex and GPCRs (Mukhopadhyay et al., 2010), or the MJR link between IFT88 and the guanylyl cyclase GC1 (Bhowmick et al., 2009), but it is not known if they undergo IFT and how they function precisely.

Exit from cilia

Protein removal from cilia can play a role in signaling. For example the dopamine receptor D1 is translocated from cilia in response to agonist binding (Domire et al., 2011). Similarly, the SHH protein SMO should be removed from the cilia when stimulation is terminated. Little is known about how signaling proteins are removed from the cilia, but the BBSome has been shown to function in this process. In Chlamydomonas, signaling proteins are accumulated in the flagella of *bbs* mutants (Lechtreck et al., 2009). This function may partly be mediated by IFT retrograde proteins, as a retrograde protein mutation also leads to accumulation of some of these signaling proteins. Similarly, BBS proteins are also required for the removal of the D1 protein in neuronal cilia (Domire et al., 2011). Another factor seems to be important for ciliary protein removal is ubiquitination. In *C. elegans*, the TRP channel PKD-2 is localized in the cilia, but the PKD-2-ubiquitin fusion is absent from the cilia (Hu et al., 2007). The early endosomal complex STAM1/Hrs is localized at the ciliary base and is required for the removal of ubiquitinated PKD-2 (Hu et al., 2007). Therefore, ubiquinitation followed by degradation could be used as a step in regulating the amount of signaling proteins in the cilia.

Another aspect of exiting from the cilium is that there could be a barrier preventing soluble signals created within the cilium from exiting the ciliary lumen and entering the cytoplasm. For example, Ca^{2+} ions entering through channels located at the proximal region of the cilium seem to only spread to the distal region and do not enter the cytoplasm through the ciliary base (Delling et al., 2013). There could be charged structures at the base of the cilium that bind and prevent small ions from escaping the ciliary lumen, as similar to what has been proposed as a role of F-actin in microvilli (Lange, 1999).

In summary, the model for the trafficking of ciliary proteins is mostly through the vesicular transport system, with some cases of lateral diffusion from the plasma membrane. Which route is taken may depend on the system, with high demands for signaling components favoring active transport, such as for photoreceptor outer segment, and slower signaling processes happening through diffusion of proteins as in the Hedgehog pathway. The third route, direct entrance into the lumen, is unlikely due to the ciliary gate, and may be applicable only to small soluble molecules such as ions and small proteins. Finally, as mentioned previously, the lipid content of the ciliary membrane

is distinct from that of the plasma membrane, so there also must be a way to transport specific lipids to the cilium and retain them there. One way of transporting specific lipids is to move them in the same vesicles with membrane proteins destined to the cilium during vesicular transport; and the diffusion barrier described earlier could also function to keep these lipids within the ciliary membrane. Mutations that prevent lipidation of ciliary proteins abolished ciliary localization (Follit et al., 2010; Tao et al., 2009). Therefore, the binding of specific lipids to certain proteins during vesicle transport may promote the ciliary transport and localization of both the proteins and lipids mutually.

1.1.4. Scope of research

Recently, our laboratory highlighted the fact that cyclic GMP (cGMP) signaling is found almost exclusively in ciliated organisms (Johnson and Leroux, 2010). The second messenger cGMP is widely utilized in biological systems, including sensory organs, and is present throughout the eukaryotic domain (Johnson and Leroux, 2010). cGMP is produced by GCs and broken down by PDEs, whose activities can be modulated by GPCRs or through direct ligand binding. cGMP can directly activate CNG channels and cGMP-dependent protein kinases (PKG), ultimately leading to various short and long-term downstream effects, including activation of neurons (Figure 1.3A). The correlation between cilia and the cGMP pathway during evolution suggests that ciliary proteins might be important in modulating cGMP signaling, and indeed this appears to be the case in vertebrate photoreceptors (Insinna and Besharse, 2008). Retinal degeneration, often associated with mislocalization of cGMP signaling proteins, is a feature of many ciliopathies, such as in Bardet-Biedl syndrome (BBS) (Beales et al., 1999; Adams et al., 2007). However, other examples of ciliary proteins functioning in cGMP signaling are largely lacking.

In particular, up until this study, little was known about how ciliary proteins function in cGMP signaling outside of the photoreceptor context. Signaling components known to require BBS proteins for proper trafficking into (or out of) cilia include GPCR proteins, which could function upstream of cGMP production (Nishimura et al., 2004; Berbari et al., 2008; Domire et al., 2011). Other components such as CNG channels and GCs are often found in the cilia, and they seem to interact with the IFT machinery, but their precise mechanism of ciliary localization is unclear (Jenkins et al., 2006; Bhowmick

et al., 2009). As for the regulation of the signaling transduction process downstream of sensory perception, even less is known about the function of different ciliary modules such as the transition zone proteins, BBS and IFT proteins. There is some genetic evidence implicating BBS proteins in cGMP signaling (Mok et al., 2011), but the molecular basis of their involvement remains undetermined. One of a few ciliary proteins associated with cGMP signaling is the *C. elegans* DAF-25 protein (also termed CHB-3; ortholog of mammalian Ankmy2) (Jensen et al., 2010; Fujiwara et al., 2010). Disruption of DAF-25 results in failure of two different GC proteins (DAF-11 and GCY-12) to target to cilia in sensory neurons, leading to sensory defects. It remains unclear, however, what the mechanism of DAF-25 function is, and whether it represents a general modulator of GC localization and function. *C. elegans* can be used to study these links between cilia and cGMP signaling, as it has been successfully used to study many aspects of ciliary biology and has a large and well explored repertoire of cGMP signaling components (Bae and Barr, 2008; Johnson and Leroux, 2010). The following section will give a brief description of *C. elegans* and an overview of its cilia, with a focus on a ciliated cell type that uses cGMP signaling in temperature sensing, the AFD neurons.

1.2. The model system: *C. elegans* cilia and AFD neurons

1.2.1. *C. elegans* as a model system

The nematode Caenorhabditis elegans has been used extensively to study numerous biological processes, many of which are conserved among species (Riddle et al., 1997) . As a free-living nematode, *C. elegans* is often found in rotten plant materials where they eat bacteria growing in the composted food source (Félix and Braendle, 2010). Developing from eggs, the worm undergoes 4 larval stages (L1-4), separated by molts, to reach the size of 1mm at the reproductive stage. Under optimum conditions, this life cycle from egg to adulthood takes place within 3 days at 20°C and wild-type worms live for about 2 weeks. Under harsh conditions, a special larval stage, dauer, can be formed that has high resistance to stress to allow long term survival. The small size and short life cycle of the worm allows a large number of animals to be studied, and experiments can be carried out in a reasonably short period of time. They also exhibit several complex physiological and behavioral phenotypes, so that various processes

can be studied at different levels. *C. elegans* exist as two sexes, self-fertilizing hermaphrodites and males. The hermaphrodites are XX animals; they first produce sperm and at a later stage switch to oocyte production. Since they do not suffer from inbreeding depression, most loci can be studied as homozygous. At the same time, the existence of males, which are XO animals and arise from chromosomal nondisjunction during meiosis, allows the possibility of crossing worms of different genotypes. A large brood size (~300) also increases the use of these genetic crosses. Moreover, worms with severe sickness can still be propagated and studied under laboratory conditions as they do not have to move in order to feed or reproduce. Most of the strains studied in different laboratories come from the same original Bristol strain, N2, so the differences in genetic backgrounds are kept at a minimum. Additionally, different genetic strains can also be stored indefinitely in liquid nitrogen to reduce the risk of genetic changes due to spontaneous mutations. Thanks to its many advantages as a multicellular model organism, a large amount of knowledge is now available about the molecular and genetic aspects of this round worm.

The amount of data and tools accumulated from 50 years of research in turn also confers a large advantage in using *C. elegans* as a model. To illustrate, mutant worms can easily be generated using different mutagens, and mutations can be mapped by standard genetic techniques. At the same time, next generation sequencing techniques are now also used to facilitate the identification of the molecular lesions in the mutated strains. Also, various techniques have been developed, such as RNA interference (RNAi), which allows one to assess quickly the effect of knocking down a specific gene (Fire et al., 1998). Microinjection of DNA (Stinchcomb et al., 1985), which allows the creation of transgenic animals, facilitates gene mapping and the study of gene expression and protein localization. Various techniques making use of transposon insertions and homologous recombination were recently developed as tools to engineer the genome at will (Robert and Bessereau, 2007; Frøkjaer-Jensen et al., 2008, 2010). It was also the first multicellular organism to have its genome completely sequenced. This opens new possibilities to the study of gene function when combined with the above techniques and allows the collection of data at a very large scale. At present, work is being performed to characterize the location, expression and interaction of many genes (such as the *C. elegans* modENCODE project, Gerstein et al., 2010). Thanks to it being

transparent and having a fixed number of somatic cells (959 in hermaphrodites and 1031 in males), the complete cell linage of this nematode has been elucidated, and the physical connections of its nervous system have been well mapped out. Finally, to facilitate research within the worm research community, a large collection of mutants are available from the Caenorhabditis Genetic Center (CGC), and a wealth of *C. elegans* information can be accessed through a central database (www.wormbase.org). This database provides links between genetic and physical mapping, as well as phenotypic and molecular data for individual genes.

1.2.2. Cilia of *C. elegans*

Unlike many organisms, the only ciliated cells in *C. elegans* are sensory neurons, which helps simplify the dissection of ciliary functions (reviewed in Inglis et al., 2007). At the same time, these neurons play important functions in *C elegans* biology, and many proteins involved in ciliogenesis in worms also have disease-related human counterparts, thus keeping relevant the studies of cilia in this model organism. Of the 302 neurons found in adult hermaphrodites, 60 are ciliated. These neurons are bipolar cells, with an un-branched dendrite-like projection running in the opposite direction of the axon-like projection. At the distal end of the dendrite is the cilium, which is non-motile. Electron microscopy studies revealed that *C. elegans* has a high diversity in ciliary shapes and structures, and these can be grouped into several types (Ward et al., 1975; Perkins et al., 1986). The amphid and phasmid cilia, with length ranges from 1.5 to 7.5 μm, are located at the lateral sensory organs in the head and tail of the worm, respectively. Each sensillum contains supporting cells called sheath cells and socket cells that make up a cylindrical channel open to the outside environment. The amphid channel contains 10 cilia from 8 neurons (ASE, ADF, ASG, ASH, ASI, ASJ, ASK, ADL); these cilia are of single or double rod shapes and are exposed to the external medium. The bundle within the lumen of the sheath cell also contains dendrites of the wing cells (AWA, AWB, AWC), but their elaborated ciliary structures invaginate the sheath cell instead of entering the lumen of the socket cell. The dendrite of the last amphid cell, AFD, stays separated from the rest and its sensory endings are completely embedded in the sheath cell. The phasmid contains PHA and PHB cells, the cilia of which are single rods exposed to the outside environment. Other groups of ciliated cells in the head and

tail include 6 pairs of inner lateral labial (IL1, IL2), 2 lateral outer labial (OLL), 4 quadrant outer labial (OLQ), 4 cephalic (CEP), and 4 cervical deirid neurons (2 ADEs at the anterior and 2 PDE at the posterior). The cilia of these cells have a general rod shape, but the inner appearance can be quite different from each other with specialized structures. Another group of cilia which includes that of the AQR and PQR neurons are exposed to the pseudocoelomic cavity of the worm and have complex, sometimes variable structures. Other cilia with complex structures are of the bilateral BAG and FLP neurons, the dendrites of which terminate in the tip of the head. Finally, there are also male-specific ciliated neurons, 4 of which are located in the head (CEM neurons), while the rest are within the specialized male tail structure.

1.2.3. Ciliogenesis in *C. elegans*

The cilia of worms have some deviations from the structure of the generic cilium in Figure 1.1A. In particular, ultrastructure studies of the amphid cilia revealed that *C. elegans* has no apparent basal bodies (Perkins et al., 1986). Instead, the very proximal end contains connections between the doublets and membrane that are reminiscent of the transition fibers. The transition zone contains Y-links and is ~1 μm long. The nine doublets, which originate from the proximal end, continue for another 4 μm before the outer tubules (B-tubules) terminate, this region is often called the 'middle segment'. The inner tubules (A-tubules) then form the singlets that extend 2.5 μm until the distal end, composing the 'distal segment' of the cilium. There are also a variable number of singlet tubules running in the middle and along the entire length of the cilium, and they are distinct from the central pair in motile cilia.

Thanks to its transparency, *C. elegans* is one of the few organisms in which IFT can be observed and studied routinely (Orozco et al., 1999). Elegant work using genetics and time-lapse microscopy has revealed considerable details about the IFT process in the amphid and phasmid neurons. Measurements made using different fluorescent markers gave an average speed of ~1.1 μm/s for retrograde IFT, and 0.7 μm/s and 1.3 μm/s for anterograde IFT in the middle and distal segments, respectively (Snow et al., 2004). This is because while retrograde is carried out by one cytoplasmic dynein motor complex, dynein-2, as in other organisms, *C elegans* has two anterograde IFT kinesin-2 motors, heterotrimeric kinesin-II complex and homodimeric OSM-3. These

two motors work together in the middle segment in such a way that the net speed is nearly average that between kinesin-II (~0.5 µm/s) and OSM-3 (~1.3 µm/s). However, only OSM-3 functions as the anterograde motor in the distal segment, resulting in a higher speed of transport in this part of the axoneme. Therefore, mutants lacking the functional kinesin-II complex (*klp-11*, *klp-20*, *kap-1*) can still have full-length cilia while *osm-3* mutants only have short cilia, and double mutants such as *kap-1; osm-3* cannot build cilia at all (Snow et al., 2004). Mutations of the dynein complex, on the other hand, result in cilia that are short and often have IFT particles accumulated at the distal tip (Wicks et al., 2000; Schafer et al., 2003).

Severely stunted cilia sometimes accompanied by dendritic accumulation at the base and short cilia with accumulation at the distal tip are phenotypes also often observed in mutants of the IFT complex B and A, respectively. Using these phenotypic criteria, many ciliary mutants could be assigned to either complex A or B, facilitating their identification. Cloned ciliary genes could also be assigned to complex A or B based on the anterograde speed of the corresponding proteins in *bbs* mutants. This is because as noted above, the two kinesin motors are detached in these mutants, such that complex A proteins move at the speed of kinesin-II, and complex B at the speed of OSM-3. Using these approaches, a model of IFT components has been described for *C. elegans*, results which largely agree with, and are complementary to the biochemical studies in Chlamydomonas (Scholey, 2003; Ou et al., 2007).

DAF-19 is the first RFX transcription factors to be associated with ciliogenesis in any organism (Swoboda et al., 2000). Being the only RFX member in *C. elegans*, it controls the expression of many ciliary genes, such as those encoding IFT and BBS proteins, by binding to the X-box sequences in their promoter. Mutants of *daf-19* lack all cilia and only vestigial centrioles are found at the dendritic tips in some neurons (Perkins et al., 1986). Some isoforms of DAF-19 have also been found in all other non-ciliated neurons where they function in synaptic maintenance (Senti and Swoboda, 2008).

1.2.4. Ciliary phenotypes

The general structure of cilia can be assessed through the dye filling assay in *C. elegans*, which tests for the ability of worms to take up fluorescent dyes (DiI, DiO, or

FITC).(Perkins et al., 1986) These dyes can enter the bilateral sensory organs called amphid and phasmid sensilla to stain some neurons (ADL, ASH, ASI, ASJ, ASK, AWB, PHA, PHB). These cells take up dyes presumably through the openings in the cuticle, but the precise mechanism is not known as there are cells in the amphid channel that do not take up dyes. Mutants that do not form cilia or have cilia that are too short, too long, or displaced from the amphid/phasmid channels often have reduced or complete loss of dye filling capacity (i.e. Dyf phenotype), and many ciliary mutants have been identified through dye fill experiments. It is noteworthy that mutants with defective ciliary functions, but otherwise form normal ciliary structures, cannot be picked up in these screens, however.

One way of accessing the functions of cilia is through physiological processes operating through cilia, including body size, dauer formation, and lifespan phenotypes (reviewed in Inglis et al., 2007). This is because cues leading to the formation and exit of the dauer stage often come from environmental stimuli. Furthermore, specific ciliated sensory neurons have been implicated in dauer formation, and many ciliary mutants either form dauers constitutively (Daf-c phenotype), or fail to enter the dauer stage (Daf-d phenotype). It is not clear why defects in ciliary functions can lead to opposite effects in dauer formation, and studying the mechanism of this difference could provide insights into the the role of different ciliary proteins in signaling. Interestingly, cilia can also affect lifespan independently of the dauer pathway. Laser ablation of ciliated neurons results in increased lifespan, and some ciliary mutants are long lived.

Another way to test for ciliary functions is through behavioral assays, since many behaviors in *C. elegans* are mediated through ciliated sensory neurons (Bae and Barr, 2008). Worms can react to many volatile and non-volatile chemicals, most of which are sensed by ciliated neurons in the head and tail. These neurons are also important for the avoidance of solutions with high osmolarity. Ciliary mutants are therefore often defective in chemotaxis and osmoavoidance behaviors, which lead to the Che and Osm phenotypes, respectively. Ciliated cells also mediate many behaviors involving mechanosensation such as nose-touch response, and basal slowing response. Ciliary mutant males have reduced mating behaviors, which involve chemical and mechanical sensation. The mechanisms of chemosensation and mechanosensation in worms are similar to vertebrate olfactory and insect touch receptors, respectively (Bargmann, 2006;

Goodman, 2006). Ciliated cells have also been implicated in light sensing in worms (Ward et al., 2008). Finally, there is some evidence for the involvement of cilia in thermosensation as thermosensory cells are ciliated, and some ciliary mutants seem to have defects in behaviors related to thermosensation (Tan et al., 2007; Kimata et al., 2012).

1.2.5. cGMP signaling

Many of the behaviors described above function through cGMP signaling. Indeed, *C. elegans* boast an abundance of GPCRs and GCs, and has virtually all other known components used in cGMP signaling. In particular, worms have genes coding for 34 GCs (27 of which are membrane proteins), 6 PDEs, 2 PKGs, 6 CNG subunits, as well as genes known to modulate cGMP signaling such as CaM and NCS (Johnson and Leroux, 2010). They also have genes coding for ~1000 GPCRs that could function through various G proteins to activate the cGMP pathway (Bargmann, 1998). Many of these components are expressed exclusively in ciliated neurons, which mediate many if not all the physiological and behavioral phenotypes described for ciliary mutants as above (de Bono and Maricq, 2005; Hobert, 2003). Some components have also been shown to localize to the ciliated end of these neurons, including the 3 GCs which have been implicated in a temperature-related behavior, thermotaxis (Inada et al., 2006).

1.2.6. Thermotaxis behavior and circuit

Hedgecock and Russell (1975) first described the thermotaxis behavior in *C. elegans*. In this rather complex behavior, worms remember the cultivation temperature and will move toward the corresponding zone on a linear temperature gradient. Once they've reached that zone, worms move isothermally along a narrow temperature range (isothermal tracking). The authors also observed the movement of worms away from the temperature zone that is associated with their starving conditions (negative thermotaxis). Subsequent studies confirmed the movement of worms toward lower temperature (cryophilic movement) and the isothermal tracking behavior, however the movement toward higher temperature (thermophilic movement) is observed only in certain assay conditions, and few have succeeded in replicating negative thermotaxis. Because of its experience-dependent plasticity, thermotaxis is used extensively as a model of how

sensory information is remembered to modify behaviors (reviewed in Kimata et al., 2012).

Components of the neural circuit mediating themotaxis behavior were first identified through laser ablation (Mori and Ohshima, 1995). In the model proposed in this study, the AFD neurons are the major thermoreceptor cells, and the interneurons AIY and AIZ drive thermophilic and cryophilic movements, respectively, possibly through controlling downstream interneurons RIA, RIB, RIM and other inter- and motor neurons (Figure 1.3B). Sensory inputs to the first layer interneurons are thought to control reversals and head turns, leading to biased random walk and weathervane behaviors in thermotaxis (Gray et al., 2005; Luo et al., 2014). The proposed role of AFD neurons in the thermotaxis circuit is consistent with previous findings that in a thermotaxis defect mutant, *ttx-1*, the AFD neurons have abnormal morphology while other sensory neurons are normal (Hedgecock and Russell, 1975; Perkins et al., 1986). Importantly, AFD neurons were subsequently shown to be able to respond to temperature changes through calcium imaging (Kimura et al., 2004; Clark et al., 2006) and electrophysiological studies (Ramot et al., 2008). The presence of additional sensory neurons with more minor roles in sensing temperature was also proposed in the ablation study because the effect of killing AFDs could not account for all the effects of killing AFDs together with AIZs (Mori and Ohshima, 1995). Indeed, the AWC olfactory neurons were later identified as a second site of temperature sensing through genetic and calcium imaging analyses (Kuhara et al., 2008; Biron et al., 2008). A recent study showed that yet another pair of sensory neurons implicated in gustatory functions, ASI, can also respond to temperature changes, and that these neurons can mediate thermotaxis in combination with AFD and/or AWC under different conditions (Beverly et al., 2011). The authors suggested that the way these three types of neurons function in thermotaxis is an example of degeneracy in the nervous system, which means multiple ways of creating the same output under different conditions.

How information is processed to modulate thermotaxis behavior is complex and involves integration at multiple levels. At the sensory level, calcium imaging studies showed that the threshold in which AFD and AWC neurons start to react to temperature stimuli depends on the past cultivation temperature (Clark et al., 2006; Kuhara et al., 2008). For example, AFD neurons in worms previously cultivated at 15, 20, and 25°C

react to temperature stimuli above 15, 17, and 21°C, respectively (Clark et al., 2006). This indicates that these neurons serve not only as the temperature sensors but also as a memory device in the circuit (Kimata et al., 2012). Clark et al.(2006) further pinpointed the site of memory storage in AFD neurons to be the sensory endings, as this site still retained the ability to respond to temperatures above the threshold temperature even when disconnected from the cell body. The mechanism of single-cell memory in this behavior is currently unknown. At the first layer of interneurons, studies have been focused on how information is transmitted from AFD and AWC neurons to AIY neurons, which is the post-synaptic partner of all three sensory neurons, AFD, AWC, and ASI. The AFD neurons can both inhibit the AIY neurons through glutamatergic transmission, and excite them through peptidergic transmission (Narayan et al., 2011; Ohnishi et al., 2011). Moreover, a reduced response in AFD hyperactivates AIY, while a complete inactivation of AFD results in the loss of AIY response (Kuhara et al., 2011). Similarly, AWC can both upregulate and downregulate AIY activity, with the former process being glutamate-dependent (Kuhara et al., 2008; Ohnishi et al., 2011). AWC and AIY also function in the olfactory circuit, and the exposure of AWC to odorants relieves the glutamate-dependent inhibition of AIY (Chalasani et al., 2007). These studies showed that a simple circuit involving just three neurons can possess an intricate flow of information that ultimately contributes to a complex behavior such as thermotaxis (Figure 1.3C). Furthermore, the study of how information from temperature and odor stimuli is discriminated and/or integrated will also give insights into environmental cues can have both short and long term effects on behaviors. Finally, the downstream interneurons and motor neurons of the circuit have been shown to regulate turn frequencies, which can affect the biased random walk component of the taxis behavior (Gray et al., 2005).

1.2.7. AFD neurons

The major thermosensors, AFD neurons, are two bipolar cells located in the head area, with the cell body and axon in the nerve ring, where they make chemical synapses with the AIY interneurons, gap junctions with the AIB interneurons, and receive chemical synapses in the axon from AWA, ASE and AIN neurons (White et al., 1986). TEM (transmission electron microscopy) showed that embedded in the sheath cells at the bilateral amphid sensilia, the dendritic ends of AFD neurons terminate in numerous

membrane projections called fingers or villi, and a 'rudimentary' cilium at the very distal end (Perkins et al., 1986). No internal microfilaments or microtubules were observed in the fingers of AFD neurons by EM in this study, but the authors noted that the fingers tend to orient in the anterior-posterior direction. The high surface area-to-volume ratio resulting from finger membranes presumably contributes to the sensitivity of this neuron to small temperature changes. Supporting this hypothesis is the observation that the thermotaxis defective mutant *ttx-1* completely lack AFD fingers, and possess a sack of membrane instead (Perkins et al., 1986). In contrast, the function of the short cilium in AFD neurons is not known. It was suggested that the cilium is dispensable for the finger formation, as the *daf-19* mutant, which lacks all cilia, still possesses AFD fingers (Swoboda et al., 2000).

The molecular pathway functioning in AFD neurons involves cGMP signaling (Figure 1.3A). Three GC proteins, GCY-8, -18, and -23, were found to be expressed exclusively in AFD neurons, and double or triple mutants of genes encoding these proteins have defective thermotaxis behavior (Inada et al., 2006; Wasserman et al., 2011). The CNG channel consisting of TAX-2 and TAX-4 subunits is expressed in many sensory neurons including AFD, and is required for thermotaxis (Coburn and Bargmann, 1996; Komatsu et al., 1996). Mutants of *tax-2* and *tax-4*, as well as the triple mutant *gcy-23, -8, -18* lack the thermoreceptor current in AFD neurons in response to temperature changes, and the *tax-4* mutant does not show an increase in intracellular calcium concentration in AFD neurons during warming (Kimura et al., 2004; Ramot et al., 2008). PDE-2 has recently been shown to function in AFD neurons in thermotaxis (Wang et al., 2013), but the sensor molecule has not been identified. However, a GPCR, SRTX-1, was found to be expressed specifically in AFD and AWC, and its mutation leads to hyperactive AWC as well as defective isothermal tracking behavior (Colosimo et al., 2004; Biron et al., 2008). Similarly, the signaling pathway in AWC for temperature sensing is also based on cGMP (Kuhara et al., 2008). *C. elegans* contains two PKG proteins, ELG-4 and PKG-2. Whereas little is known about the function of PKG-2, EGL-4 has been shown to function in olfactory adaptation (L'Etoile et al., 2002), as well as regulation of sensory function in ASH neurons (Krzyzanowski et al., 2013). EGL-4 has not been shown to be expressed in AFD neurons, however it can play a role in regulating thermotaxis in response to starvation, even though this role is likely mediated

through AWC neurons (Nishio et al., 2012). Downstream of temperature sensing, various regulatory molecules have been identified in AFD that modulate its activity and plasticity. These include the CaM kinase CMK-1, the calcineurin A subunit TAX-6, the PKC-epsilon/eta TTX-4, the diacylglycerol kinase DGK-1, and the CREB protein CHR-1 (reviewed in Kimata et al., 2012). Besides functioning in thermotaxis, AFD neurons also take part in CO_2 sensing as well as noxious temperature avoidance behaviors (Bretscher et al., 2011; Liu et al., 2012).

While being sensitive to different stimuli, AFD neurons and vertebrate photoreceptor cells have been suggested to be closely linked evolutionary because they share remarkable similarities at many levels (Erclik et al., 2009; Ramot et al., 2008; Satterlee et al., 2001; Svendsen and McGhee, 1995). At the morphological level, both types of cells possess elaborate membrane structure, discs in photoreceptors and fingers in AFDs. The high surface-to-volume ratio is known to contribute to photoreceptor sensitivity. AFD neurons can respond to exquisitely small temperature changes (Clark et al., 2006), and mutants with altered finger structures have thermotaxis defects, suggesting that the finger structures are needed for their function as a sensitive device. Interestingly, the AFD sensory structure is similar to those of the invertebrate photoreceptors, with a small cilium and many villi (reviewed in(Arendt, 2003)). At the molecular levels, both cell types use cGMP signaling in the transduction of stimuli, and the signaling pathways are composed of components that are closely related between *C. elegans* and vertebrates. Finally, at the circuit level, several components of the neuronal network mediating thermotaxis are specified by the same families of transcription factors as those functioning in the retina. Specifically, AFD neurons are specified by TTX-1, while photoreceptor-specific genes are regulated by CRX, both are members of the *otd/otx* transcription factors. AIY neurons, which receive direct inputs from AFDs, requirethe CEH-10 and TTX-3 homeobox proteins, while their homologs, VSX and LHX, respectively, have been implicated in the development of bipolar cells, the primary post-synaptic partners of vertebrate photoreceptors. This raises the intriguing possibility that the thermosensation circuit in *C. elegans* and the photosensation circuit in vertebrate retina are ancestrally related. However, it is also possible that the same transcription factor network is used to specify anterior neuronal circuits in general, as for example,

AWC neurons are also connected to AIY neurons, and are specified by another member of the *otd/otx* family, CEH-36 (Koga and Ohshima, 2004).

1.2.8. Research goals

For this dissertation, I chose to study the role of ciliary proteins in cGMP signaling of the AFD neurons in *C. elegans* thermotaxis behavior because of the relatively well characterized nature of the system as well as its potential implications in many aspects of cilium biology. More specifically, as described above, AFD neurons use cGMP signaling, components of this pathway in AFD have been identified and their functions in thermotaxis have been confirmed by various studies. This facilitates the investigation of the interaction between ciliary proteins and cGMP signaling components. At the same time, the role of the AFD cilium is currently unknown, as there is evidence for the involvement of ciliary proteins in thermotaxis but their precise function remains unclear (Tan et al., 2007). More generally, unlike for other sensory modalities, little is known about the connection between cilia and temperature sensing across species, in particular whether the cilium can function as a thermal sensory device. In fact, *C. elegans* has the best studied thermosensor system involving ciliated cells so far. Therefore, these neurons can be used to investigate the function of cilia in thermosensation. The AFD neurons also have a unique ciliated end, and studying how this structure is formed could provide insights into the mechanism of how ciliary structural diversity is generated. Furthermore, since AFD neurons themselves show plasticity, any step in the signaling pathway could be modified by past experiences, so there is a unique opportunity to explore how signal sensing by cilia can influence learning and memory within the single-cell context. Lastly, the connection between AFD neurons and vertebrate photoreceptors described above implies that findings in this model system may help provide insights into the mechanism of normal retinal function and degeneration in the context of ciliopathies.

In particular, the goal of my research is to investigate the role of the cilium in AFD neurons. Does the cilium function as the device that initiates the cGMP-based sensory transduction like cilia in other sensory receptor cells? Or does it act as a regulator of the cGMP signaling pathway, similar to the role of primary cilia in developmental signaling? Toward this goal, I set out to answer the following questions:

1. Where are the cGMP signaling components localized in respect to the cilium in AFD neurons?

2. How are these localization patterns affected by mutations in various ciliary functional modules?

3. Does the lack of ciliary proteins, or of the cilium itself, result in defects in AFD function?

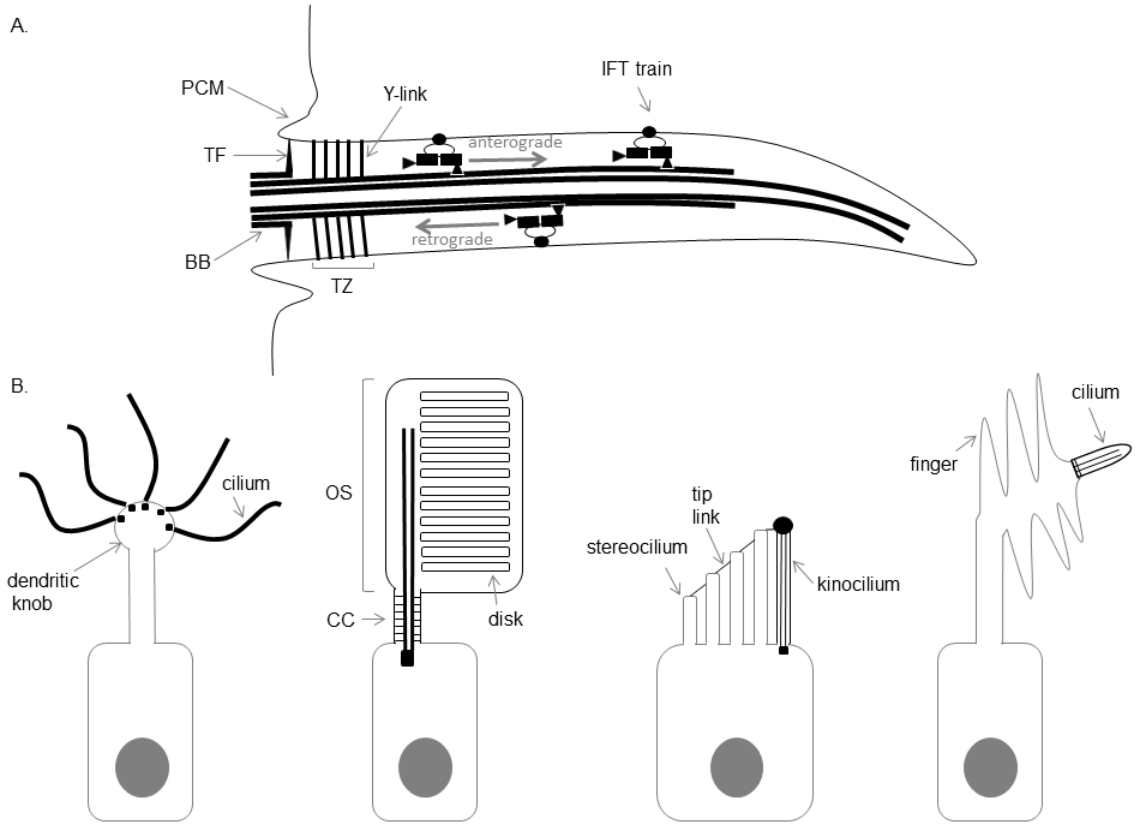

Figure 1.1. Ciliary structures.

(A) Schematic drawing showing basic features of a generic cilium. (B) Structures of specialized cilia in sensory cells (left to right): an olfactory neuron, a rod photoreceptor, a hair cell (in mammals), and an AFD neuron in *C. elegans*. Ciliary structures are in black, the rest of the cells are in gray. BB - basal body, TF – transition fibers, TZ – transition zone, PCM – periciliary membrane, IFT – intraflagellar transport, OS – outer segment, CC – connecting cilium.

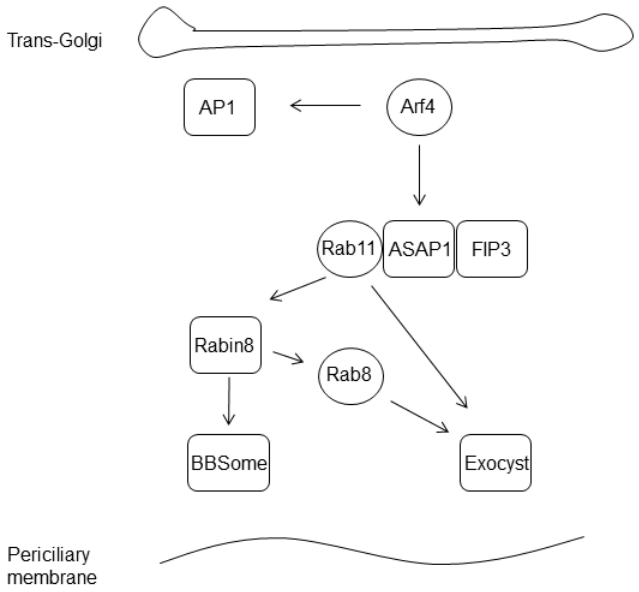

Figure 1.2. Interaction network in vesicular transport to cilia.

Summary of known interaction between various components of the vesicular transport machinery from the trans-Golgi network to the periciliary membrane. Small GTPases are drawn as circles to highlight the role of various GTPases in this process (based on Nachury et al., 2010).

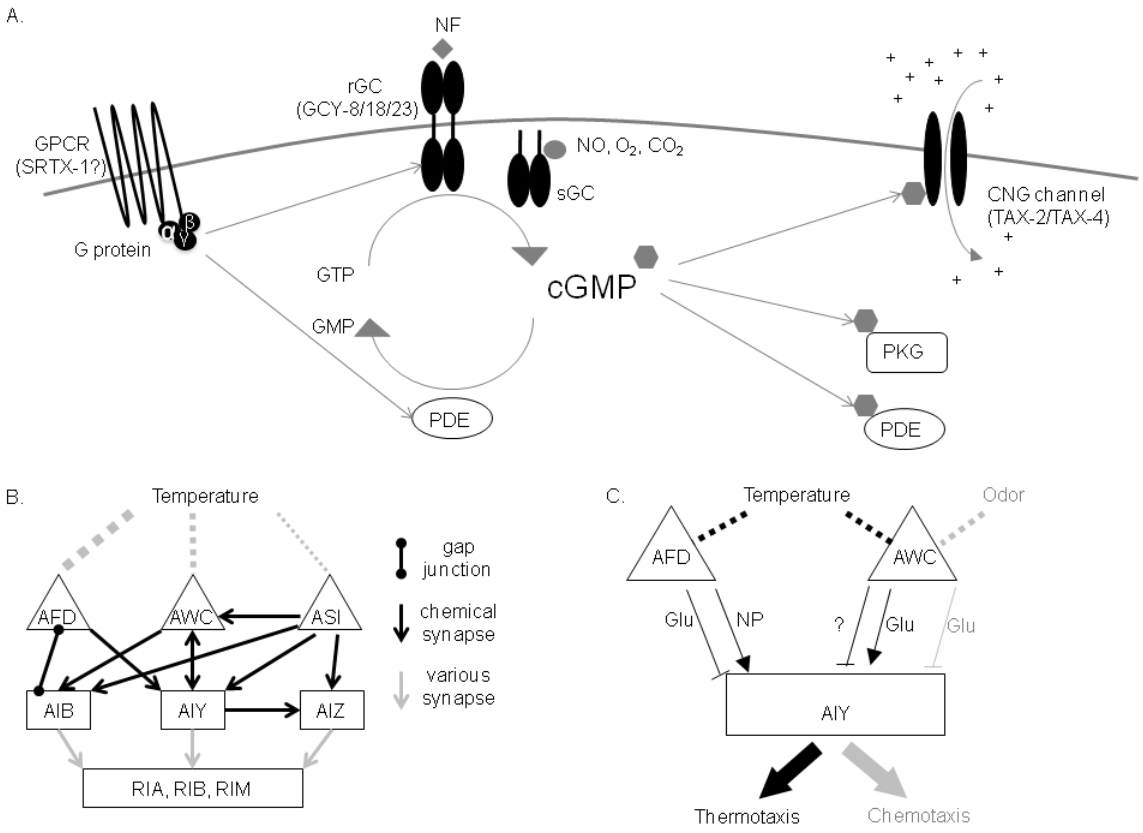

Figure 1.3. Molecular and neuronal networks in *C. elegans* thermotaxis.

(A) cGMP signaling components. Names of proteins functioning in AFD neurons during thermotaxis are given in brackets. (B) Neural connections among sensory neurons and layer 1 interneurons that mediate thermotaxis behaviors in *C. elegans*. (C) A model for neuronal regulation of the AIY interneuron by AFD and AWC sensory neurons. Regulation steps during thermotaxis are in black, and during chemotaxis are in gray. GPCR – G protein-coupled receptor, rGC – receptor guanylyl cyclase, sGC – soluble guanylyl cyclase, CNG – cyclic nucleotide-gated, PDE – phosphodiesterase, PKG – cGMP-dependent protein kinase, Glu – glutamate. (B and C are based on Kimata et al., 2012).

Chapter 2. Materials and methods

2.1. General *C. elegans* techniques

Strains and culturing conditions

All strains were cultured on OP50 bacteria at 20°C using standard techniques (Brenner, 1974). The Bristol strain N2 was used as the wild type. The mutant strains used were MX52 *bbs-8(nx77)*, MX972 *daf-25(m362); daf-12(sa204)*, JT204 *daf-12(sa204)*, IK597 *gcy-23(nj37) gcy-8(oy44) gcy-18(nj38)*, MT3645 *osm-12(n1606)*, PR813 *osm-5(p813)*, CB3330 *che-11(e1810)*, MX1331 *nphp-2(gk653),* MX754 *mks-5(tm3100)*, MX27 *mksr-2(tm2452)*, MX642 *mks-6(gk674)*, FX925 *nphp-4(tm925)*. Transgenic strains used are listed in Appendix C. All crosses with mutants carrying no visible phenotype were followed by PCR of the corresponding mutation, except for the following crosses: (1) crosses that involve *daf-12(sa204)* were done by backcrossing F1 males with *daf-12(sa204)*, since the *sa204* mutation has not been characterized but is on LGX, and the Lon phenotype of *daf-12* worms was hard to follow; (2) crosses that involve the strain carrying multiple copies of *FLP* were followed by semi-quantitative PCR of the *pes-10* promoter.

Dye filling

Animals were incubated with 5μM DiI ($DiIC_{18}(3)$, Vybrant DiI cell-labeling solution, Molecular Probes) in M9 for 1 hour before being imaged (Blacque et al., 2004).

2.2. Transgenic strain construction

Construction of fluorescent transgenic strains

In general, full-length translational fusion constructs were created by stitch PCR (Hobert, 2002) using Expand Long Template PCR system (Roche) and were injected into N2, CB907 *dpy-5(e907)* or PS3729 *unc-119(ed4) III; syIs78 [ajm-1::GFP + unc-119(+)]* worms. The AFD-specific constructs were made by using the 1.5kb upstream region of the *gcy-8* gene as the promoter. All stitched constructs carry *GFP* or *mCherry* with *unc-54 3'UTR* amplified from plasmids *pPD95.77* or *pLV-mCherry* (Addgene), respectively. Templates for PCR amplification of genes of interest (GOI) were listed in Table 1. Constructs were injected at the 5-10ng/µl range, together with co-injection markers *unc-122::gfp* (20ng/µl), *rol-6(su1006)* (50ng/µl), or *dpy-5(+)* (100ng/µl). Empty DNA vectors, such as *pUC19*, were sometimes added to make the final DNA concentration reach 100ng/µl. Integration of extra-chromosomal arrays was done with X-ray at 1500 rads.

A few exceptions and specifications in making some constructs are described here. For the *gcy-8p::gfp::gasr-8* construct, the *gfp::gasr-8* fragment was previously made by Chunmei Li, which contain the ~1kb downstream of the predicted stop codon for *gasr-8* (as of WS240) as the *3'UTR*. For translational constructs of *egl-2* and *mks-5*, stitch PCR was unsuccessful due to their large size, so they were made using a modified ligation-independent cloning (LIC) method instead (see below). For *ajm-1*, a truncated version containing exons 4 to 9 was used as it was shown to be localized similarly to the full-length construct (Köppen et al., 2001). For calcium imaging experiments, wild-type strain carrying a *gcy-8*p::YC3.60-containing extrachromosomal array described in Clark et al. (2007) was obtained from Piali Sengupta (Brandeis University).

Construction of cell-specific knockdown strains

Double-stranded RNA (dsRNA) constructs were made using the protocol described by Esposito et al. (2007). Primers used to amplify genomic fragments (from N2) or the *gfp* fragment (from *pPD95.77*) are listed in Table 2. The *gcy-8* promoter was used to drive the constructs specifically in AFD neurons. The constructs were injected at 100ng/µl into N2 and integrated into the genome, the resulting strains were outcrossed at least 5 times. For *gfp* knockdown, three independent lines were isolated from the integration that showed normal phenotype visually and on the Multi-Worm Tracker (Swierczek et al., 2011). Therefore they were used without outcrossing, and all three

lines gave similar results, suggesting no important mutations present in their background.

Construction of cell-specific knockout strains

All single copy insertions were done using the MosSCI method (Frøkjaer-Jensen et al., 2008), with the following co-injection plasmids (Addgene): *pCFJ601* (*eft-3p::Mos1 transposase*) (50ng/μl), *pMA122* (*Phsp::peel-1*) (10ng/μl), *pCFJ90* (*myo-2p::mCherry::unc-54 3'*UTR) (1ng/μl), *pCFJ104* (*myo-3p::mCherry::unc-54 3'*UTR) (10ng/μl), *pGH8* (*Prab-3::mCherry::unc-54 3'*UTR) (10ng/μl), *pUC19* (junk DNA) (15 ng/μl).

Single copy insertion on LGII: IE36198 *daf-19*(*ttTi36198*), a strain containing the Mos1 transposon inserted near the DNA binding domain (DBD) of *daf-19*, was obtained from Maite Carre-Pierrat (UMS 3421-CNRS) and crossed into *unc-119(ed3)* to make MX1689. A plasmid containing the 1.5kb left and right homology arms, *cb-unc-119(+)*, and *daf-19* DBD flanked by the 34-nucleotide *FRT* or scrambled *FRT* (*FRTsc*) sites (GAAGTTCCTATTCtctagaaaGTATAGGAACTTC and ATAACTCATCTTAAGGTATGCTAACGTGTCAGAT, respectively) inserted into *pNIC28-Bsa4* vector (Addgene) was made with the Golden Gate cloning method (Engler et al., 2008) using BsaI (NEB) and T4 Ligase (NEB) enzymes. This plasmid was confirmed by sequencing and then injected at 10ng/μl into MX1689 and the resulting strains were outcrossed 6 times to make MX1768 (or MX1769), a strain carrying *FRT* (or *FRTsc*) sites flanking genomic *daf-19* DBD.

Single copy insertion on LGIV: A plasmid was made that contains a single copy of *QF* with *unc-54 3'UTR* driven by the *gcy-8* promoter, and *FLP* with *let-858 3'UTR* driven by the 5x*QUAS* + Δ*pes-10* promoter put into the *pNIC28-Bsa4* vector using the Golden Gate cloning method. Templates for amplifying *QF* and *FLP* with *let-858 3'UTR* are from *pAC-QF* and *pGC133* (Addgene), respectively. The *QF* + *FLP* gene cassette was then cloned into the *pCFJ178* plasmid at *XmaI*/*KpnI* sites. This plasmid was confirmed by sequencing and then injected at 10ng/μl into the EG6256 strain and the resulting strain was outcrossed 6 times to make MX1772, which contains the insertion on LGIV at locus *cxTi10882*, using the MosSCI method.

Single copy insertions into both sites were confirmed by PCR on genomic DNA with Expand Long Template PCR system (Roche) for LGII and LongAmp Taq DNA Polymerase (NEB) for LGIV using primers flanking the homology arms (Figure 2.1). The primers used are: CCACAGTGCAATACCATGTAC and GGAGAAGTGAGATCTATGGTAG for LGII, CAAACGGAGCACCAGGAAAGC and AAACTCCAAACACACCAGTCAC for LGIV. A low copy number for the *gcy-8* promoter was also confirmed by qPCR, which showed that the mutant strains carry no more than twice the number of copies compared to N2 (see Section 2.3). Double mutants carrying insertions on both LGII and LGIV were made through genetic crosses, and these are worms carrying a single copy of *FLP* (MX1776 and MX1778). To make knockout strains carrying multiple copies of *FLP*, a PCR fragment containing the 5x*QUAS* + Δ*pes-10* promoter, *FLP*, and *let-858 3'UTR* was injected and integrated into wild-type worms, and the resulting strain was crossed into MX1776 and MX1778 to make MX2141 and MX2142, respectively.

2.3. Molecular biology

Modified ligation-independent cloning (LIC)

The *gcy-8* promoter was cloned into *pPD95.77* at the *PstI*/*SalI* sites to make the *pPD95.77-gcy-8p* plasmid. Mutations were incorporated into the primers to turn the *TAA* stop codon 35bp downstream of the *MscI* site into *GCT*, creating the *F-pPD95.77-gcy-8p* plasmid. This plasmid was digested with *MscI* and treated with T4 DNA Polymerase (NEB) and dATP to create a linear LIC vector with unique overhangs. PCR fragments for genes of interest were in turn treated with T4 DNA Polymerase and dTTP to create complementary overhangs. The two fragments were then ligated with T4 Ligase (NEB) in order to increase cloning efficiency. All resulted plasmids were sequenced to confirm the presence of correct promoter and exon sequences.

qPCR to test for low copy numbers of the *gcy-8* promoter

Genomic DNA was extracted using Gentra Puregene kit (Qiagen), and was diluted to the 6ng/µl range. Primers for amplifying *gcy-8* promoter are

TAACAGTTGTCGCTGCATACC and TGGATGGTCTCACCCGTAAT, and for *cdc-42* (as the control) are TTTCCTTCTGAGATATGTGCCG and ATCCTAATGTGTATGGCTCGC, using the KAPA SYBR FAST qPCR mix (Kapa Biosystems) in the StepOne Real-Time PCR system (Applied Biosystems). Standard curve was used to determine the amplification efficiency as 106% and 99% for *gcy-8* promoter and *cdc-42*, respectively. Three replicated were done in each trial, and the results from 2 trials showed a 1.98 to 2.34 fold increase in the copy numbers of *gcy-8* promoter in MX1772 compared to N2.

PCR to detect somatic deletion in the cell-specific knockout strain

This method is based on the protocol described in Edgley et al. (2002), using poison primers followed by nested PCR to detect rare deletions. In brief, L3/L4 larvae were used for single-worm lysis, all of which was used as template for the first round of PCR with the use of a poison primer. A 0.2μl from the first PCR reaction was used as template for the second round with the nested primers. To enrich for the mutant and long wild-type fragments, only the nested forward primer was used for the first 10 cycles of the 2nd round, followed by 25 cycles with equal amount of forward and reverse nested primers. Deletion of *daf-19* DBD results in a ~250bp band, while no deletion is indicated with the presence of the ~800bp wild-type band only (Figure 2.2). Primers used for the 1st round are: CCCTTGTTGGGAGTTAATAACCGG (F1), GCTGAACATCGAATGGATCCAG (P), and GTAATGGAGCAGGTTGTTGCG (R1); for the 2nd round are: CCAATTCATCCCGGTTTCTGTC (F2) and CGTTGATGGTATGACTGAGTGG (R2)

2.4. Microscopy

Fluorescent microscopy

Live animals were anaesthetized with 10mM levamisole, mounted on 5% agarose pads with 0.1μm-diameter polystyrene beads (Polysciences, PA), and observed under epifluorescence or spinning disk confocal microscopes. Image analyses were carried out using Volocity (Improvision) for deconvolution and co-localization.

To follow ciliogenesis in the embryos, worms were used in *unc-54(e190)* background to reduce movement of embryos. On a 5% agarose pad without polystyrene beads, gravid adults were cut open in M9 to release embryos of different stages. A cover slip was put on slightly, the space was filled with M9 and then sealed with Vaseline. Under this condition, ciliogenesis can be followed for a couple of hours before the embryo stops developing.

Electron microscopy

Sample preparation was carried out essentially as described in (Hall et al., 2012).. Briefly, one-day adult worms were fixed in 2.5% glutaldehyde, 1% paraformaldehyde at room temperature for 2-4 hours. Samples were then refixed in 1% osmium tetroxide on ice for 1 hour, and stained with 1% uranium acetate at room temperature for 90 minutes. After dehydration, samples were embedded in Embed-812 resin medium mixture (EMS) and sectioned on a diamond knife. Electron micrographs were collected with a Philips CM10 at 13500-19000X.

2.5. Behavioral assays

Thermotaxis assay

Thermotaxis plates were made with thermotaxis medium consisting of 2% agar, 0.3% NaCl and 25 mM potassium phosphate (Mori and Ohshima, 1995) in a 9-cm plate. About 100 to 300 one-day old adults raised at 20°C were collected and washed with M9 twice at room temperature before being put on the 23°C zone (in the middle) of thermotaxis plates on a linear temperature gradient (0.5°C/cm) as described in Tan et al., 2007. After 30 minutes, the plates were scanned and the resulting images were analyzed as followed: the plate was divided longitudinally into 4 equal parts, each part corresponding roughly to a one-degree zone; the number of worms in each part was counted and a thermotaxis index was calculated as (2a+b-c-2d)/(a+b+c+d), with a being the number of worms on the hottest part, d the coldest part (Figure 2.3A). The data from at least 10 different repeats were used to test for significance using Student's t-test or one-way ANOVA with Bonferroni *post hoc* correction.

Locomotory assay – On food

A single, well-fed one-day old adult was put on a 6-cm plate (with a thin lawn of OP50 bacteria covering most of the plate) and was allowed to move freely for 18-20 hours. The extent of locomotion was then analyzed by counting the number of 5x5mm squares the worm travelled through. Each strain was analyzed at least 3 times, 10 worms each time, and Student's t-test or one-way ANOVA with Bonferroni *post hoc* correction was used to test for significant difference.

Locomotory assay – Off food

Worms were prepared as for thermotaxis assay and put in the center of the thermotaxis plate without a temperature gradient. After 30 minutes, the plates were scanned and the resulting images were analyzed as followed: the plate was divided into 4 concentric circles; the number of worms in each part was counted and a dispersal index was calculated as (a+2b+3c+4d)/(a+b+c+d), with a being the number of worms on the most inner circle, d the most outter (Figure 2.3B). The data from 3 repeats were used to test for significance using one-way ANOVA with Bonferroni *post hoc* correction.

Table 1. Source of templates for PCR amplification of genes of interest

GOI	Source of template
arl-13	genomic DNA from N2
srtx-1	genomic DNA from N2
gcy-8	genomic DNA from N2
gcy-18	genomic DNA from N2
gcy-23	genomic DNA from N2
tax-2	genomic DNA from N2
tax-4	genomic DNA from N2
egl-2	genomic DNA from N2
ttx-4	genomic DNA from N2
tax-6	genomic DNA from N2
odr-1	genomic DNA from N2
xbx-1	Plasmid *p328 (osm-5p::xbx-1::tdTomato)* - Bradley Yoder (University of Alabama)
gasr-8	PCR product *bbs-8p::gfp::gasr-8* - Chunmei Li (SFU)
nphp-1	Plasmid *p344 (nphp-1::tdTomato)* - B. Yoder
mks-5	genomic DNA from YH930 - B. Yoder
mks-6	Plasmid *p342.1 (osm-5p::mks-6::gfp)* - B. Yoder
mksr-2	PCR product *mksr-2::gfp* – C. Li; plasmid *p356 (mksr-2::tdTomato)* - B. Yoder
bbs-8	construct already made previously by C. Li
tram-1	genomic DNA from N2
ajm-1	genomic DNA from N2
nphp-2	construct already made previously by C. Li

Table 2. List of primers for dsRNA constructs

GOI	Primers
bbs-8	AGTAGATCAACCAATGGCGG TTTTTGCAATGCTCATGCTC
daf-25	TCTCAAACCTTGGATCTCGC TCAAATATTGGGGTTCAGCC
daf-19	GGTGCACCATGACACTATCG AAACGAGCGAGAAAGGACAA
unc-122	GACACGTTGGACGCTGAGTA TTCTGCATTCCAATCATCCA
gfp	TTTGTATAGTTCATCCATGCC AACTTTTCACTGGAGTTGTCC

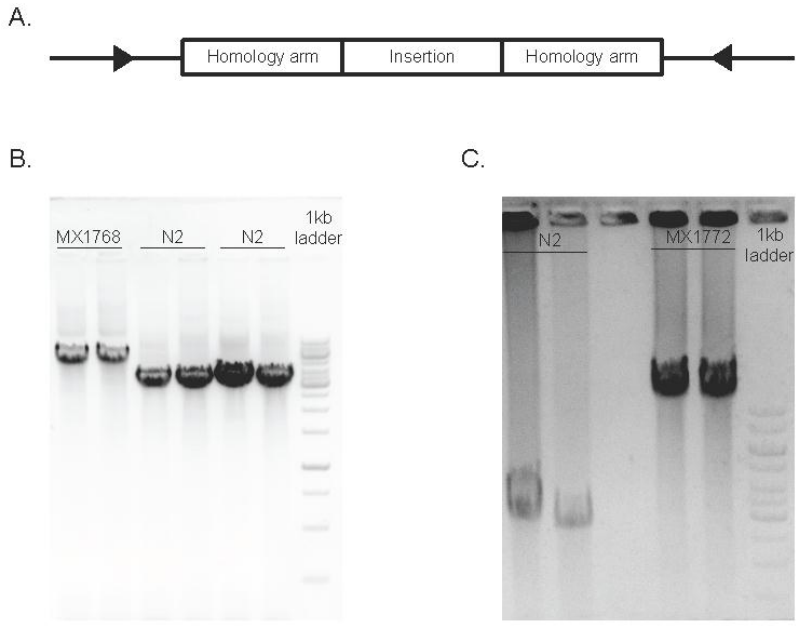

Figure 2.1. PCR to confirm single copy insertions.

(A) Positions of the primers used for PCR (arrowheads). (B) DNA gel showing products of PCR for the LGII insertion. (C) DNA gel showing products of PCR for the LGIV insertion.

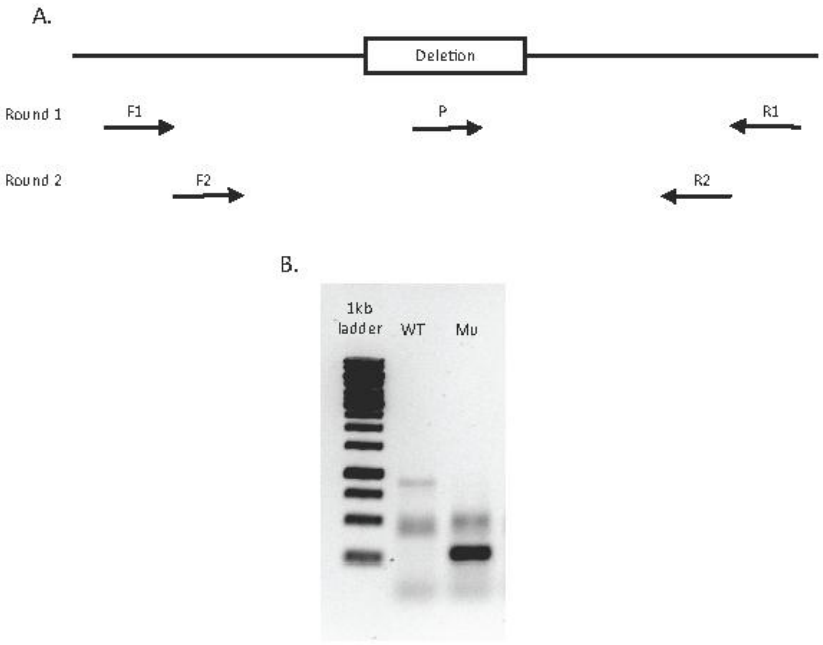

Figure 2.2. PCR to test for somatic deletion of *daf-19* DNA binding domain.

(A) Position of primers used for PCR (arrows). (B) DNA gel after the 2nd round of PCR shows an example of a worm without the deletion (WT) having a ~800bp band, and another worm with the deletion (Mu) having a ~300bp band. Note that the ~500bp bands in both lanes are products of the 1st round of PCR.

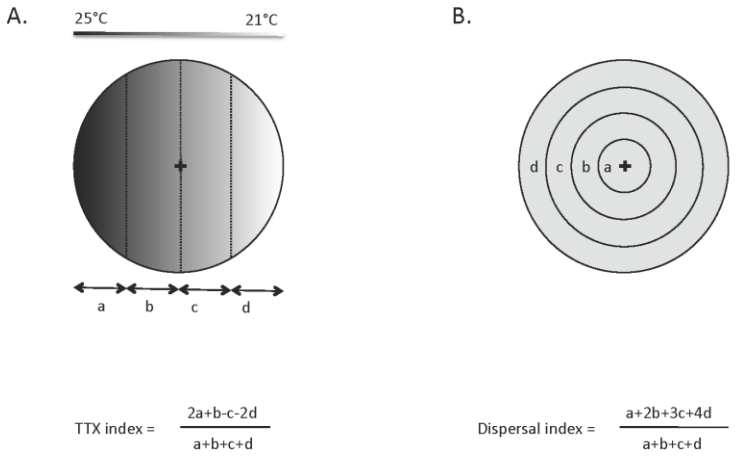

Figure 2.3. Behavioral measurements.

(A) Thermotaxis (TTX) index is measured as the weighted proportion of worms in each temperature zone (a to d) after 30 minutes. (B) Dispersal index is measured as the weighted proportion of worms in each concentric circle (a to d). Crosses represent the initial positions where worms are put at the beginning of each assay.

Chapter 3. Description of the AFD sensory end

3.1. Localization patterns of cGMP signaling proteins

Before this study, there had been few detailed descriptions published about the dendritic end of the AFD neurons, even though these neurons are a well-studied model for learning and memory in *C. elegans* (Kimata et al., 2012). Perkins et al. (1986) gave a brief view of the structure from their TEM studies, with no information regarding proteins functioning in this area. Other studies indicated localization of signaling proteins (Colosimo et al., 2004; Inada et al., 2006), but due to the lack of co-markers, it was difficult to have an organized picture of protein localization in relation to each other. In particular, it was not known which proteins function in the cilium, which proteins in the fingers.

In order to test the role of ciliary proteins in the signaling cascade of AFD neurons, I first set out to investigate the localization of different proteins relative to each other. In this section, I will describe the localization of signaling proteins, in particular those functioning in cGMP cascade, with relation to the fingers and the cilium of AFD neurons. If the AFD cilium functions in temperature sensing, I would predict that signaling components are present in the cilium. The results indicate discrete, differential localization of signaling proteins in and around the AFD cilium, and suggest that the cilium could play a role in this organization.

As a marker for the cilium in AFD neurons, I used the AFD-specific promoter *gcy-8p* to drive a GFP-tagged version of ARL-13, a small GTPase shown to be a ciliary membrane-associated protein (Cevik et al., 2010). In AFD neurons, ARL-13 is localized predominantly to one single projection distal to the many fingers (Figure 3.1), consistent with the location of the cilium observed by TEM at the very distal end of the AFD dendrite (Perkins et al., 1986) (In the following studies, ‘proximal’ and ‘distal’ were used

in relation to the dendrite). Interestingly, less intense ARL-13 signal is also observed in the finger membrane, but is absent in the dendritic membrane. The cilium is often elongated and possesses extra membrane, which is normally seen in transgenic animals overexpressing ARL-13 (Cevik et al., 2010).

Among cGMP signaling proteins tested, the fluorescently tagged versions of the GPCR SRTX-1 and the 3 GC proteins (GCY-8, -18, and -23) under their own promoter are expressed only in AFD neurons, similar to previous reports (Colosimo et al., 2004; Inada et al., 2006). The promoter used for SRTX-1 in this study does not seem to result in expression of this protein in AWC, however. More specifically, the encoded proteins localize exclusively to the finger membrane, but not to the cilium of AFD neurons (Figure 3.1A). The CNG channel subunit TAX-4, however, is present in various ciliated neurons. In AFD neurons, it is found exclusively at the proximal part of the cilium, and not in the fingers (Figure 3.1B). This is consistent with the location of the subunits TAX-2 and TAX-4 at the proximal region of the ciliated AWB and ASK neurons (Mukhopadhyay et al., 2008; Wojtyniak et al., 2013). The fingers, as marked by SRTX-1 and GC proteins, are generally oriented along the anterior-posterior axis, as noted by Perkin et al 1986, the significance of which is currently unclear. However, this orientation is not apparent in every worm, which could be caused by overexpression of membrane proteins in this area, as I noticed the finger membrane seems to be very sensitive to the amount of membrane proteins localized there.

Downstream of CNG channels, various voltage-gated ion channels can help propagate and modulate neuronal activation. *C. elegans* is not known to possess voltage-gated sodium channels, and little is known about voltage-gated calcium channels in sensory neurons. In contrast, EGL-2 is a voltage-gated potassium channel of the ether-a-go-go (EAG) family that has been found to be expressed in various sensory neurons, including AFD (Weinshenker et al., 1999). A dominant mutation in EGL-2 has been found to affect taxis behavior, most likely through its function in sensory processes. Therefore, I investigated the localization of this voltage-gated potassium channel in relation to the AFD dendritic ends. With STRX-1 as the finger marker, an AFD-specific GFP fusion of EGL-2 is found to exclusively localize in a ring-like area, between the finger and dendritic membranes (Figure 3.1C).

The segregation of signaling proteins into different membrane domains seen in AFD neurons is also observed in other ciliary structures, such as the vertebrate olfactory cilia, and the outer segment of mammalian photoreceptors (Section 1.1.2). The localization of the *C. elegans* GPCR and GC proteins on the extensive membrane area of the fingers in AFD neurons may help increase its sensitivity to temperature changes. Indeed, AFD neurons have striking sensitivity to temperature changes (as small as 0.05°C) (Clark et al., 2006). However, the advantage of having the ion channels present only near the cilia but not in the fingers, close to other signaling proteins, is not clear. One possibility is the lipid environment needed for the ion channel function is different from that needed for the thermosensing function. Indeed, in the cilia of *Paramecium tetraurelia*, the calcium channels and guanylyl cyclases were reported to segregate into distinct lipid environments (Thiele et al., 1982). Therefore, I probed the lipid composition of the dendritic endings in AFD neurons using GFP constructs carrying different lipid anchors (Zacharias et al., 2002). Two GFP constructs with saturated fatty acid chains (myristoylated plus palmitoylated, and tandemly palmitoylated) are present throughout the dendritic, finger, and ciliary membranes of the AFD neurons (Figure 3.2). In contrast, geranylgeranylated GFP, which has an unsaturated fatty acid anchor, localizes specifically to the finger compartment (Figure 3.2). This suggests a different lipid composition between the finger compartment and the rest of the membrane at the AFD dendritic end.

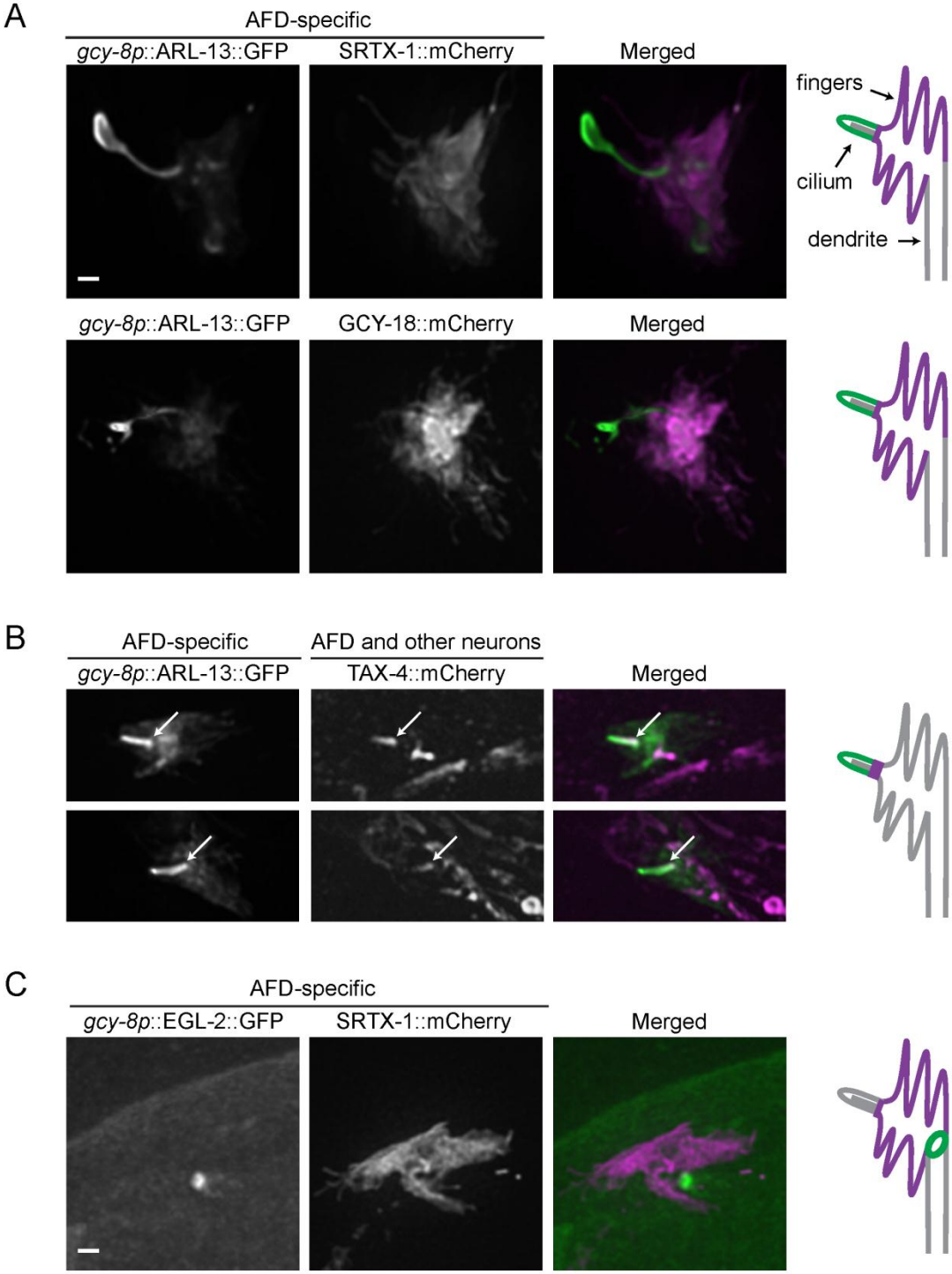
A
AFD-specific
gcy-8p::ARL-13::GFP
SRTX-1::mCherry
Merged
fingers
cilium
dendrite
gcy-8p::ARL-13::GFP
GCY-18::mCherry
Merged
B
AFD-specific
AFD and other neurons
gcy-8p::ARL-13::GFP
TAX-4::mCherry
Merged
C
AFD-specific
gcy-8p::EGL-2::GFP
SRTX-1::mCherry
Merged

Figure 3.1. cGMP signaling components are localized to two distinct compartments in AFD neurons.

(A-B) Fluorescently-tagged membrane proteins in the cGMP signaling pathway are co-expressed with ARL-13, a ciliary membrane marker, driven by an AFD-specific promoter. (A) SRTX-1 and GCY-18 are AFD-specific, and present within the finger membrane but not the cilium. (B) TAX-4 is expressed in many ciliated neurons besides AFD neurons, and localized specifically to the proximal part of the AFD cilium (arrows). Two representative images are shown for TAX-4. (C) EGL-2, an EAG K^+ channel, shows ring-like localization pattern at the base of the finger compartment in AFD neurons, as marked by SRTX-1. Scale bars are 1 μm. Schematics of the two compartments and localization of signaling components are depicted on the right of the panels (only 6 fingers are drawn, there are normally about 60).

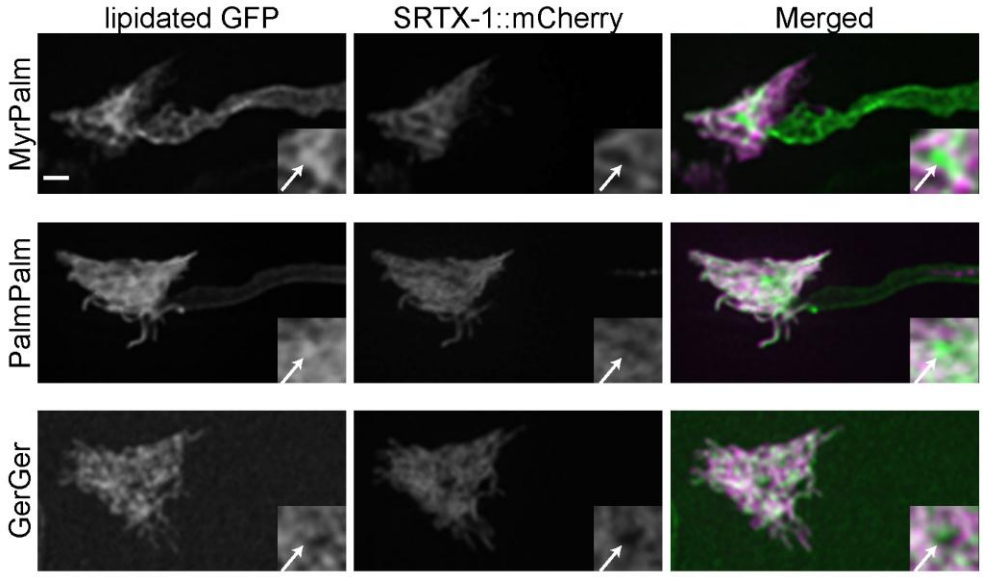

Figure 3.2. Different lipidated GFP constructs localize to different membrane compartments in the AFD neurons.

Acylated GFP (PalmMyr and MyrMyr GFP) is present throughout the dendritic, finger, and possibly ciliary membranes, whereas prenylated GFP (GerGer GFP) is localized specifically to the finger membrane (marked with SRTX-1). Arrows indicate the position of the cilium, as inferred by the lack of SRTX-1 signal. Scale bar is 1 μm.

3.2. Localization patterns of ciliary proteins

The observation that the ciliary membrane marker ARL-13 is also present on the fingers but absent from the dendritic membrane in AFD neurons (Figure 3.1) suggests that the ciliary and finger membranes are distinct from each other but potentially more similar in composition than to the dendritic membrane. To investigate the possibility that the finger membrane may be functionally related to a ciliary compartment, I analyzed the localization of various ciliary proteins in AFD neurons to better define the ciliary structure in these neurons. In these studies, I used fluorescently labeled SRTX-1 as the marker for the finger, and observed the localization patterns of various ciliary proteins driven by an AFD-specific promoter.

I first looked at XBX-1, a dynein motor subunit in IFT present at the base (basal body/transition fibers) and along the length of the axonemes in other neurons with canonical cilia (Schafer et al., 2003; Williams et al., 2011). In AFD neurons, XBX-1 is also localized at the base of the cilium and along the axoneme (Figure 3.3A) as expected, since microtubule tracks can be observed within the short cilium of AFD neurons in TEM (Perkins et al., 1986).

Next I looked at several members of the transition zone (TZ) protein network. NPHP-1, MKSR-2, and MKS-6 can be found at a similar localization, a single dot among the fingers (arrow heads in Figure 3.3), which is presumably the TZ. The fact that this dot (when marked by NPHP-1) is near the base of the cilium (marked by ARL-13) supported the hypothesis that it represents the TZ in AFD neurons (Figure 3.3G). However, to our surprise, MKSR-2 and MKS-6 also display a second localization, as a ring-like structure between the distal end of the dendrite and the finger compartment (Figure 3.3C-D), similar to EGL-2 localization (Figure 3.1C). That MKSR-2 and MKS-6 show a somewhat different localization pattern than NPHP-1 might reflect their involvement in two related but distinct TZ protein modules (MKS and NPHP modules, respectively) (Williams et al., 2011; Sang et al., 2011).

In other neurons, BBS-8 is specifically found at the basal body, where IFT particles dock, and along the ciliary axoneme, in association with moving IFT particles (Deane et al., 2001; Blacque et al., 2004). Surprisingly, BBS-8 is also found at two

different locations in AFD neurons: in the cilium, and in the ring-like pattern at the entrance of the finger compartment (Figure 3.3E). Since the BBSome facilitates the trafficking of ciliary proteins at the base of cilia (Nachury et al., 2007), such a function could be carried out at the ring structure, which is where vesicles likely dock before membrane proteins disperse into the finger compartment, and more distally, the cilium.

To support the hypothesis that the finger compartment represents a cilium-related domain, we localized AFD neuron-expressed TRAM-1a, a membrane protein normally found immediately outside the base of cilia (Bae et al., 2006; Williams et al., 2011). TRAM-1a is also observed as a ring structure just outside of the finger compartment (Figure 3.3F), suggesting that the ring structure at the base of the finger compartment may serve as a barrier between the finger and dendritic membranes in AFD neurons.

Together, the presence of BBS, IFT, and TZ proteins in the distal end of the AFD neuron provides further evidence that this region is a *bona fide* cilium. The presence of a barrier and trafficking hub between the fingers and the dendrite where ciliary proteins are found suggests that the fingers represent a *bona fide* subcompartment of the ciliary membrane in the AFD neurons. This compartment is distinct from the periciliary membrane compartment (PCMC) described recently in *C. elegans* (Kaplan et al., 2012). In fact, several observations support this distinction between the finger compartment in AFD neurons and the PCMC in other neurons (Figure 3.4). Firstly, whereas ARL-13 is consistently present in the finger membrane, even at injection low concentration (Figure 3.1), it does not normally stain the PCMC membrane (Cevik et al., 2010). Secondly, signaling proteins are present specifically in the finger membrane (Figure 3.1) and therefore are likely to function there, but no signaling transduction has been described in PCMC. In particular, the fact that in the *daf-25* mutant, which is defective in cGMP signaling, the guanylyl cyclase DAF-11 is still localized at the PCMC but no longer present in the cilium of amphid neurons (Jensen et al., 2010) suggests that DAF-11 functions in the cilium and not in the PCMC. Lastly, TRAM-1a is found between the finger and dendritic membranes (Figure 3.3F) in AFD neurons, but is normally localized between the ciliary and PCMC membranes (Bae et al., 2006; Williams et al., 2011; Kaplan et al., 2012). Therefore, I propose that the AFD finger compartment is a newly identified ciliary subcompartment.

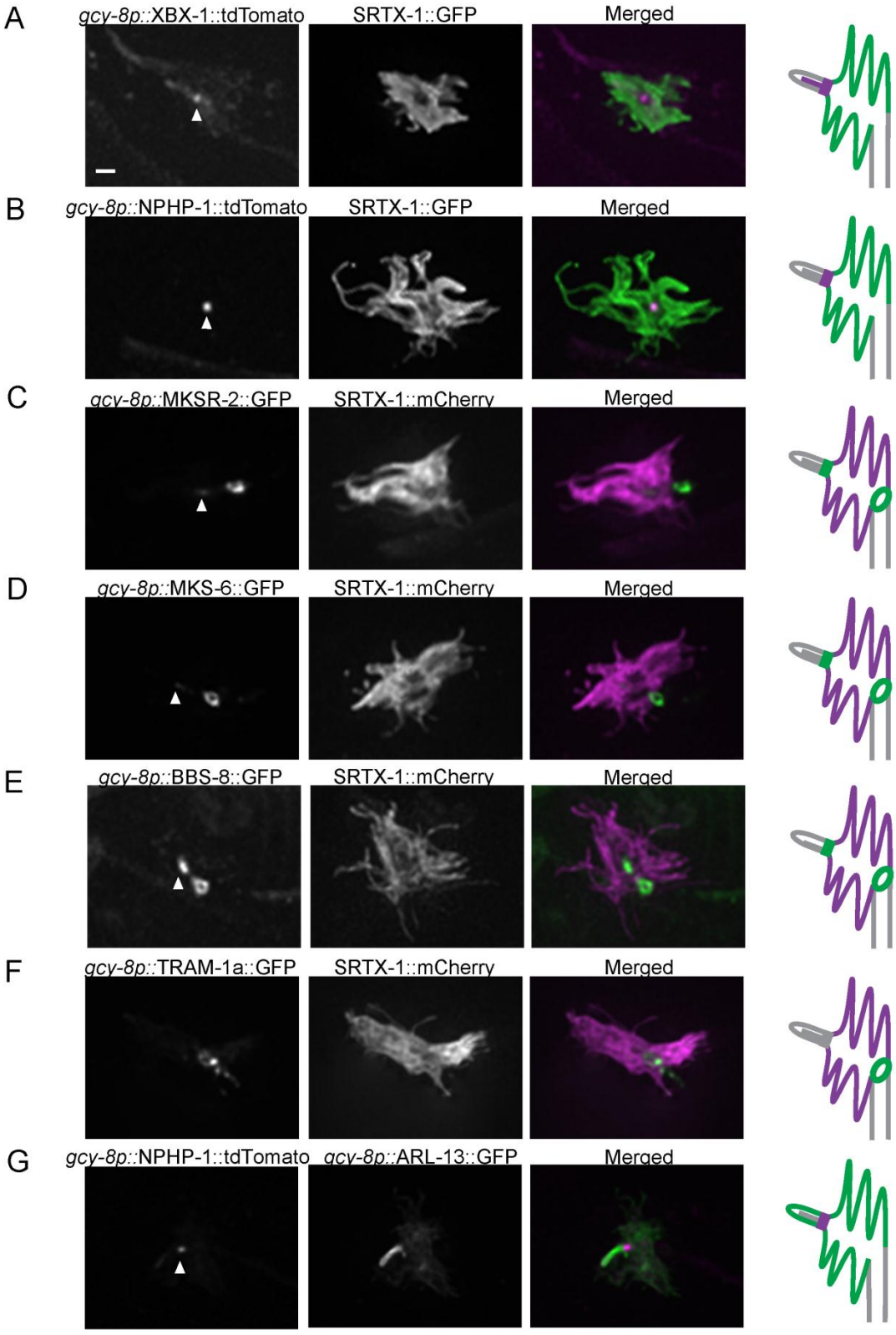
A
gcy-8p::XBX-1::tdTomato
SRTX-1::GFP
Merged
B
gcy-8p::NPHP-1::tdTomato
SRTX-1::GFP
Merged
C
gcy-8p::MKSR-2::GFP
SRTX-1::mCherry
Merged
D
gcy-8p::MKS-6::GFP
SRTX-1::mCherry
Merged
E
gcy-8p::BBS-8::GFP
SRTX-1::mCherry
Merged
F
gcy-8p::TRAM-1a::GFP
SRTX-1::mCherry
Merged
G
gcy-8p::NPHP-1::tdTomato
gcy-8p::ARL-13::GFP
Merged

Figure 3.3. Localization of ciliary and dendritic protein markers uncovers the AFD finger compartment as a *bona fide* ciliary sub-compartment.

Fluorescently-tagged ciliary proteins were produced specifically in the AFD neurons and co-expressed with SRTX-1, a marker of the AFD finger membrane. The IFT-dynein subunit XBX-1 (A) and TZ protein NPHP-1 (B) are enriched at the base of the cilium. The TZ proteins MKSR-2 (C) and MKS-6 (D) are localized at the base of the cilium and are also present as ring structures at a second location, between the finger and dendritic membranes. (E) BBS-8 is also localized at these two different locations. (F) TRAM-1a, which is normally found at the dendritic tips but not inside cilia, is present as a ring outside of the finger compartment in AFD neurons. (G) NPHP-1 localization at the base of the cilium marked by ARL-13 confirms that the puncta (arrowheads) often seen among the fingers are at the position of the canonical transition zone in AFD neurons. Scale bar is 1 μm.

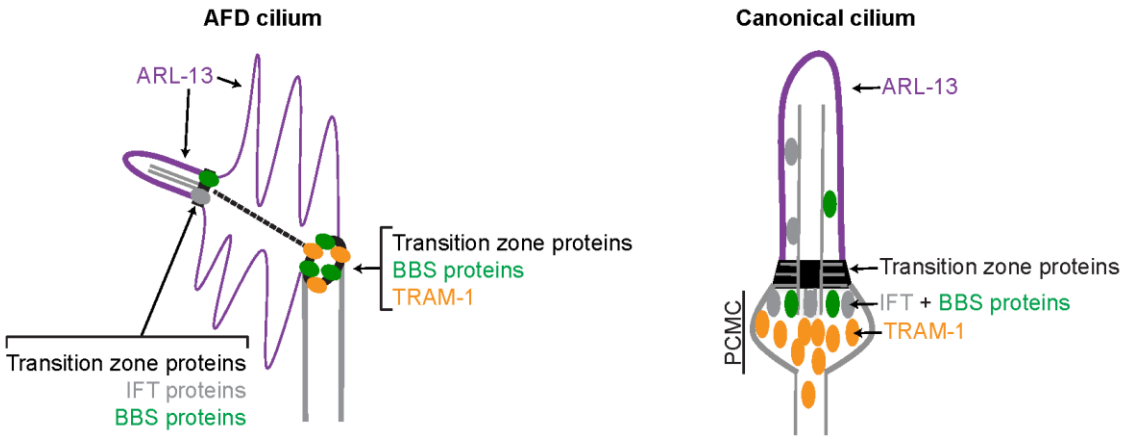

Figure 3.4. AFD sensory end is a special ciliary structure.

In AFD neurons, besides being present in the *bona fide* cilium at the distal part, ciliary proteins are also found at the base of the finger compartment, establishing it as a ciliary subcompartment. Due to its protein composition, it is distinct from the periciliary membrane compartment (PCMC) found in other cilia.

3.3. Development of the two signaling compartments

Having established the spatial relationship between the two presumptive signaling compartments, I was interested to know whether the cilium or the fingers are formed first. The temporal relation between these two compartments could potentially give us insight into how the cGMP signaling cascade is set up in AFD neurons. To investigate the development of these two compartments, fluorescently-tagged SRTX-1 (finger membrane marker), ARL-13 (ciliary membrane marker) and MKS-6 (TZ marker) were followed during embryogenesis. ARL-13 appears early at the site of the developing cilium at the 2-fold stage (Figure 3.5A), consistent with the onset of ciliogenesis (Swoboda et al., 2000). Around this time, MKS-6 signal shows the formation of a TZ as one distinct punctum (Figure 3.5B). When SRTX-1 becomes visible at the early 3-fold stage, it overlaps with ARL-13 in a rod shape and gradually separate, albeit not completely, before any fingers are detectable (Figure 3.5A). In the meantime, a second MKS-6 signal appears at a location posterior to the original TZ, and these two signals move away from each other as the finger compartment grows (Figure 3.5B). Our observations suggest the cilium forms before the fingers, and further support the finding that the two membranes are related. In adult worms, I also observed a relatively constant angle between the cilium and the fingers relative to the dendrite, suggesting a potential role of the cilium in orienting the developing fingers. However, the orientation of the fingers in ciliary mutants has not yet been quantified.

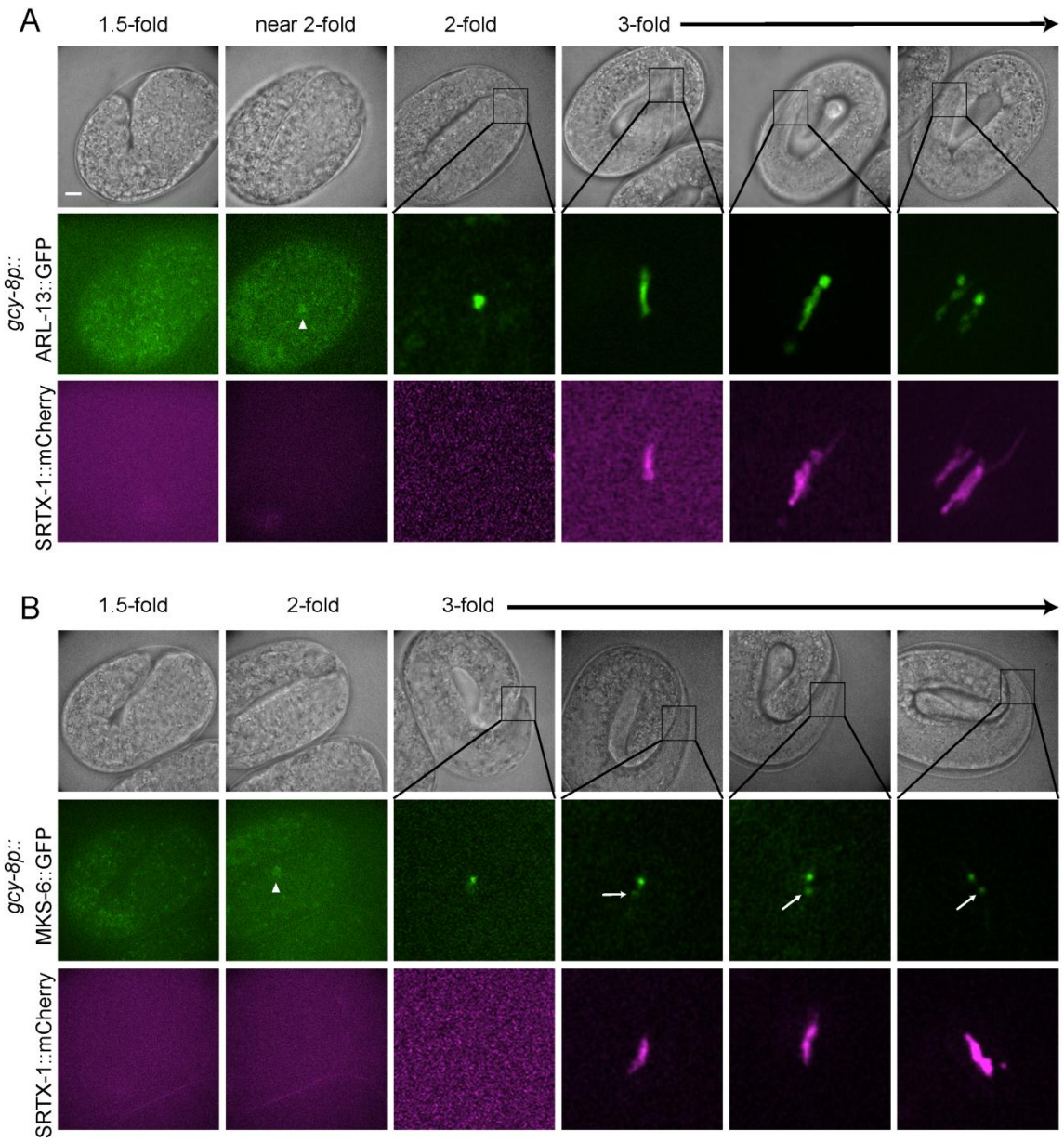

Figure 3.5. Development of the cilium precedes finger formation.

The development of the ciliary and finger compartments in AFD neurons are followed during embryogenesis. (A) Ciliary membrane (marked by ARL-13) appears before the fingers (marked by SRTX-1) are formed. (B) The TZ protein MKS-6 appears first at the base of the cilium, and then at a more posterior second location (arrows), as the finger compartment (marked by SRTX-1) develops. Arrowheads indicate AFD cell bodies. Scale bar is 5 μm.

3.4. Cytoskeletal structures of the finger compartment

How are proteins destined to the cilium transported from the apical junction area across the finger compartment to the ciliary base in AFD neurons? We hypothesized that microtubules might form the cytoskeletal tracks needed for this purpose. To address this, our collaborators carried out TEM tomography of the AFD cilium (Appendix A). To our surprise, no apparent microtubule structures within the finger compartment are visible, but instead structured that resemble intermediate filaments (IFs) are seen running in the middle of the compartment, with occasional vesicles attached. Incidentally, high expression lines or increased exposure of fluorescently tagged MKS-6 also show signals along a filamentous structure that could be the same as the IFs seen in TEM (see Figure 3.7 below). The current tomography data were collected from samples prepared by a high-pressure freezing procedure, so the vesicles observed in these samples were unlikely to be artifacts often associated with chemical fixation methods. Even though no motor molecules have been found to move along IFs, these cytoskeletal tracks have been shown to interact with membrane-bound organelles (Styers et al., 2005), and play an important role in directional mobility of vesicles in astrocytes, independent of their interaction with microtubules (Potokar et al., 2007). Our observations suggest that in AFD neurons, proteins could potentially be transported within vesicles along IFs; the role of IFs could be to render diffusion more efficient by restricting it to one dimension instead of three. High-pressure freezing combined with EM tomography, which tend to preserve intricate structures better than normal chemical fixation procedures, also allowed us to observe actin filaments throughout the compartment, supporting the extensive membranous fingers; this finding establishes them as true microvilli, which was speculated but not demonstrated (Perkins et al., 1986). Microfilaments could be involved in trafficking, or be used to help anchor signaling proteins such as GCs and SRTX-1 within the finger membranes, as seen for Na^+ channels in the node of Ranvier (Kaplan et al., 2001)

3.5. The nature of the ring structure

Because of its potential role in the compartmentalization and trafficking of proteins in the AFD dendritic end, I investigated further the ring-like structure around the base of the finger compartment as observed thus far with several of our tested proteins. To test if this structure is dependent on the ciliary machinery, I looked at MKS-6 signal in the *daf-19* mutant, which lacks the transcription factor required for ciliogenesis, and in the *mks-5* mutant, which lacks a core TZ protein required for proper localization of many TZ proteins (Williams et al., 2011). Even though the MKS-6 signal disappeared from the canonical TZ as expected, the signal at the ring structure is still present (Figure 3.6A). This is consistent with the observation that MKS-5 is not present at the ring (Figure 3.6B). This suggests that the ring structure is independent of DAF-19 and MKS-5.

The ring is located at a distance similar to that between the cilium base and the dendritic tip as estimated through TEM (Perkins et al., 1986) (Figure 3.7). TEM images from previous studies also show that at this distance: (1) there is no cytoplasmic structure reminiscent of the Y-links often seen in normal TZ, suggesting this ring might be only a membrane barrier; (2) dark material at the membrane, typical of apical junctions (belt junctions), is often observed around this area (Perkins et al., 1986). Indeed, AJM-1, an apical junction marker (Köppen et al., 2001), also shows localization with ring-like patterns around the base of amphid cilia (Figure 3.8A). Moreover, when AJM-1 is expressed in AFD neurons, it co-localizes with MKS-6 at the ring structure, but is absent at the canonical TZ (Figure 3.8B). NPHP-1, on the contrary, is only localized at the canonical TZ (Figure 3.8C). The apical junctions are still present at the dendritic ends in the *daf-19* mutant (Perkins et al., 1986), so if the ring structure marked by MKS-6 is the same as the apical junction in AFD neurons, it should still be there in *daf-19* mutants. This is indeed what I found (Figure 3.6A). These data strongly suggest that the ring structure observed with many fluorescent proteins in AFD neurons is a cellular junction.

Interestingly, several TZ proteins have been found at adherens junction in previous studies (NPHP1, NPHP4; Donaldson et al., 2000; Mollet et al., 2005), although their function there remains largely unclear (Figure 3.8D). To test for the function of TZ proteins at the ring, I looked at the localization of signaling proteins as well as of TRAM-

1a in several single and double TZ mutants. Supporting the ciliary gating function of TZ proteins, Williams et al. (2011) showed that TRAM-1a leaked into the cilia of TZ mutants. Similarly, I expected TRAM-1a to leak into, and signaling proteins to leak out of the finger compartment in the AFD neurons of TZ mutants if they indeed function as a gate at the boundary between dendritic and finger membranes. However, these proteins have normal localizations in the mutants tested (Table 3); therefore I have not found any evidence for a functional role of TZ proteins at the ring structure. Further studies looking at triple TZ mutants might give a more complete result as Wojtyniak et al. (2013) have found that the triple mutant *mks-1; mksr-2; mksr-1* showed mislocalized signaling proteins in a subset of AWB neurons. Alternatively, I speculate that in AFD neurons, the belt junction is only the docking site for some TZ proteins before being transported to the cilium to function there. The fact that MKS-5 and NPHP-1 are not seen at the ring implies that: (1) they are only needed in a small amount; and/or (2) they are more stable and do not need to be constantly supplied/renewed at the TZ. However, the pool of BBS-8 found at the ring might have some function there (see Chapter 4).

Table 3. Localization of signaling proteins in transition zone mutants

	mksr-2	*mks-6*	*mks-6; mksr-2*	*mksr-2; nphp-4*
GCY-18::GFP	Normal	Not done	Normal	Normal
SRTX-1::GFP	Not done	Normal	Normal	Not done
TRAM-1a::GFP	Normal	Not done	Not done	Normal

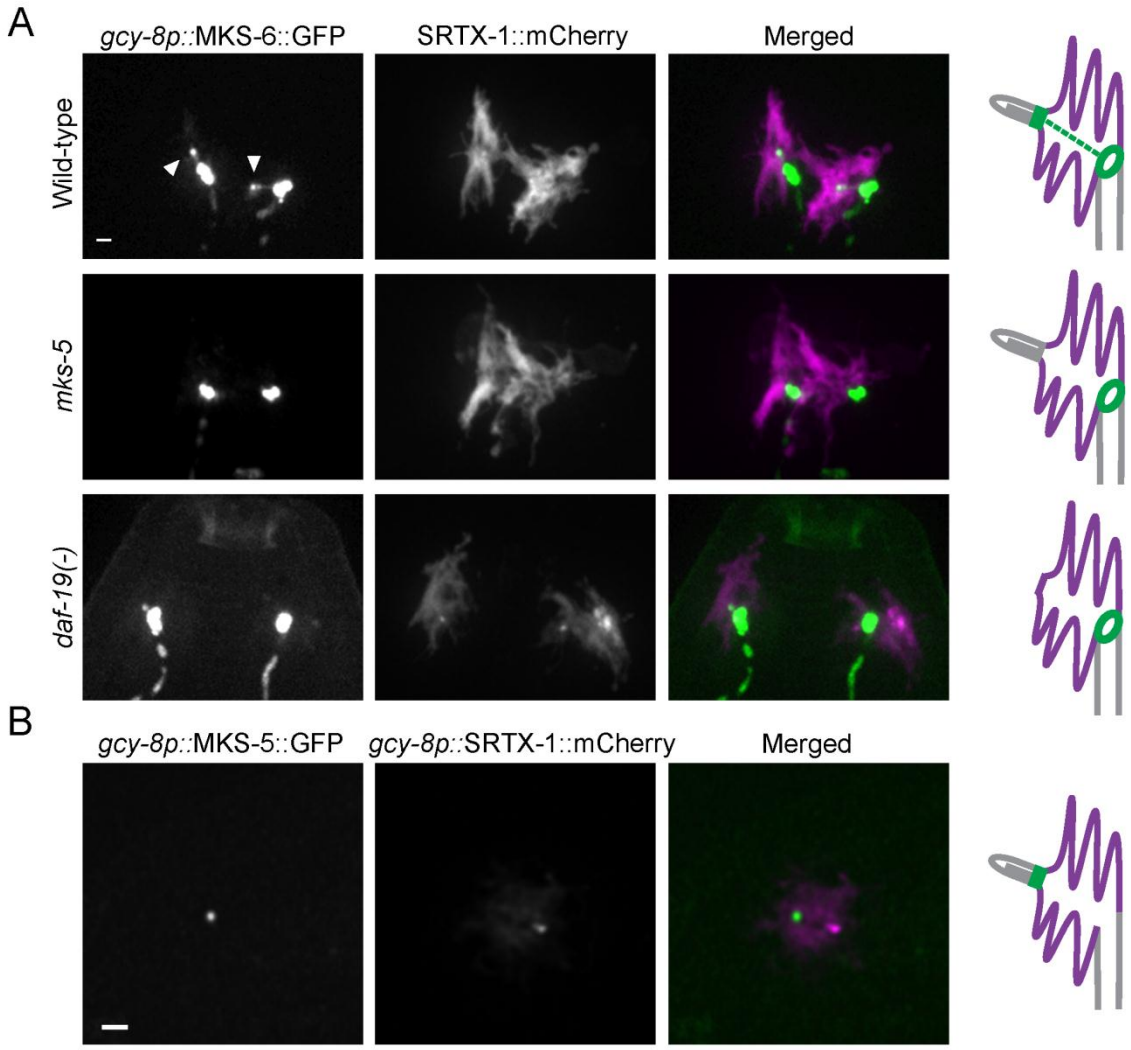

Figure 3.6. The ring structure is independent of ciliary proteins DAF-19 and MKS-5.

(A) The ring structure at the base of the finger compartment is still present in mutants lacking the ciliary transcription factor DAF-19 or the essential TZ protein MKS-5. Two neurons are shown for each worm. GFP signals are overexposed to highlight the complete absence of the canonical TZ in the mutants (arrowheads in wild-type). Overexposure also shows a filamentous structure decorated with MKS-6 that could be intermediate filaments in wild-type worms. (B) In wild-type worms, MKS-5 is present only at the canonical TZ and not at the ring structure. Scale bars are 1 μm.

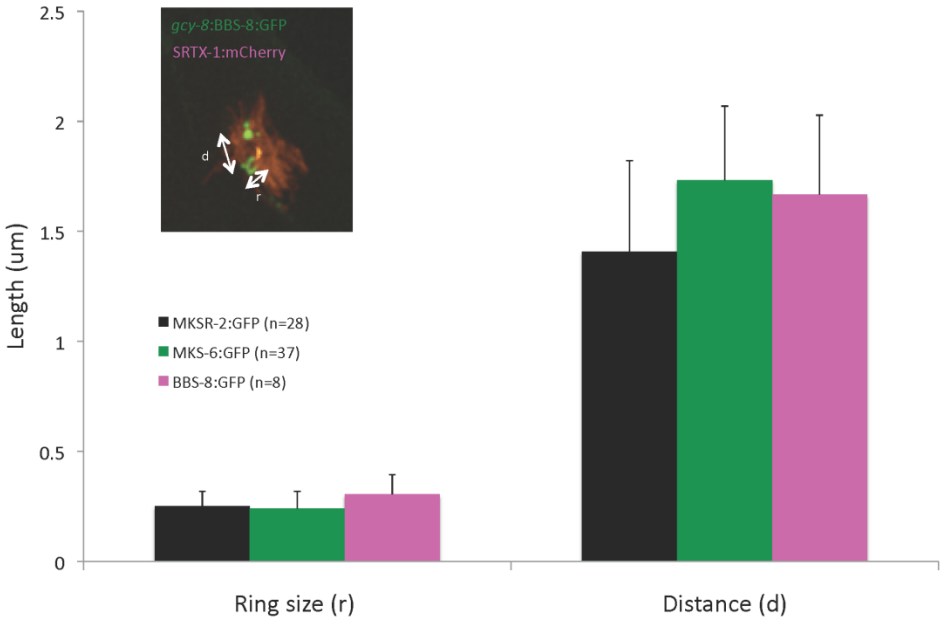

Figure 3.7. Dimensions of the ring structure.

The inner diameter of the ring (r) and the distance between the ring and the canonical TZ (d) are consistent among three different markers. A representative image is shown to indicate the dimensions being measured in 3D. Because the size of the ring (r) is under light microscopy resolution limit, accurate measurements of this feature cannot be done with the current method.

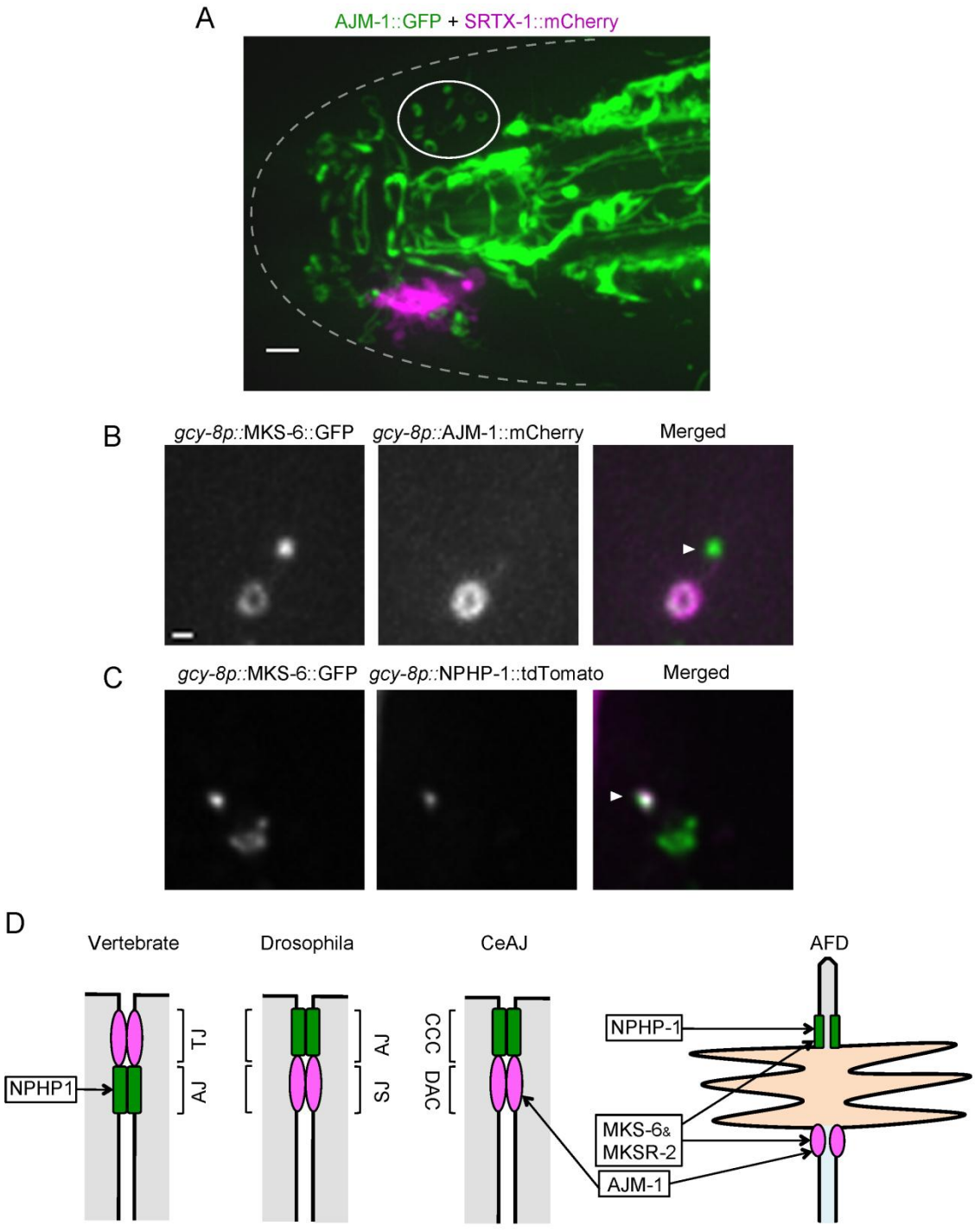
A
AJM-1::GFP + SRTX-1::mCherry
B
gcy-8p::MKS-6::GFP
gcy-8p::AJM-1::mCherry
Merged
C
gcy-8p::MKS-6::GFP
gcy-8p::NPHP-1::tdTomato
Merged
D
Vertebrate
Drosophila
CeAJ
AFD
NPHP1
TJ
AJ
SJ
CCC
DAC
NPHP-1
MKS-6&
MKSR-2
AJM-1

Figure 3.8. The ring structure is an apical junction.

(A) In the head, apical junctions (marked by AJM-1) are seen as ring-like structures at the base of cilia in the bilateral amphid channels (one side is circled). The position of the amphid channels can be inferred from the signal of the AFD finger marker SRTX-1. Scale bar is 2 μm. (B) AJM-1 is co-localized with MKS-6 at the ring. Note the absence of AJM-1 at the canonical TZ (arrowhead). Scale bar is 0.5 μm. (C) MKS-6, a MKS module protein, and NPHP-1, a NPHP module protein, co-localize at the canonical TZ (arrowhead), but not at the ring structure. (D) A comparison of protein composition of adhesion complexes in vertebrates, Drosophila, *C. elegans* epithelia and AFD neurons suggests a functional difference between MKS and NPHP modules. CeAJ - *C. elegans* apical junction, AJ - adherens junction, TJ - tight junction, SJ - septate junction, CCC - cadherin-catenin complex, DAG – DLG-1/AM-1 complex. The drawings of complexes in epithelial cells are based on WormBook (http://www.wormbook.org/).

3.6. Discussion

The functions of the two signaling compartments

In AFD sensory endings, the cGMP signaling components are segregated into two nearby but distinct compartments, i.e. TAX-4 in the cilium, and SRTX-1 and GCs in the finger membrane (Figure 3.1). The thermosensor molecule has not been identified for AFD neurons, but is likely present in the finger membrane too. Besides an extensive membrane structure, this compartment also seems to have a distinct lipid composition, which is preferentially labeled by unsaturated lipids (Figure 3.2). Both features likely contribute to the temperature sensing function of AFD neurons. As mentioned previously, sensory cells often have specialized structures with a high surface-to-volume ratio designed to maximize their sensitivity, either by increasing the sensory surface or by increasing the speed of transduction. The function of this special membrane composition for temperature sensing is not clear, as the identity and the mode of action of the thermosensor molecule are still unknown, but it is likely to be relevant to the function of the sensor. In phototransduction, rhodopsin has lipid anchors (Ovchinnikov et al., 1988), and is sensitive to its lipid environment (reviewed in Brown., 1997). Moreover, the outer segment of photoreceptors is rich in unsaturated lipids (Boesze-Battaglia and Schimmel, 1997), and this is thought to allow the fast diffusion rate of rhodopsin, contributing to the high speed of the phototransduction process. Similarly, the unsaturated lipids in the AFD finger membrane could allow the thermosensory molecules to be more mobile and increase the signaling process. This high fluidity lipid composition, however, might not be compatible for the function of the CNG channel. It has been shown that the composition of the lipid bilayer has significant effects on the function of various ion channels (Schmidt et al., 2006; daCosta and Baenziger, 2009). In particular, the functions of ciliary channels have been shown to require a membrane rich in sphingolipids, which are saturated fatty acids (Forte et al 1981). Therefore, a requirement for different lipid compositions could be one of the reasons why TAX-4 is localized in a separate compartment from the rest of the signaling machinery.

Another possibility for the localization of CNG channels only at the ciliary base in AFD neurons is the need to sequester or concentrate Ca^{2+} into the ciliary lumen for regulatory purposes. Consistent with this hypothesis, recent studies have shown that the

ciliary lumen is a compartment with high Ca^{2+} concentration compared to the cytoplasm (Jin et al., 2013; Collingridge et al., 2013; Delling et al., 2013). In the AFD cilium, the initial calcium signal generated by the CNG channel in the cilium would be sequestered within a relatively small space compared to the finger space, where it can act on the CNG channel to allow effective short-term adaptation to the thermal stimuli. In mammalian olfactory neurons and photoreceptors, CNG channels bind to Ca2+-calmodulin to modulate adaptation (Hsu and Molday, 1993; Chen et al., 1994; Chen and Yau, 1994). Even though regulation by Ca^{2+} has not been demonstrated directly for the TAX-2/TAX-4 channel in *C. elegans*, TAX-4 has a potential phosphorylation site by CaMKII in the cytoplasmic domain (Komatsu et al, 1999), and therefore can potentially be regulated by Ca^{2+} indirectly. CNG channels are also partially blocked by divalent cations, so TAX-2/TAX-4 channels could also be regulated by Ca^{2+} directly (Komatsu et al, 1999). AFD neurons have been shown to have fast adaptation, allowing it to react to quick temperature change as the worm is moving along the temperature gradient. This high temporal resolution also contributes to the high sensitivity of AFD neurons to temperature changes.

Furthermore, this sequestration of Ca^{2+} would could mean that there are cilium-specific localization of Ca^{2+}-regulated proteins in AFD neurons. To test this hypothesis, I started to look at the localization of various Ca^{2+}-regulated signaling proteins known to function in AFD neurons (TTX-4, TAX-6, CMK-1, UNC-43, NCS-1) in relation to SRTX-1. A fluorescent signal in any projection not marked by SRTX-1 is likely to be ciliary localization. So far I have not identified any Ca^{2+}-regulated protein that is exclusive to the cilium, which would first suggest that ciliary localization of these proteins might be transient. More likely, however, overexpression of soluble proteins could override any potential accumulation of such proteins in the cilioplasm. Single-copy insertion of GFP constructs together with high-resolution microscopy might be a better method of addressing this issue. Alternatively, even if signaling regulatory proteins are present throughout different cellular compartments, they are activated only locally by nearby flux of Ca^{2+}, which is known as 'Ca^{2+} micro-domains'. Another explanation is that Ca^{2+} could regulate signaling indirectly by modulating ciliary processes. Indeed, during the course of this study, several laboratories have published evidence for the role of Ca^{2+} entering through several ciliary-specific ion channels to regulate IFT, thereby affecting ciliary

signaling (Jin et al., 2013; Collingridge et al., 2013; Su et al., 2013; Delling et al., 2013; DeCaen et al., 2013). In these cases, IFT proteins are the effector molecules of Ca^{2+} themselves.

Lastly, a third possibility that could result in CNG localization away from the fingers is the energy cost of chemical signaling compared to that of electrical signaling in neurons. In general, electrical signaling is fast but of high cost, due to the energy consumption of various ion pumps used to regulate membrane potential; in contrast, chemical signaling is slower but also consumes less energy through enzymatic reactions (Niven and Laughlin, 2008; Okawa et al., 2008). Thermotaxis is a slow, sustained behavior, compared to reflexes such as avoidance behaviors; therefore AFD function does not require a fast, expensive signaling cascade. This would require the CNG channels to be away from the fingers, where the thermosensors are most likely to be present. This means it is the second messenger cGMP that is the summation signal of the temperature sensed by various receptors. This arrangement is in contrast to the case in which CNG channels are localized throughout the finger membrane, next to the thermosensors, as would be expected if the cations are the summation signal from these receptors (Figure 3.9). At this moment, I have not done any experiment to test this hypothesis. However, it is of note that in neurons mediating avoidance behaviors, which require fast reactions, such as in ASH, PVD or touch receptor neurons, direct electrical signaling through ionotropic receptors such as TRP channels is more likely to be used instead of chemical signaling through metabotropic receptors such as GPCRs cGMP/CNG channels (Tobin et al., 2002; Johnson and Leroux, 2010). One way of testing this is to mislocalize the CNG channel to the finger membrane, or the GC to the cilium, and measure the current compared to the normal localization. However, since the membrane composition might have an effect on CNG function, it would first require the identification of a version of CNG channels that is functional in the finger membrane environment. Moreover, the localization signals on these proteins are currently not known, so this might involve looking for specific factors required for their proper localization first.

EAG channel localization

The localization of a voltage-gated EAG channel at the ring structure is of interest. This is in close proximity to the cGMP signaling compartment and just before the electrical signal propagates down the dendrite, thus the EGL-2 channel could be regulated by cGMP signaling directly or indirectly to help set the excitability of AFD neurons for optimal thermotaxis. Interestingly, EAG channels are closely related to CNG channels and possess a cGMP-binding domain, though it has not been shown that cGMP can directly regulate these channels (Christie, 1995; Dubin et al., 1998). In any case, the unique localization of EGL-2 suggests that it could be a potential point of integration for past experiences that leads to the memory found in AFD (Engel and Wu, 1998; Clark et al., 2006).

The development of the compartments

The developmental sequence of the two compartments suggests that the cilium may play a role in orienting the finger growth. The cilium forms first, followed by finger growths, and this results in a relatively fixed orientation between the dendrite, the microvillar fingers, and the axis between the ciliary base and the apical junction. This is reminiscent of the situation in hair cells, where the kinocilium plays a role in orienting the growth of the microvillar stereocilia through Wnt/PCP signaling. The growth and orientation of AFD sensory structures can be looked at in some ciliary and PCP mutants to test this hypothesis. In particular, the *nphp-2* mutant would be of particular interest, as its protein product, Inversin, has a central role in PCP signaling through cilia, and NPHP-2 has a role in positioning the cilia in other neurons (Warburton-Pitt et al., 2012)

The apical junction structure

The observation that MKS-6 and MKSR-2 have different localization patterns compared to NPHP-1 may reflect a functional difference between NPHP and MKS modules at cellular junctions in AFD neurons (Figure 3.8D). As mentioned above, NPHP1 and NPHP4 have been found at adherens junction in mammalian cells (Donaldson et al., 2000; Mollet et al., 2005), and their *C. elegans* homologs stain both the TZ and the basal body of the cilium (Williams et al., 2011). Adherens junctions function in cell-cell adhesion, and are composed of E-cadherin and b-catenin, which, in

C. elegans epithelia, form the cadherin-catenin complex (CCC) (Costa et al., 1998). CCC is localized to the apical junctions, which are a special type of cell junctions found in *C. elegans* through TEM (McMahon et al., 2001). Also present at the apical junctions, and basal to the CCC, is the DLG-1/AJM-1 complex (DAC). DAC has been shown to have distinct composition and some non-redundant function from CCC. Besides functioning with CCC in cell-cell adhesion, the DAC is thought to also act as the paracellular gate, regulating ion flow between apical and basal sides of epithelia (Köppen et al., 2001; Asano et al., 2003). In other organisms this is the function of tight junctions or septate junctions. In ciliated neurons of *C. elegans*, cellular junctions are found in the form of belt junctions (Perkins et al., 1986), which my data suggest to contain AJM-1 proteins, and therefore indicating that they are apical junctions. However, belt junctions might be a special type of apical junctions, since I did not observe GFP signal in the amphid of worms with an integrated *dlg-1::gfp* construct (data not shown). Nevertheless, there seems to be an association between the NPHP module and CCC, and of the MKS module with DAC in *C. elegans* ciliated neurons, pointing to the common function of TZ and apical junctions as cellular gates. In AFD neurons, these distinct modules are easily observed due to the special separation between the TZ and the apical junction by the finger compartment (Figure 3.8). Interestingly, associated with both CCC and DAC are 4-pass membrane proteins of the Claudin family needed for localization of apical junction components and often associated with paracellular barrier function (reviewed in Simske and Hardin, 2011). In ciliary TZ, there have been several 4-pass membrane proteins identified so far with unknown mechanism of function (Szymanska and Johnson, 2012). It would be interesting to investigate the localization of CCC components such as HMR-1 and HMP-1 in ciliated neurons, as well as the equivalence between TMEM proteins and Claudin in gating function at ciliary TZ.

In mammalian cells, septins are thought to form a diffusion barrier at the base of the cilium, in the form of a ring structure. Therefore, it was hypothesized that septins may also present at the ring structure at the base of the finger compartment in AFD neurons. However, preliminary data showed that GFP constructs of septin homologs in *C. elegans*, UNC-59 and UNC-61, are localized diffusely throughout this cell. Moreover, a ciliary phenotype was not observed for *unc-59* and *unc-61* mutants in terms of signaling protein localization in other ciliated neurons in worms (Wojtyniak et al., 2013).

Therefore, it is currently unclear if septins play a role in protein localization in *C. elegans* cilia.In conclusion, the data in this chapter showed that cGMP signaling proteins are localized within the ciliary structure of AFD neurons.

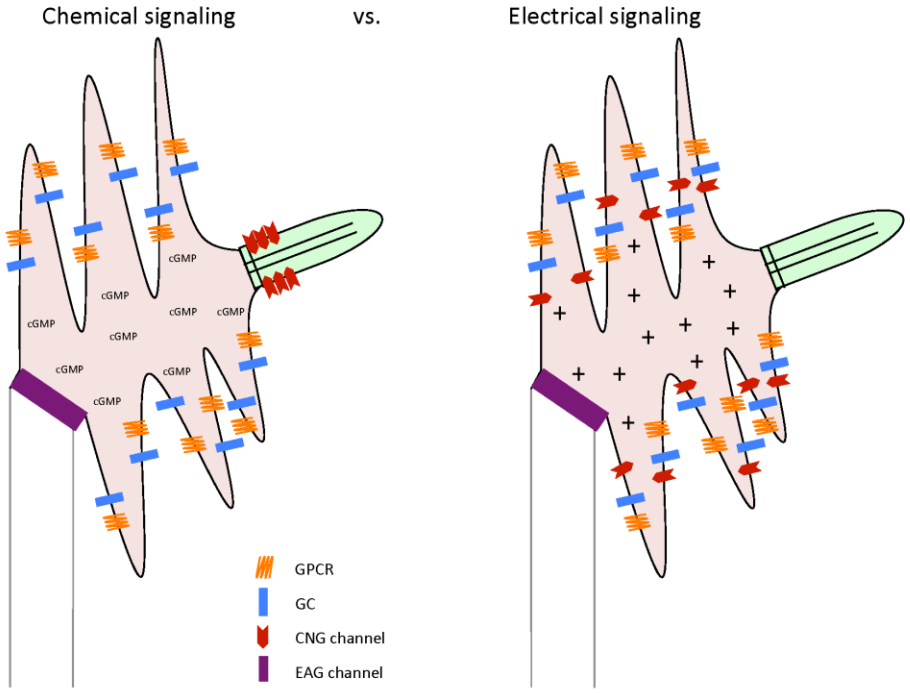

Figure 3.9. CNG channel localization can have an effect on the type of summation signals used in AFD sensory end.

In chemical signaling, cGMP is the second messenger, which needs to reach a certain threshold to activate CNG channels located away from the thermal sensors. In electrical signaling, each thermal sensor activates a nearby CNG channel, and the level of cations reaching voltage-gated ion channels determines whether neuronal activation will happen.

Chapter 4. The role of ciliary proteins in the localization of cGMP signaling in the AFD neurons

Given the close spatial relationship between cGMP signaling proteins and ciliary proteins at the AFD dendritic ends, I tested for the role of ciliary proteins in cGMP signaling by first looking at the signaling protein localization in various ciliary mutants. I focused on signaling proteins localized to specific regions in/around the cilium, i.e. SRTX-1, GCY-8,-18,-23, and TAX-4, since their specific targeting would more likely require ciliary proteins.

4.1. Guanylyl cyclase localization

In the *daf-25* mutant

I first examined the *daf-25* mutant, in which other cilia have recently been shown to lack the membrane GCs DAF-11 and GCY-12, but the mechanism of DAF-25 function is not clear (Jensen et al., 2010; Fujiwara et al., 2010). In *daf-25(-)* worms, the three AFD-specific GC's (GCY-8, -18, and -23) are 100% absent from the AFD fingers, and in certain worms these proteins could be seen along the dendrite instead (Figure 4.1A). Using SRTX-1 as the finger marker, I observed a variety of defects in this structure: 35% have no signal in fingers, 55% have stunted fingers, and 10% have long, protruding fingers (Figure 4.1B).

Consistent with these observations of abnormal AFD fingers, my TEM data reveal that in the *daf-25* mutant AFD dendritic ends have few, if any, fingers, which are also unorganized, compared to ~30 fingers seen running parallel to each other in wild-type worms (Figure 4.1C). Other cilia in the amphid neurons of *daf-25* mutant worms are superficially normal, similar to findings by Jensen et al. (2010). Since GCs are completely absent from 100% of *daf-25* worms early on during development, whereas the fingers are still present in most adult worms, albeit abnormal, I believe that the

abnormal finger phenotype is not the cause for the absence of GCs in these animals. These data suggest that DAF-25 plays a role in not only the trafficking of GCs but also the morphogenesis of a specialized sensory compartment. Given that the mammalian ortholog (Ankmy2) binds the photoreceptor guanylyl cyclase GC1 (Jensen et al., 2010), it may play a role in the formation/function of ciliary photoreceptor development, function and degeneration.

Since GCs are observed along the dendrite but not in the fingers of *daf-25* worms, I wondered about the integrity of the ring structure that separates the two membranes in this strain. I found that in the *daf-25* mutant, MKS-6 signal is markedly reduced or completely absent from the ring structure, and increased along the filamentous structure between the ring and the canonical TZ (Figure 4.1D). Even though TEM showed superficially normal apical junctions in all amphid cilia of *daf-25(-)* worms, my observations suggest the integrity of this barrier is compromised in the AFD neurons of this strain, resulting in some protein (MKS-6) leaking out of the docking zone while others (GC's) being prevented from entering the finger compartment.

Interestingly, I noticed that MKS-6 signal at the TZ seems to be expanding in the *daf-25* mutant, compared to wild-type worms (Figure 4.1D). The daf-25 mutation also showed similar effect on the NPHP-1 signal (Figure 4.1E). This expansion of TZ markers is reminiscent of the defects seen in TZ mutants, where signal sometimes can be seen to separate into two dots (Chunmei Li, personal communication). However, other cilia in the *daf-25* mutant show normal TZ protein localization (Chunmei Li, personal communication), and their TZ are superficially intact through TEM (Jensen et al., 2010). Therefore, DAF-25 might not function as a typical TZ protein, and the TZ defects in AFD could be secondary to defects in protein trafficking to the cilium through the ring-like gate.

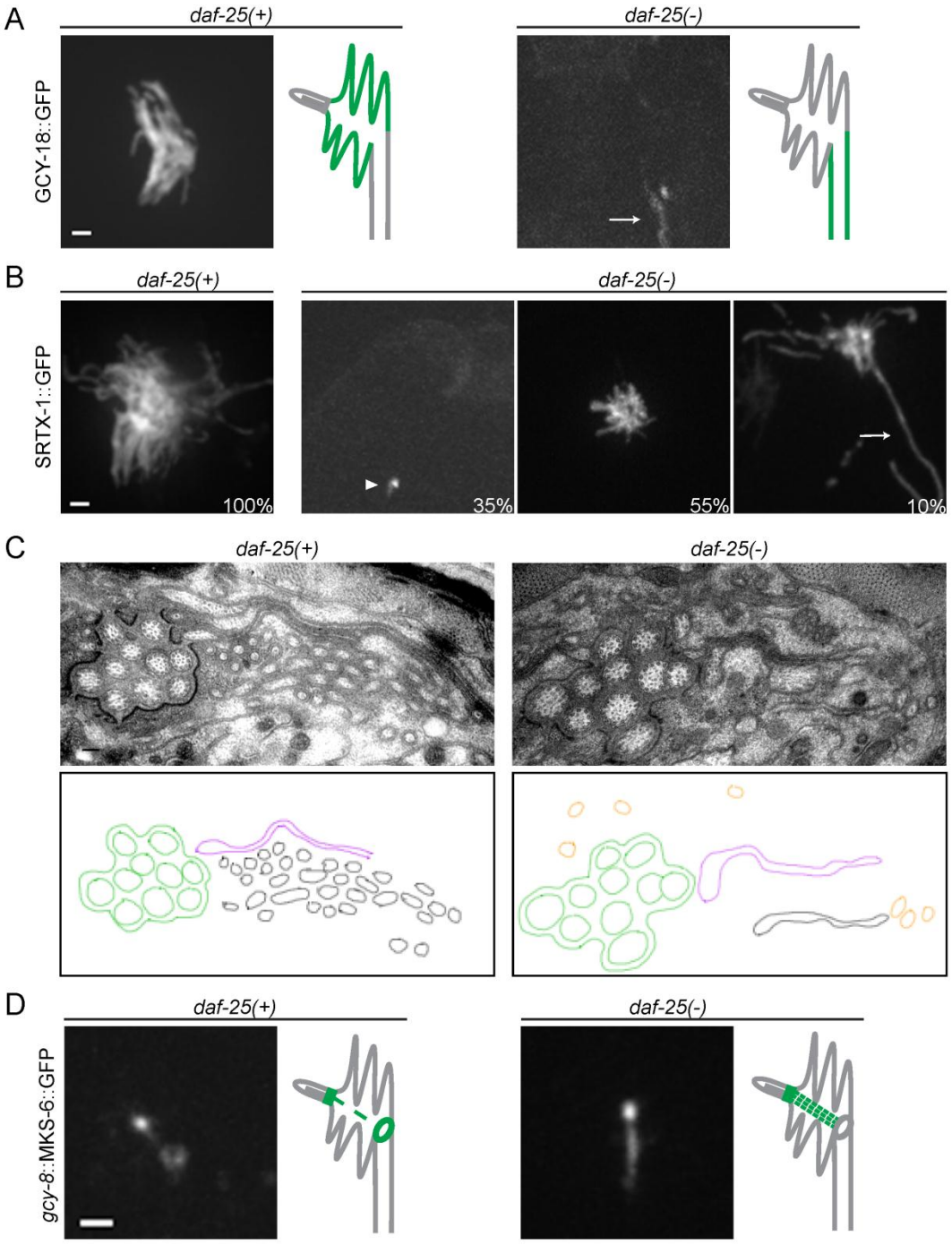
A
daf-25(+)
daf-25(-)
GCY-18::GFP
B
daf-25(+)
daf-25(-)
SRTX-1::GFP
100%
35%
55%
10%
C
daf-25(+)
daf-25(-)
D
daf-25(+)
daf-25(-)
gcy-8::MKS-6::GFP

Figure 4.1. The *daf-25* mutant shows various defects at the AFD sensory end.

(A) Localization of GCs in wild-type and *daf-25(-)* worms. GCs, represented here by GCY-18, are absent from AFD fingers of the *daf-25* mutant, and are seen along the dendrite (arrow) instead. Scale bar is 1 μm. (B) *daf-25(-)* worms show various defects in finger formation compared to wild-type worms. The numbers are the percentages of worms with each phenotype (n=100). The arrowhead indicates a complete absence of fingers, and the arrow points to an extra-long finger. Scale bar is 1 μm. (C) TEM data support the finding of abnormal finger formation in *daf-25* worms. About 30 fingers (illustrated in black) can be seen in wild-type worms, whereas in *daf-25* worms they cannot be distinguished as easily. Double-membrane structures seen in mutant worms (orange) could be part of AWA cilia, due to the presence of microtubules in the middle, and their location relative to the amphid bundle (green) and the AWC wing structure (magenta). Scale bar is 200 nm. (D) The TZ protein MKS-6 displays an altered localization in *daf-25* worms, as it is no longer seen at the ring structure but appears stronger at the filamentous structure connecting the cilium and the ring structure. Scale bar is 1 μm. (E) In *daf-*25 worms, NPHP-1 signal at the canonical TZ is longer than in wild-type worms. An increased signal length can also be seen for MKS-6 in *daf-25(-)* (D) but is less obvious. Signals from two neurons of the same worm are shown for each genotype. Scale bar is 1 μm.

In the *bbs-8* mutant

I also examined mutations in BBS-8, given its presence at both locations relevant to cGMP signaling protein localization, namely at the base of the cilium, which harbors the cGMP-gated channel TAX-4, and at the ring structure at the entrance of the finger/villi compartment, where the GPCR SRTX-1 and the GCs are found. Among all of the cGMP signaling components tested (SRTX-1, GCY-8/18/23, TAX-2/4, TTX-4, and TAX-6), the *bbs-8* mutant shows abnormalities specifically in the localization of the 3 GC proteins (26%, 46%, and 30% abnormal for GCY-8, 18, and -23, respectively) (Figure 4.2A, C). Whereas wild-type worms show GC localization only in the finger compartment, *bbs-8* worms also have GCs sometimes present along the dendrite, and variable, strong accumulation in the fingers. This is not caused by a general increased expression of GCs in the AFD neurons of the *bbs-8* mutant (as quantified with the *gcy-8p::GFP* construct using Volocity, data not shown). Importantly, I confirmed this phenotype in a separate *bbs* mutant, *bbs-7* (Figure 4.2B), providing evidence that the overall function of the BBSome is important for GC localization in AFD neurons. Also significant is the fact that the phenotype is not observed in two IFT mutants tested, namely *osm-5*, which disrupts anterograde IFT, and *che-11*, which abrogates retrograde transport (Figure 4.2B). This suggests that BBS proteins might act in an IFT-independent manner to facilitate GC protein localization to the finger compartment, which is consistent with the fact that no microtubule or IFT is observed in this compartment.

In Chlamydomonas, *bbs* mutants accumulate signaling proteins in their motile cilia, and possess a phototaxis phenotype (Lechtreck et al., 2009). Lack of BBS proteins also leads to accumulation of the dopamine receptor D1 in cilia of mouse brains (Domire et al., 2011). The accumulations of signaling proteins in Chlamydomonas mutants were explained by the function of BBS proteins in exporting signaling proteins from the flagella via IFT, since mutants of retrograde IFT also showed this phenotype. However, I do not think this is the case for BBS-8 function in AFD neurons, since no IFT is observed in the fingers and IFT proteins are not seen at the ring structure; furthermore, the retrograde IFT mutant *che-11* does not show severe mislocalization like bbs mutants (9% in *che-11* vs. 35% and 31% in *bbs-8* and *bbs-7*, respectively) (Figure 4.2B). Disruption of BBS proteins have been reported to result in mislocalization of GPCRs, such as MCHR1, SSTR3, and D1 (Berbari et al., 2008b; Domire et al., 2011), but this is the first time BBS

is reported to be involved specifically in the trafficking of GCs, a central and upstream component of cGMP signaling.

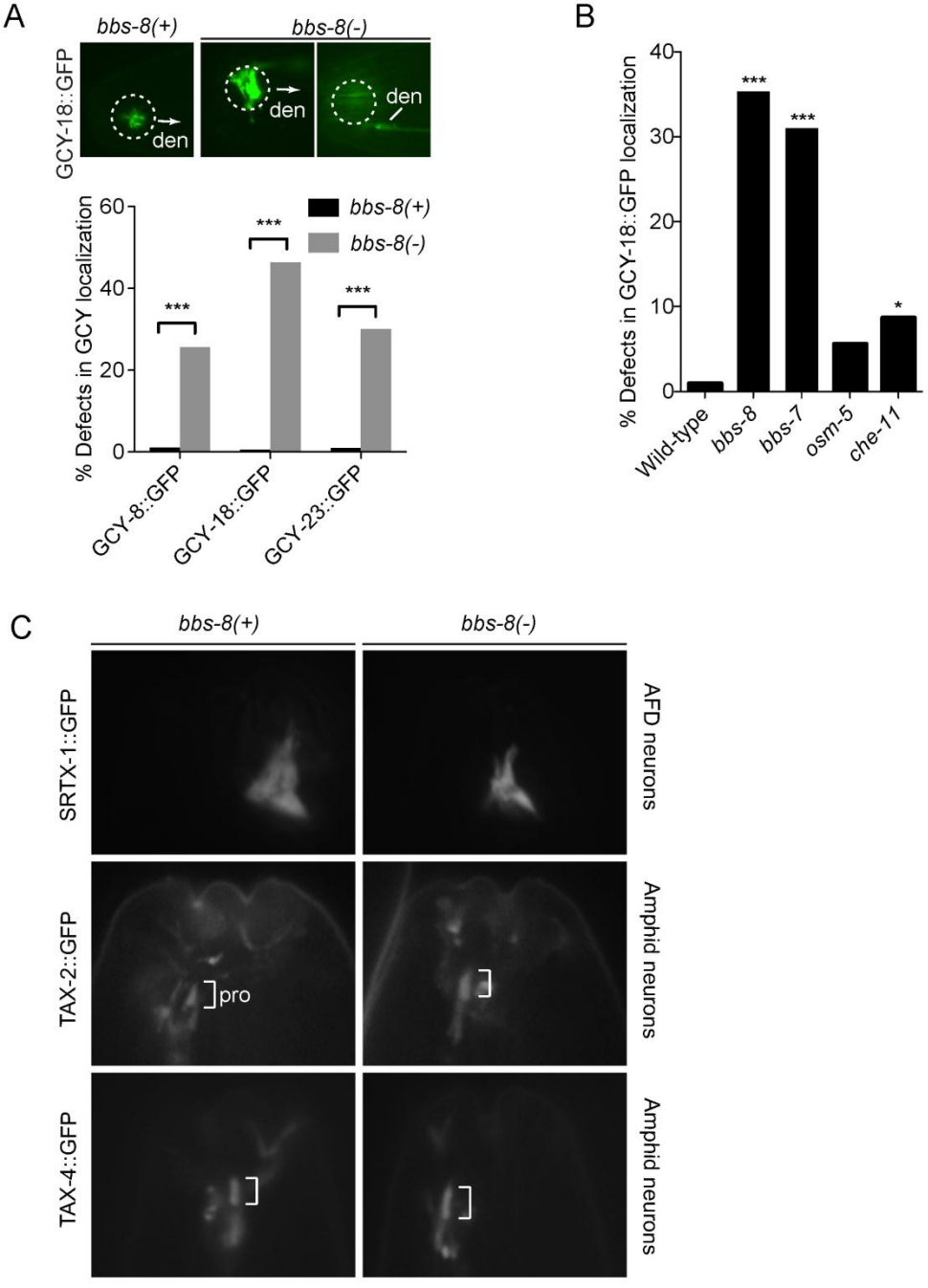
A
bbs-8(+)
bbs-8(-)
GCY-18::GFP
den
den
den
% Defects in GCY localization
bbs-8(+)
bbs-8(-)
GCY-8::GFP
GCY-18::GFP
GCY-23::GFP
B
% Defects in GCY-18::GFP localization
Wild-type
bbs-8
bbs-7
osm-5
che-11
C
bbs-8(+)
bbs-8(-)
SRTX-1::GFP
AFD neurons
TAX-2::GFP
pro
Amphid neurons
TAX-4::GFP
Amphid neurons

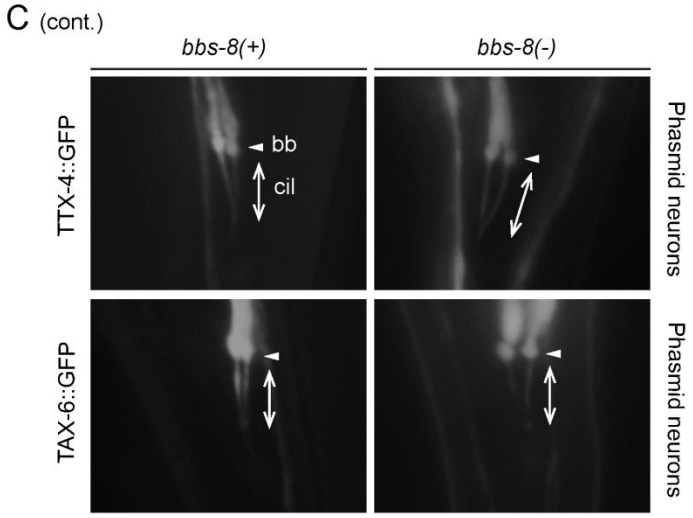

Figure 4.2. The *bbs* mutants specifically show defects in the localization of GCs.

(A) Localization of a representative GC (GCY-18::GFP) in wild-type and *bbs-8* worms. GCY-18 is localized specifically in the finger compartment of wild-type AFD neurons, but accumulates in the fingers and along the dendrite of the *bbs-8* mutant. In the image on the right for *bbs-8(-)*, the plane was focused on the dendrite to highlight the accumulation there, this neuron still has GFP signal in the finger compartment. Dotted circles indicate the position of the finger compartment; arrows indicate the direction of the dendrite ('den') when it is not visible. The graph shows the percentage of AFD neurons with defective localization of GCY-8, GCY-18, or GCY-23 (n>100). *** indicates significant difference at p<0.001. (B) Mislocalization of GCY-18 is a prominent phenotype in bbs mutants (*bbs-7*, *bbs-8*) but not other mutants that affect IFT (*osm-5* and *che-11*). The bar graph shows the percentage of AFD neurons with defective GCY-18 localization (n>100). *** indicates significant difference from wild-type at p<0.001; *, p<0.05. (C) Other cGMP signaling proteins (SRTX-1, TAX-2, TAX-4, TTX-4, and TAX-6) localize normally in the *bbs-8* mutant. Since the AFD cilia are too short for the phenotype in wild-type and mutant worms to be scored confidently, the localization data are based on the patterns seen in the amphid cilia for TAX-2 and TAX-4, and in the phasmid cilia for TTX-4 and TAX-6 (the two latter proteins are also present in many non-neuronal cells in the head, obscuring the amphid localization). 'pro' (brackets) indicates ciliary proximal region; 'cil' (double-headed arrows), cilia; 'bb' (arrowheads), basal body.

4.2. CNG channel localization

Since the CNG channel subunit TAX-4 localizes within the proximal part of the AFD cilium, but this localization is not affected by disrupting BBS-8 or DAF-25 (Figure 3.1, 4.2, and Jensen et al., 2010), I wondered if other ciliary proteins are required for proper localization of this cGMP-gated channel subunit.

In the *daf-19* mutant

DAF-19 is the transcription factor regulating ciliary gene expression, and mutations in daf-19 result in the absence of all cilia in *C. elegans* (Swoboda et al., 2000). In AFD neurons of the *daf-19* mutant, the cilium is missing but the fingers are still present (Perkins et al., 1986; Swoboda et al., 2000). Since TAX-4 is present in the cilium of AFD neurons (Figure 4.3), I wondered where it would be located in the absence of the cilium. When an AFD-specific version of TAX-4 is expressed in wild-type worms, it is localized near the base of the canonical cilium and sometimes seen accumulated at the ring structure in AFD neurons (Figure 4.3). In contrast, *daf-19* animals show TAX-4 signal within the finger compartment, possibly along the filamentous structure between the cilium and the ring structure (Figure 4.3). This may suggest that intermediate filaments (IFs) and their associated vesicles might be the trafficking route for TAX-4 in the AFD dendritic end in the normal situation. These data also suggest that the filamentous structure is somewhat independent of the ciliogenesis machinery, since I could still observe indirectly its presence in the *daf-19* mutant. Supporting this hypothesis, IFs can still be seen in the *daf-19* mutant through TEM (Perkins et al., 1986).

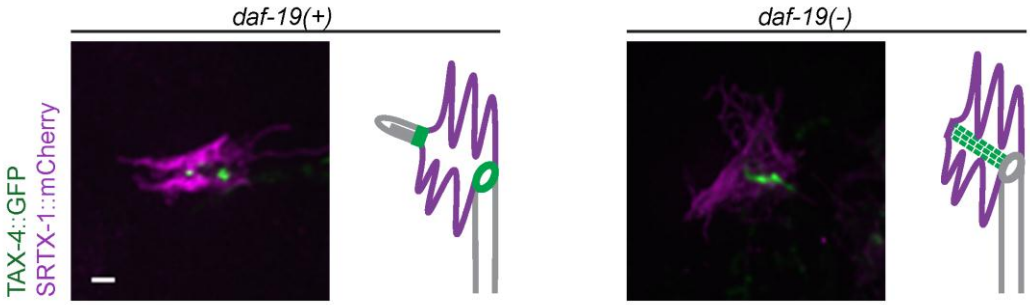

Figure 4.3. The *daf-19* mutant shows defects in the localization of TAX-4.

Instead of its usual discrete localization at the ciliary base, TAX-4 in the *daf-19* mutant is seen in the finger compartment, probably decorating the filamentous structure connecting the cilium and the ring structure. Scale bar is 1 μm.

In the *nphp-2* mutant

In the amphid cilia, TAX-4 is also localized to a distinct part of the cilium, distal to the TZ (Figure 4.4A). This localization is reminiscent of the so-called 'Inv' compartment described for cilia of mammalian cells (Shiba et al., 2009). It has also been shown that Inversin/NPHP2 is required for the localization of two other proteins, NPHP3 and NEK8, which together may form a functional complex within this compartment (Mahjoub et al., 2005; Shiba et al., 2010). Therefore, I specifically asked if the *C. elegans* Inversin homolog, NPHP-2 (Warburton-Pitt et al., 2012), is also required for anchoring TAX-4 to this proximal region of the cilium.

I first confirmed that a GFP-tagged version of NPHP-2 co-localizes with TAX-4 in the proximal segment of various cilia (Figure 4.4A), indicating that TAX-4 is localized at the Inv compartment. Interestingly, in the *nphp-2* mutant, TAX-4 does not localize tightly to the proximal part of the channel cilia, but instead, is partially delocalized to the distal part, and seems to have a cytoplasmic localization rather than membrane localization as in wild-type worms (Figure 4.4B). The altered localization of TAX-4 in the *nphp-2* mutant is thus similar to what was reported in AWB neurons recently (Wojtyniak et al., 2013), but milder than the phenotype seen in mammalian Inv mutant cells (Shiba et al., 2010). In these cells, ciliary proteins NPHP3 and NEK8 are no longer seen concentrated in the Inv compartment but are localized to the whole length of the cilia. The milder phenotype could be due to the nature of the *gk653* mutation in the *nphp-2* mutant worms. This is a deletion removing only the first exon of the gene, resulting in a near full-length protein missing only an ankyrin repeat (Warburton-Pitt et al., 2012). Thus, in *nphp-2* worms, the NPHP-2 protein would be predicted to still localize to the Inv compartment since the C-terminal region required for proper localization is intact (Shiba et al., 2009), but have reduced ability to interact with binding partners due to the missing ankyrin repeat. Therefore, some of the TAX-4 proteins may not be bound tightly to the truncated NPHP-2, and could leak into the more distal part of the cilia. Alternatively, NPHP3 and NEK8 might represent true interacting partners of NPHP2, whereas TAX-4 may interact with NPHP-2 indirectly or transiently, such that the requirement of NPHP-2 for TAX-4 localization is less strict compared to that of NPHP3 and NEK8 localization.

Since the cilium of the AFD neurons is short and the signal of TAX-4::GFP in these neurons is even smaller, I was not able to conclusively test whether TAX-4 is mislocalized in AFD neurons of the *nphp-2* mutant. Behavioral data suggest that TAX-4 localization might be disrupted in AFD neurons (see below), even though I cannot exclude the possibility that TAX-4 mislocalization in other cilia also contribute to this thermotaxis phenotype in the *nphp-2* mutant.

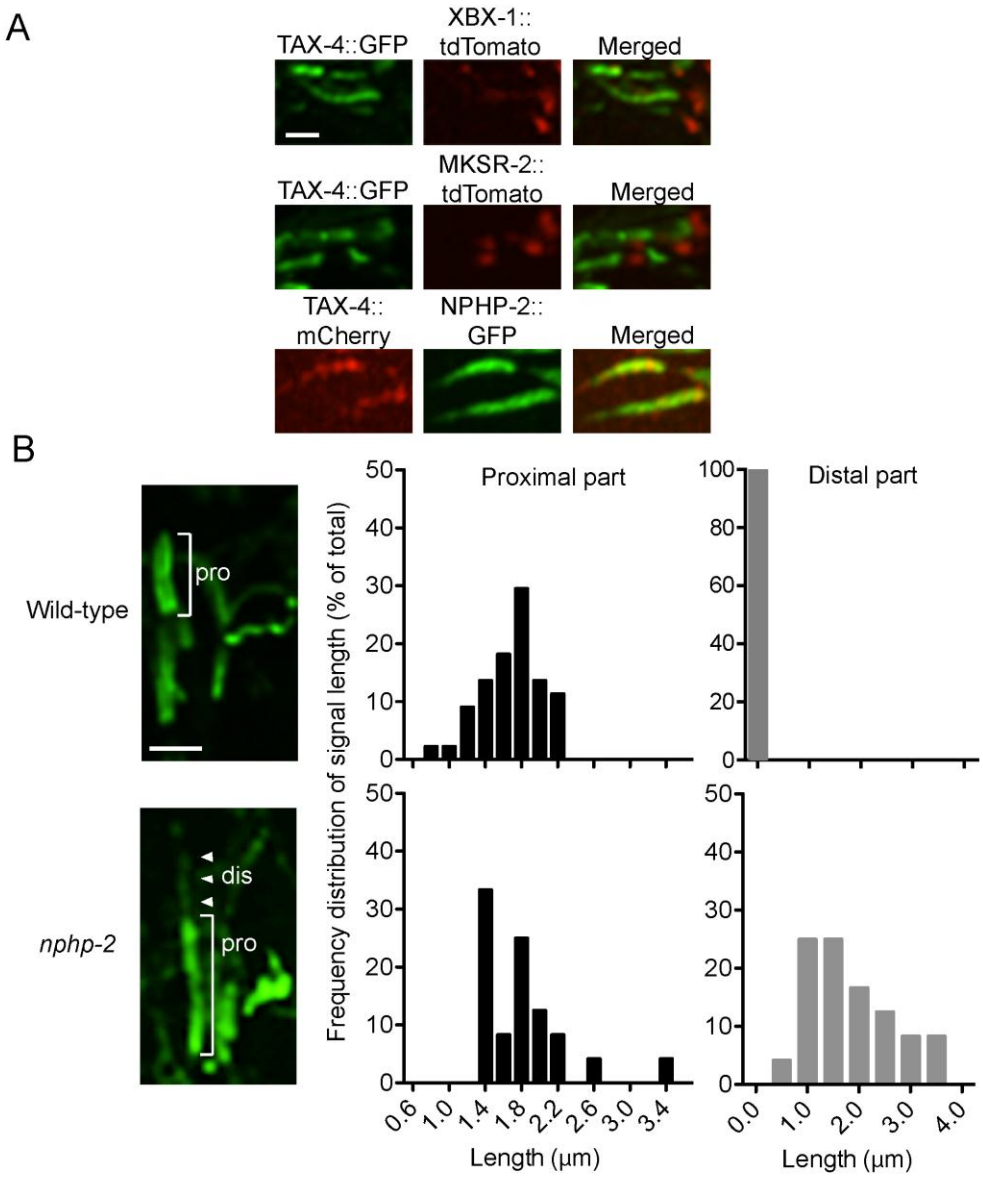

Figure 4.4. TAX-4 is mislocalized from the Inv compartment in amphid cilia of the *nphp-2* mutant.

(A) In amphid channel cilia, TAX-4 colocalizes with NPHP-2 in the Inv compartment of the cilium, which locates above the transition zone (marked by MKSR-2) and the basal body (marked by XBX-1). Scale bar is 1 μm. (B) Wild-type cilia display discrete localization of TAX-4 at the proximal ('pro', bracket) and not in the distal part of the cilia, whereas *nphp-2* cilia show GFP signal leaking into the distal part of cilia ('dis', arrowheads). Scale bar is 1 μm. The histograms show the frequency distribution of signal length at proximal and distal parts in cilia of wild-type (n=44) and *nphp-2* (n=24) worms.

4.3. Discussion

Regulation of GC localization

The loss of GCs from the finger membrane in the *daf-25* mutant suggests that the normal function of DAF-25 is to keep GCs in the finger compartment. This means that DAF-25 functions in at least one of these three steps: (1) bringing GCs to the base of the finger compartment, (2) carrying them through the gate and preventing them from diffusing out, (3) anchoring them in the compartment. Because in the *daf*-25 mutant, GCs could be observed along the dendrite, up to the area near the base of the finger compartment, it suggests DAF-25 is not absolutely required for the first step.

DAF-25 could also function in preventing GC from getting out of the compartment (step 3). DAF-25 is a well conserved protein but its function is not known. It has three ankyrin repeats at its N-terminus, and a zinc finger MYND domain at its C-terminus, both of which can mediate protein-protein interactions (Jensen et al., 2010). A member of the ankyrin protein family, Ankyrin-G (ANK3), is thought to help channel clustering in the axon hillock by connecting these membrane proteins with the spectrin-actin cytoskeleton. The human ortholog of DAF-25, Ankmy2, is also able to bind retinal GC in an *in vitro* assay (Jensen et al., 2010). Taken together, these data suggest that one function of DAF-25 in AFD neurons is to anchor the GCs to the actin network underneath the finger membrane. This could be one of the reasons why GCs still localize normally in the finger compartment of transition zone mutants (Table 3).

Another function of DAF-25 can be at the gate of the finger compartment (step 2), because DAF-25 is needed for the integrity of the gate. In the *daf-25* mutant, MKS-6 is also mislocalized from the apical junction and is present inside the compartment, along the IFs instead. Thus, DAF-25 can also function at the apical junction in AFD neurons, there it can interact with actin bundles connecting with apical junction components to gate the entry and exit of different proteins. These two functions of DAF-25 are not mutually exclusive, and may be linked by its ability to bind GCs. Supporting the hypothesis that DAF-25 functions as a specific adaptor for GC trafficking is the observations that other signaling proteins are localized normally in many neurons of *daf-25* mutants.

Deletion analyses of GCY-18 did not identify a region carrying the targeting signal needed for its localization at the finger membrane (data not shown). Constructs with either the extracellular and cytoplasmic domain deleted can localize normally, and the transmembrane domain is necessary but not sufficient for normal localization. Similarly, a specific CLS also has not been found for the GC localization in photoreceptor outer segment (Karan et al., 2011), suggesting that GC localization in general involves multiple processes. Therefore, DAF-25/Ankmy2 may be only one of the factors involved in GC localization. Moreover, in the case of AFD neurons, the data also suggest that GCs can be anchored both to the inside and outside of the cell. On the outside, AFD fingers are in contact with the sheath cell, for example, therefore GCs can anchor to this site and function as a structural component as well. This would be similar to the situation in vertebrate photoreceptors, where rhodopsin is also a structural component of the outer segment. A reduced level of this membrane protein results in the failure to form the outer segment and ultimately leads to degeneration (Lem et al., 1999). In the *daf-25* mutant, the lack of the structural link to the sheath cell provided by GCs resulted in abnormal finger morphology. Another direct way DAF-25 mutations can affect AFD finger morphology is that GCs also play a structural role at the finger membrane, such as the lack of these proteins results in deformed fingers.

Taken together, my data suggest the following model for the trafficking of GCs in AFD neurons: At the base of the finger compartment, DAF-25 binds to GCs and interacts with the gating mechanism to get these proteins into the compartment. Once inside, GCs are anchored to the actin network in the cytoplasmic site through DAF-25, and to the sheath cell through the interactions at its extracellular domain. GCs can be taken out by the BBSome at the gate, and this does not require its interaction with the IFT machinery. The finding that only GC localization is affected in both bbs and daf-25 mutants provides evidence that the trafficking of GCs is an important step in the regulation of cGMP signaling by ciliary proteins. Since *daf-25* mutants also lack GCs in other cilia (Jensen et al., 2010; Fujiwara et al., 2010), and because I also observed that the *bbs-8* mutant shows accumulations of the GC DAF-11 in a channel cilium, the function of these proteins in GC localization may be more general.

Many important details are still missing, however, and one of them is the localization of DAF-25 in AFD neurons, as it could help provide clues as to which steps

this protein functions in. Attempts to localize DAF-25 in AFD neurons have not resulted in a specific localization pattern so far, however, as the fluorescent signal is present throughout the cytoplasm of AFD neurons How GCs are transported to the base of the finger compartment is also not known. GCs are still present in the finger compartment in the *bbs-8* mutant, suggesting that BBS-8 is not needed for this process. Mapping the DAF-25 binding site on GC proteins would also provide clues to how the GC constructs without the cytoplasmic end can interact with DAF-25 to get through the gate. This could involve the binding of DAF-25 to the transmembrane segment of GCs either directly or indirectly, giving rise to the need of this segment in GC localization, as suggested by the deletion studies. Since the *daf-25* mutation leads to opposite effects on different proteins, there should be other proteins mediating DAF-25 function, which would be interesting to identify through future interaction studies.

Regulation of TAX-4 localization

TAX-4 is localized at the proximal end of the cilium in AFD neurons, and not in the finger compartment. There are different ways TAX-4 could possibly get to the ciliary base in AFD neurons. One way is for TAX-4 to be incorporated into the cilium during development, before the finger compartment forms. Alternatively, later on, TAX-4 can be transported through the finger compartment into the cilium, either by moving through the finger membrane, or by following a more direct route from the apical junction area directly to the ciliary base. The incorporation of signaling components into the sensory end of AFD neurons has not been followed during development, so it is not clear which route TAX-4 takes to get to the ciliary base. Nevertheless, my data support the direct route, as the tomography data and ciliary mutant phenotype suggest that TAX-4 are carried in vesicles that move along intermediate filaments (either by active transport or restricted diffusion) to get to the AFD ciliary base. Similar to mammalian olfactory CNG channels, TAX-4 could be carried into the cilium by the IFT machinery, and anchored in the Inv compartment by the action of NPHP-2/Inversin. TAX-4 also carries a VxPx (RVxP) motif at its C-terminus, but unlike olfactory CNG channels, my preliminary data showed that it does not need this sequence for its ciliary localization in worm sensory neurons.

For AFD neurons, I have not identified any specific factors involved in CNG channel localization, with only an inferred role for NPHP-2/Inversin function. It is currently unknown if the expanded signal of TAX-4 in the *nphp-2* mutant cilia is caused by an expansion of the Inv compartment within the cilium, or because of the increased length of the whole cilium in this mutant (Warburton-Pitt et al., 2012). The Inv compartment is thought to coincide with the middle segment, where the axoneme is composed of doublets and where the kinesin-II functions (Warburton-Pitt et al., 2012), the length of the middle segment in the *nphp-2* mutant could be indicative of the status of the Inv compartment.

In conclusion, the data in this chapter showed that cGMP signaling proteins are mislocalized in ciliary mutants. The four ciliary mutants described above show various protein mislocalization patterns, but ultimately are all expected to result in defective sensory transduction through the misregulation of key signaling components (Figure 4.5). As observed in other sensory cell types, a phenotype caused by misregulated signaling might be different from that arising from a complete lack of signaling proteins. Indeed, the mislocalization of the GPCR MCHR1 from the cilia of bbs mutant mice is linked to obesity (Berbari et al., 2008b), which is the opposite to the phenotype of mice lacking MCHR1 expression (Chen et al., 2002), and indicative of increased signaling in bbs mutants. In the next chapter, I describe the consequences of mislocalized signaling components in ciliary mutant phenotypes.

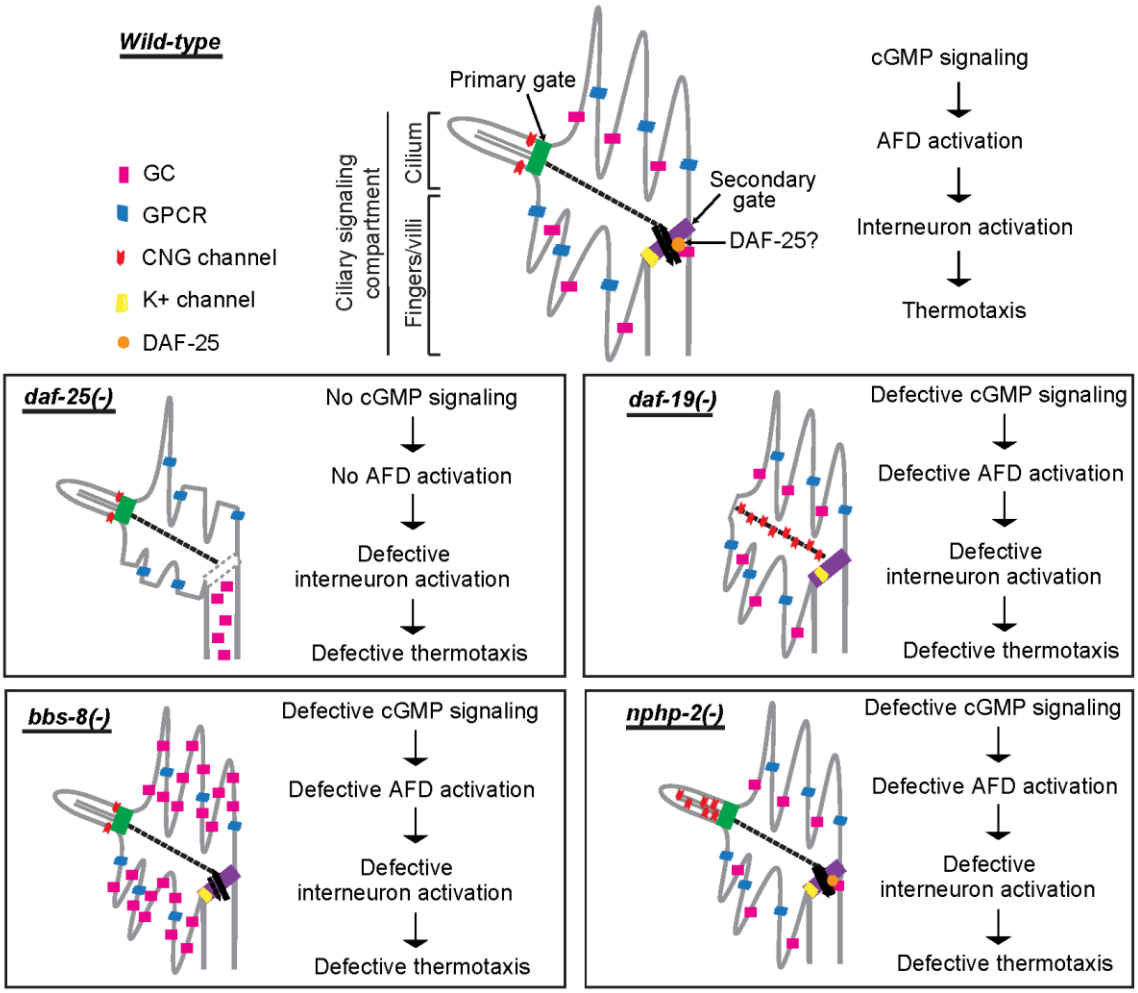

Figure 4.5. Summary of protein localization patterns in ciliary mutants.

Based on the mislocalization patterns, it is expected that in the AFD neurons of the *daf-25* mutant, no cGMP is made in the signaling compartment, leading to no AFD activation. In the *bbs-8* mutant, it is expected that the cGMP baseline level is higher than normal, which could lead to CNG channels being opened more easily or closed slower than normal, and therefore defective AFD activation. In both *daf-19* and *nphp-2* mutants, TAX-4 is mislocalized and is likely to be non-functional, leading to no AFD activation. All mutants are expected to have defective AIY activation and thermotaxis.

Chapter 5. Behavioral phenotypes

Given the mislocalisation in AFD neurons of GCs in the *daf-25* and *bbs* mutants, and of TAX-4 in the *daf-19* and *nphp-2* mutants, I expect that these mutants would have thermotaxis (TTX) defects. This behaviour has only been looked at in *bbs* mutants, with data showing an abnormal TTX index for these mutants (Tan et al., 2007). However, in the thermotaxis assay described in that study, the TTX index alone did not specify the nature of the thermotaxis defects. This is because a low index could be the result of either worms dispersing more or less equally along the temperature gradient, or inversely, from worms staying in a limited area but away from the targeted temperature zone. Therefore, I carried out a thermotaxis assay for ciliary mutants in order to clarify the nature of their defects.

5.1. Ciliary mutants

The thermotaxis assay I used for the experiments described below involves worms raised at 20°C and put at the 23°C zone, and the movement of worms down a linear temperature gradient (0.5°C/cm) is measured as the thermotaxis index. I chose to use this assay because the ability of worms to move toward colder temperature is more robust and has been observed in many studies in comparison to the movement toward higher temperature or negative thermotaxis behavior; it is also easier to quantify compared to the isothermal tracking assay. Using this assay, my data confirmed the thermotaxis defects in the *bbs-8* mutant, and also showed defects for the *daf-25*, *daf-19*, and *nphp-2* mutants, as measured by the TTX index (Figure 5.1A). The *daf-25* and *daf-19* mutants were used in the context of *daf-12* background to suppress the developmental arrest (dauer) of the *daf-25* and *daf-19* mutants, with the *daf-12* mutant alone showing normal thermotaxis behaviour. Secondly, I noticed that even though they all had a low index number, the *daf-25*, *bbs-8*, and *daf-19* mutants often stayed around the same area where they were initially placed. Moreover, in the absence of a

temperature gradient, *daf-25*, *bbs-8*, and *daf-19* mutants also showed a reduced locomotory behavior, regardless of food status. That is, in the presence of food, wild-type worms constantly moved around, covering most of the plate within 24 hours. Ciliary mutants, however, spent most their time in one small area (Figure 5.1B). Similarly, wild-type worms dispersed shortly after they were put on a plate without food, and after 30 minutes, had distributed themselves evenly on the plate. Ciliary mutants, on the other hand, stayed close to the area where they had been put, even after 30 minutes (Figure 5.1C). This reduced movement is unlikely to be caused by general muscle defects, as they can move with apparently normal gait when poked with a platinum pick, and *bbs* mutants show normal number of bends per minute during movement (Tan et al., 2007). Among the ciliary mutants tested, *nphp-2* worms did not show any apparent motility defects when not on a temperature gradient (Figure 5.1D), therefore their thermotaxis defects are likely to be caused by a defect in sensing temperature.

Previous studies have found that several other ciliary mutants have locomotory defects. Compared to wild-type worms, *che-2* - an IFT mutant - spends more time dwelling than roaming when food is present (Fujiwara et al., 2002). Similarly, in the absence of food, *osm-6*, also an IFT mutant, has increased local search behavior and reduced dispersal behavior (Gray et al., 2005). Moreover, these locomotory behaviours were shown to be mediated by various ciliated neurons (Gray et al., 2005; Mok et al., 2011). Given the involvement of ciliated neurons in various steps during thermotaxis, i.e. sensing temperature, food, and other external stimuli, as well as the subsequent taxis behavior, the thermotaxis defects of ciliary mutants are difficult to interpret as they can be caused by various reasons. Therefore, the function of ciliary proteins in cGMP signaling during thermotaxis would be better addressed in a cell-specific manner. Described below are my various attempts to test for cell-specific functions of ciliary proteins in AFD neurons. To avoid confusion, I will reserve the word ‘mutant’ to refer to a strain carrying a defective allele of a gene in the germline. For example, the *daf-19* mutant carries a null mutation in the *daf-19* sequence of the germline, therefore every cell of this strain will have a defective copy of this gene. This is in contrast to the AFD-specific knockout strain of *daf-19*, where the germline carries a modified copy of *daf-19* sequence, but this strain produces a loss of function of DAF-19 only in AFD neurons.

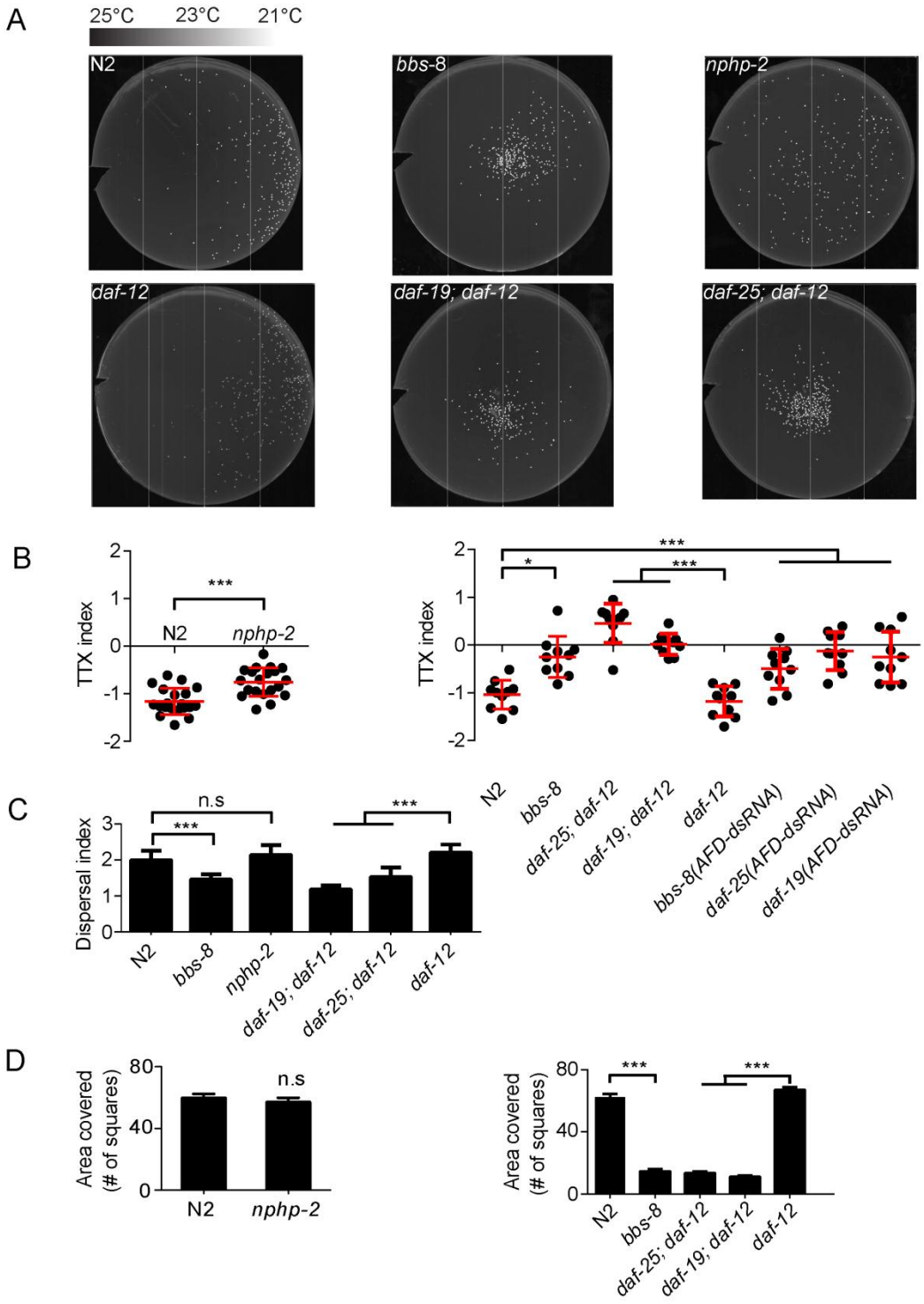

Figure 5.1. Ciliary mutants have defective thermotaxis and locomotory behaviors.

(A) Ciliary mutant worms show defective behavior when tested in a thermotaxis assay. Representative thermotaxis plates show the distribution on a linear temperature gradient of different ciliary mutant worms raised at 20°C. Worm positions are highlighted by white dots. (B) The graph represents the thermotaxis index of ciliary mutants and AFD-specific knockdown strains. Each data point is from an independent experiment, n≥10. Red bars indicate means ± SD. *** indicates significant difference at $p<0.001$; *, $p<0.05$. (C) In the presence of food, *nphp-2* worms show normal locomotion, but *bbs-8*, *daf-25*, and *daf-19* mutants have reduced locomotion, compared to wild-type worms. The bar graph represents the mean area covered ± SEM from 3 independent experiments of 10 worms each. 'n.s' indicates no significant difference, *** indicates significant difference at $p<0.001$. (D) In the absence of food, *nphp-2* worms show normal dispersal behavior, but *bbs-8*, *daf-25*, and *daf-19* mutants have reduced dispersal. The bar graph represents the mean area covered ± SD from 3 independent experiments. 'n.s' indicates no significant difference; ***, significant difference at $p<0.001$.

5.2. AFD-specific knockdown of ciliary genes

I first carried out cell-specific knockdown of *bbs-8*, *daf-25*, and *daf-19* by integrating into wild-type worms a double-stranded RNA (dsRNA) construct which targets each of these genes, and which is under the control of the AFD neuron-specific *gcy-8* promoter (Esposito et al., 2007). I first confirmed that the *bbs-8* dsRNA construct, denoted *bbs-8(AFD-dsRNA)*, is active only in AFD neurons, showing little or no leakage to the surrounding neurons. The *bbs-8(AFD-dsRNA)* construct can significantly reduce, if not abolish, the BBS-8::GFP signal in AFD neurons, but not in other ciliated neurons (Figure 5.2A). Moreover, in the *bbs-8* knockdown strain, general ciliogenesis is not affected as demonstrated by the normal dye filling capacity of neurons located in the amphid and phasmid sensory organs exposed to the environment (Figure 5.2B) (Hedgecock et al., 1985); in comparison, the *bbs-8* mutant globally affects ciliogenesis (Blacque et al., 2004).

Given the apparently successful AFD neuron-specific knockdown of *bbs-8*, I then analyzed this strain, as well as the *daf-25* knockdown strain, *daf-25(AFD-dsRNA)*, for their locomotory behaviors. Both *bbs-8* and *daf-25* mutant animals display motility defects (Figure 5.2C), which may contribute to their defects in thermotaxis assays. In contrast, the *bbs-8* and *daf-25* knockdown strains seem to have normal motility as they showed wild-type level of movement, at least on plates with food (Figure 5.2C). Finally, all three knockdown strains (for *bbs-8*, *daf-25* and *daf-19*) still show defects in a standard thermotaxis assay, where animals are placed in a linear temperature gradient (Figure 5.1B – these worms were assayed at the same time as the mutants and wild-type, so their data were graphed together in Figure 5.1B). Compared to wild-type animals, which migrate towards their cultivation temperature of 20°C, the AFD-dsRNA knockdown animals show little temperature preference during their movement and distribute themselves randomly along the gradient. However, when I tested a control strain, in which the targeted knockdown gene is *gfp*, it also showed some level of thermotaxis defects, making the effects of ciliary gene knockdown inconclusive (Figure 5.3).

This general toxicity of dsRNA constructs could be caused by the general promoter squelching effect (Gill and Ptashne, 1988). Thus, a high copy number of *gcy-8*

promoter in my knockdown strains could render AFD neurons non-functional by titrating transcription factors, such as TTX-1 (Satterlee et al., 2001), therefore inhibiting expression of other genes important for AFD function. Indeed, several other strains carrying multiple copies of the *gcy-8* promoter driving different unrelated DNA sequences also show thermotaxis defects in general (Figure 5.3).

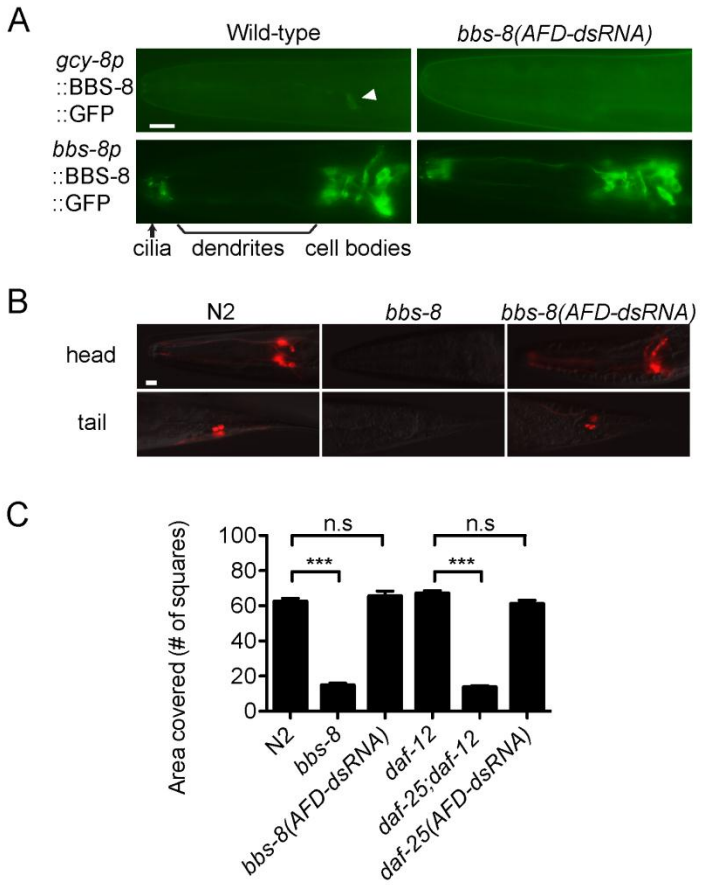

Figure 5.2. AFD-specific knockdown constructs are active only in AFD neurons.

(A) AFD-specific knockdown of *bbs-8* reduces the expression of BBS-8::GFP in AFD neurons (arrow) but not in other ciliated neurons. Top: strains carrying the BBS-8::GFP construct only in AFD neurons (arrowhead indicates an AFD cell body); bottom: strains carrying the BBS-8::GFP construct in all ciliated neurons. Scale bar is 10μm. (B) AFD-specific knockdown of *bbs-8* does not have effects on general ciliary structures, as assessed by dye filling experiments. The *bbs-8* mutant control is completely dye-fill defective. Scale bar is 10μm. (C) AFD-specific knockdown of *bbs-8* or *daf-25* does not affect the foraging behavior of worms on food. The bar graph shows the mean area covered ± SEM from 3 independent experiments of at least 10 worms each. 'n.s' indicates no significant difference, *** indicates significant difference at $p<0.001$.

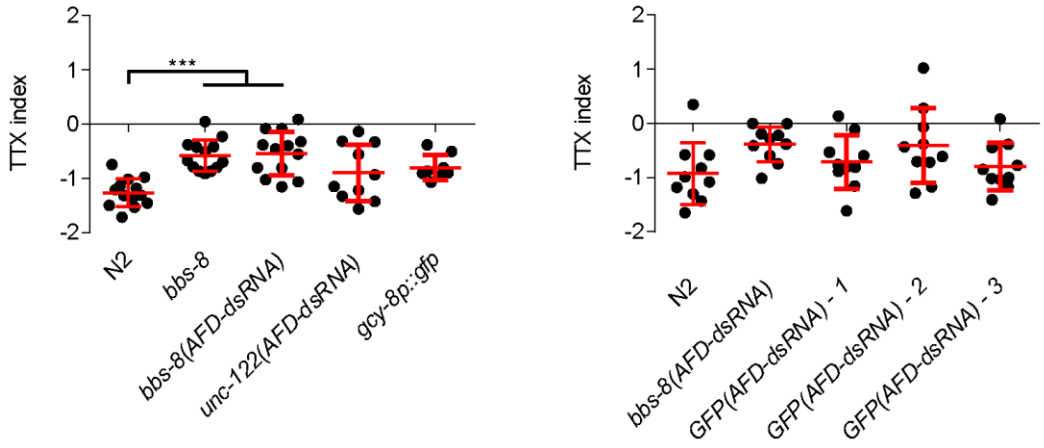

Figure 5.3. AFD-specific constructs result in a general thermotaxis defect.

The graph represents the thermotaxis index of worms with AFD-specific knockdown of *bbs-8* or non-related genes (*unc-122* and *gfp*), or worms carrying a *gfp* construct driven by the AFD-specific promoter. Only mutants and AFD-specific knockdown of *bbs-8* are significantly different from wild-type worms (*** indicates significant difference at $p<0.001$). No other pair-wise comparison reaches significant level ($p>0.05$). Each data point is from an independent experiment, $n\geq10$ (except n=8 for *gcy-8p::gfp*). Red bars indicate means ± SD.

5.3. AFD-specific knockout of *daf-19*

Continuing our attempt to test for cell-specific functions of ciliary genes in AFD neurons, I sought out another method of abrogating these genes without the use of multiple copies of the *gcy-8* promoter in order to avoid the promoter squelching effect. This new method could not be RNAi-based since it would require multiple copies of the effective molecules due to the fact that RNAi is practically not all-or-none. Therefore I combined two strategies to ensure the abrogation of ciliary genes in AFD neurons without the use of multiple copies of cell-specific promoters (Figure 5.4). First, gene knockout with the FRT/FLP system (Voutev and Hubbard, 2008) is used instead of knockdown in order to effectively eliminate ciliary gene function as much as possible. Second, a single copy of the AFD-specific promoter was used in combination with the Q system(Wei et al., 2012b) as an amplification step to ensure sufficient production of the FLP enzymes without the use of high copy numbers of promoters. In the Q system, a transcription factor from *Neurospora crassa*, QF, can be used to induce the expression of target genes under the QUAS promoter. Both aspects of this new method makes use of the transposon *Mos1* insertions available for *C. elegans* genetics, i.e. to insert *FRT* sites into the worm genome, and to ensure the addition of only one copy of the *gcy-8* promoter (through MosSCI method, Frøkjaer-Jensen et al., 2008). A more detailed description of the cell-specific knockout strategy can be found in Section 2.2.3.

Among the four ciliary genes showing defective cGMP protein localization and thermotaxis behavior described in previous sections, I chose to knockout *daf-19* in the AFD neurons for the following reasons. First, *daf-19* encodes a transcription factor regulating ciliogenesis, and thus cells lacking DAF-19 do not form cilia (Swoboda et al., 2000). Therefore, knocking out *daf-19* gene in AFD neurons would give us insights into the function of the AFD cilium in general. Second, there exists a *Mos1* insertion within a relatively short distance (1kb) to the DNA-binding domain (DBD) of *daf-19*. As the first attempt, I created a knockout strain (MX1776) containing *FRT* sites flanking a large part of the DBD of *daf-19* on LGII, and a single copy of a gene cassette on LGIV containing the coding region of the QF transcription factor driven by the *gcy-8* promoter, and the coding region of the FLP protein driven by the QF binding site, 5x*QUAS*, together with

the minimum promoter *Δpes-10* (Figure 5.4). A control strain containing scrambled *FRT* sites (*FRTsc*) flanking *daf-19* DBD was constructed in a similar manner (MX1778).

When tested in the thermotaxis assay, the *daf-19* AFD-specific knockout strain (MX1776) behaved normally compared to the control strain (MX1778) (data not shown). However, several lines of evidence suggest that the *daf-19* knockout did not happen in this strain. First, when the ciliary marker *gcy-8p*::ARL-13::GFP was put into the knockout strain, 100% of the worms examined showed normal GFP signal in the AFD neurons, indicating that the AFD cilium is still present in this strain. Second, ciliary structures can still be observed in this strain through TEM (n=3). Third, preliminary data from PCR experiments did not detect deletion in the *daf-19* coding region of the knockout strain.

There are several potential reasons why this first attempt at cell-specific knockout was not successful, one of which is that not enough FLP was made due to the single insertion of this gene into the genome. To test this hypothesis, I created a new knockout strain (MX2141) and a control strain (MX2142) carrying multiple copies of the FLP gene cassette on an extrachromosomal array that was then integrated into the genome; these strains also carry the same transgenes on LGII and LGIV as MX1776 and MX1778, respectively. The new knockout and control strains showed normal dye fill capacity, suggesting normal ciliogenesis in other neurons. From preliminary PCR data, it is estimated that 20-60% of MX2141 worms have at least one copy of the *daf-19* mutated, compared to 0% in the control strain, MX2142 (Figure 5.5). Notably, MX2141 showed a reduced thermotaxis index compared to that of MX2142 (Figure 5.5A), indicating that the DAF-19 protein in the AFD neurons is important for thermotaxis behavior. However, MX2141 also showed a reduced dispersal behavior in the absence of temperature gradient when compared to MX2142 (Figure 5.5B), even though this defect seems less severe than that of the daf-19 mutant (compared to Figure 5.1B). Indeed, AFD neurons have been shown to play a role in the local search behavior, and these data suggest DAF-19 mediates this function of AFD neurons. In summary, my data suggest that the function of ciliary proteins in AFD neurons contribute to the thermotaxis defect seen in ciliary mutants.

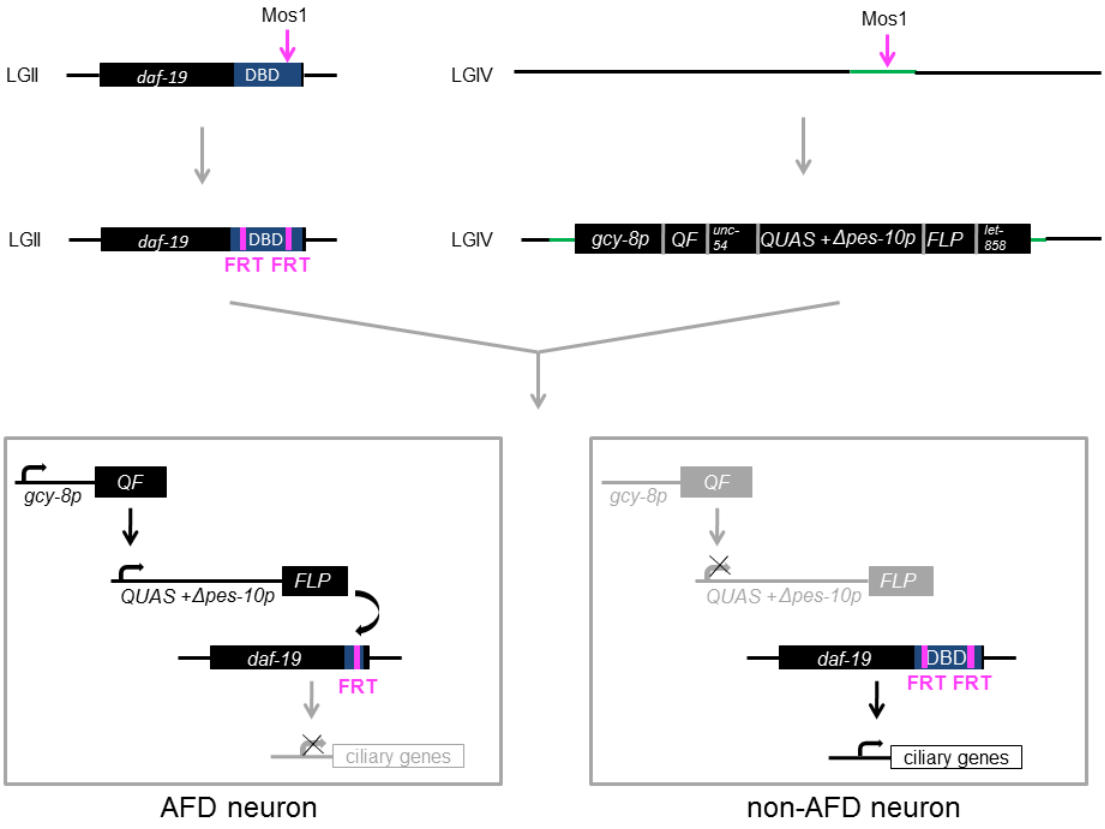

Figure 5.4. Strategy for AFD-specific knockout of *daf-19*.

On LGII, the existence of a *Mos1* transposon within the DNA-binding domain (DBD) of *daf-19* facilitates the insertion of FRT sites in this domain. On LGIV, a gene cassette is inserted in place of *Mos1* to allow AFD-specific expression of FLP. Worms carrying both of these mutations will have mutated copies of *daf-19* gene only in AFD neurons and therefore no ciliary genes expressed there.

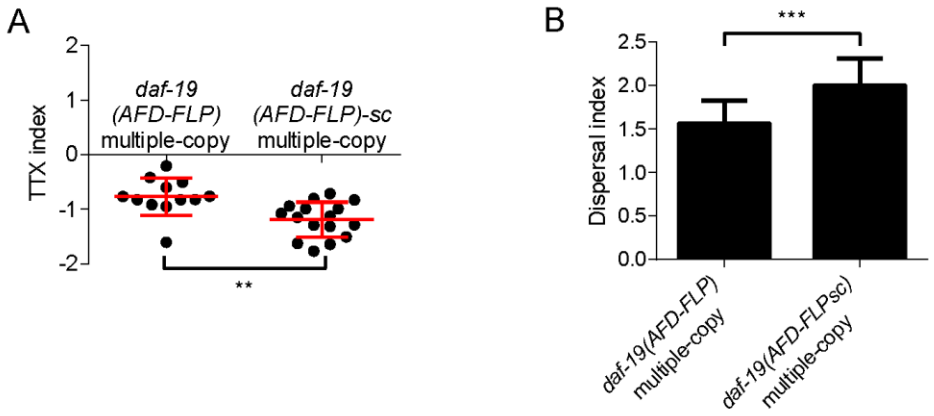

Figure 5.5. AFD-specific knockout of *daf-19* with multiple copies of *FLP* causes thermotaxis and locomotor defects.

(A) The knockout strain has a reduced thermotaxis index compared to the scramble control. Each data point is from an independent experiment, n≥10. Red bars indicate means ± SD. ** indicates significant difference at $p<0.01$. (B) In the absence of food, the knockout strain shows reduced dispersal compared to the control. The bar graph represents the mean area covered ± SD from at least 3 independent experiments. *** indicates significant difference at $p<0.001$.

5.4. AFD neuronal activities in ciliary mutants

Since disrupting DAF-19 function in AFD neurons alone results in thermotaxis defects, it suggests that the AFD neurons lacking cilia may have anomalies in activation by temperature. Our collaborator tested this hypothesis by measuring the calcium influx of AFD neurons in cilia mutants when stimulated with a temperature ramp (similar to what the worms experience when thermotaxing on a linear gradient), or a temperature oscillation (similar to the isothermal tracking condition, another temperature-mediated behavior related to thermotaxis) using the genetically-encoded calcium sensor Cameleon (Clark et al., 2006). Surprisingly, we did not observe any abnormalities in the calcium influx of the *bbs-8* mutant compared to wild-type under either temperature stimulus, unlike the null response seen in the triple mutant *gcy-23,-8,-18*, which lacks thermoreceptor current (Ramot et al., 2008) (Appendix B). These data suggest that under the conditions tested, the loss of BBS-8 function in AFD neurons affects thermosensation in a manner that is either distinct from, or potentially subtler than, a global decrease in cGMP production. We are interested in testing this hypothesis using the *daf-25* and *daf-19* mutants, however, I was unable to express the cameleon construct in these strains due to unknown reasons.

5.5. Discussion

Consequences of signaling protein mislocalization - At the level of neuronal activities

Given the accumulation of GC proteins in *bbs-8(-)* worms, I expected these animals to show defects in calcium influx in response to temperature changes. Unexpectedly, results from our collaborators showed that *bbs-8(-)* worms have normal calcium influx under the tested conditions, indicating that these animals can perceive the changes in temperature per se. At first, this seemed to contradict previous results showing olfactory neurons from *Bbs* mutant mice, including *Bbs8*$^{-/-}$, have a near complete loss of receptor currents when stimulated with odors (Kulaga et al., 2004; Tadenev et al., 2011). The *Bbs* mutations in these mice resulted in the shortening and loss of olfactory cilia, as well as mislocalization of OR, ACIII and G proteins from the ciliary layer. Therefore, the loss of receptor currents can be attributed to the lack of most transduction components from the olfactory cilia. However, there are a few significant differences between olfactory cilia of *Bbs* mutant mice and AFD cilia of *bbs-8* worms. Importantly, in the AFD neurons of *bbs-8(-)* worms, the thermal transduction machinery is still present at the major sensory site - the finger compartment, albeit with an increased level of some components. Moreover, TAX-4 localization are normal in the amphid cilia of *bbs-8(-)* animals, so it is expected that its localization is also intact in AFD neurons of these worms as well. Interestingly, although all other components of olfactory transduction are mislocalized in *bbs* mutant mice (Kulaga et al., 2004; Tadenev et al., 2011), a localization phenotype for CNG channels has not been reported for any cilium so far. In *Paramecium*, the loss of BBS proteins resulted in mislocalization of a ciliary K^+ channel and a TRP channel, but a voltage-gated calcium channel is still present in the cilia (Valentine et al., 2012). Therefore, the loss of BBS function may not affect all ion channel localization in the cilia. Finally, in *bbs-8* worms, the ASE channel cilia were shown to be shorter than in the wild-type (Blacque et al., 2004), but it is not known if this is also the case for the small cilium of AFD neurons. This could explain why the AFD neurons of *bbs-8(-)* worms can still react to temperature changes.

The *bbs-8* mutant may have defects downstream of the initial temperature reception, leading to an adaptation defect. Worms with mutated GCs of various combinations showed defective AFD calcium influxes in response to temperature

changes (Wasserman et al., 2011), including a complete loss of reaction in the triple *gcy* mutant. However, it is not known how an increase in GC levels would affect the intracellular calcium dynamics in AFD neurons. The activity of signaling components in sensory neurons are known to be tightly regulated for shut-off and adaptation purposes, and GCs are often regulated by calcium-dependent proteins known as GCAPs (guanylyl cyclase activating proteins). In photoreceptors, high Ca^{2+} levels activate GCAPs, which in turn inhibit GCs and therefore stop the production of cGMP. No GCAP has been identified to function in AFD neurons so far, but several other regulatory proteins have been found to play a role, including NCS-1, a member of calcium-regulated protein family related to GCAP (Gomez et al., 2001; Wang et al., 2013). A high level of GCs without an accompanying increase in regulatory proteins in *bbs-8* mutants could result in a sustained high level of cGMP and affect adaptation. In olfactory neurons, it has been shown that the sustained levels of cyclic nucleotides do not affect responses to odor stimuli delivered as successive quick pulses; however, the cell shows prolonged and less extensive adaptation if activated once (Takeuchi and Kurahashi, 2002). Similarly, sustained activities of ACIII decreased the onset rate of adaptation and the extent of recovery to long exposure, but not to quick deliveries of stimuli (Leinders-Zufall et al., 1999). It is conceivable that in AFD neurons, an increase in GC levels would lead to a similar effect as a reduction in PDE activity. Interestingly, in AFD neurons, Wang et al. (2013) showed that blocking PDE-2 activity led to a shift in the activating temperature and a prolonged recovery phase of the thermocurrent, without changing the magnitude of the current. This is consistent with the calcium influx data for the *bbs-8* mutant, which showed no changes in the magnitude of the influx, and a small change in the activating temperature (Appendix B). The temperature stimuli were delivered as fast pulses, so it is currently not known whether this mutant has a defect in response of AFD neurons to prolonged stimuli. The finding that only GC localization is affected in both *bbs* and *daf-25* mutants suggests that the trafficking of GCs is an important step in the regulation of cGMP signaling by ciliary proteins, which may relate to their potential role in sensory adaptation.

Testing AFD neural activities in other ciliary mutants besides *bbs-8* would also be useful, as different ciliary mutants seem to have different defects in protein localization. Studying the effect of different mislocalization patterns can provide further insights into

why signaling proteins are found in discrete compartments, and what are the consequences of disrupting their location on the signaling process. Unfortunately, calcium dynamics could not be measured for the *daf-19* and *daf-25* mutants, because they do not express the calcium sensor construct properly. The cause for this phenotype is currently unknown, but it does hint at some defects caused by mutations in these genes, different from that of the *bbs-8* mutation. My preliminary data using qPCR suggested *daf-19* and *daf-25* mutations do not affect the expression level of *gcy-8*, ruling out a transcriptional defect in these mutants. However, the qPCR results might not be able to measure the subtle changes since *gcy-8* is expressed at very low level (in only 2 AFD cells). Alternatively, the calcium sensor phenotype may reflect cell death caused by improper localization of signaling proteins in these mutants. In other systems, mutations in ciliary genes often result in degeneration of sensory cilia, followed by cell death, and in some cases, this can be attributed to ectopic proteins interfering with other signaling processes (Tsujikawa and Malicki, 2004). The mislocalization of TAX-4 and GCYs from their site of action in *daf-19* and *daf-25*, respectively, could result in low levels of calcium in sensory neurons, which would be exacerbated in AFD neurons with the use of the sensor - a calcium quencher. Because of its importance in many crucial cellular processes, calcium levels are tightly controlled, and a sustained low level of calcium could lead to cell death (Fain, 2006). Interestingly, young worms of these strains often show visible cameleon signal but older worms do not, supporting the existence of an AFD degeneration phenotype in these worms later in life. This is also consistent with an age-dependent effect of Ca^{2+} on the survival of neurons seen in cell cultures (Tong et al., 1996). Measuring the neural activities of downstream neurons such as AIY in strains carrying AFD-specific disruption of *daf-19* or *daf-25* could potentially overcome this technical problem (Biron et al., 2006).

Consequences of signaling protein mislocalization - At the behavioral level

AFD neurons are thought to regulate the turn frequency of worms during thermotaxis movement, as killing AFD neurons reduced turn frequency during cryophiphic movement (Chung et al., 2006). Thermotaxis behaviors in *C. elegans* are thought to have a biased random walk component, and changing the run length by monitoring turning rates is thought to contribute to this strategy (Ryu and Samuel, 2002, Luo et al., 2014). A prolonged activation of AFD neurons due to the slow adaptation rate

caused by accumulation of GCs in *bbs-8* mutants could result in a high turn rate. A high turn rate could in turn result in worms having short run lengths and not being able to disperse away from the initial location, a phenotype very similar to the locomotory defects seen in the AFD-specific *daf-19* knockout strain, as well as the tested ciliary mutants. The turn frequency of these strains during dispersal and thermotaxis is currently not known.

There are several indirect observations that support the hypothesis that the AFD-specific knockout of *daf-19* can cause a high turning rate, leading to the observed reduced dispersal behaviors. Several studies have found a role for AFD neurons in locomotory behaviors with no food nor a temperature gradient (Gray et al., 2005; Tsalik and Hobert, 2003; Wakabayashi et al., 2004). Killing AFD neurons resulted in reduced turning rate during locomotory behaviors. Disrupting the function of TTX-1, the transcription factor important for AFD specification, also resulted in decreased turning rates and an increase in forward run duration. AFD neurons are thought to act through AIY interneurons to modulate turning rates, as mutants lacking both cell types have a high turning rate, similar to animals lacking AIY only. So the lack of AFD neurons can release the inhibition of AIY, leading to a low turning rate. A simple explanation for the phenotype in animals with AFD-specific knockout of *daf-19* could be that an increase in AFD activities (due to slow adaptation) inhibits AIY, resulting in a high turning rate, and thus reduces dispersal. However, it was recently shown that different levels of AFD activity seem to affect AIY activity differently (Kuhara et al., 2011). In wild-type worms, normal AFD activity lead to a certain level of AIY activity; when AFD activities are reduced to a lower level, AIY activity increases, but a complete loss of AFD function eliminates AIY activation. This is because AFD has both excitatory and inhibitory effects on AIY activities. It is not known how a higher than normal level of AFD activities would affect AIY activation, so the cause for the reduced dispersal in the knockout strain may not be so simple.

The role of AFD neurons in thermotaxis and locomotory behaviors could also be mediated by interactions outside of its influence on AIY activity. For example, AFD neurons can receive inputs from other cells. AFD neurons are post-synaptic to AWA, ASE and AIN neurons (White et al., 1986), but these neurons have not been shown to have a role in thermotaxis or locomotion. Several neuromodulators have been recently

shown to modulate locomotory behaviors in worms (Barrios et al., 2012; Choi et al., 2013; Flavell et al., 2013). Among these neuromodulators, serotonin has been showed to have some effect on isothermal tracking behaviors (Li et al., 2013). AFD neurons are not known to express receptors for serotonin, as well as for NPR-1, or PDFR-1. Insulin is often involved in mediating behaviors in response to metabolic status; however, insulin's effect on thermotaxis is likely through interneurons, and starvation does not seem to affect AFD activity (Biron et al., 2006; Ramot et al., 2008; Nishio et al., 2012). So AFD neurons are either independent of other neurons' activities, or are influenced by yet unknown neuromodulators. The observation that defects in AFD function by itself resulted in locomotory defects supports the hypothesis that AFD neurons by themselves can have some influence on worm locomotion. To further support this hypothesis, it would be interesting to test AFD activities in response to temperature in gap junction mutants, such as *inx-19* mutants (Chuang et al., 2007), neurotransmitter mutants, such as *unc-13* (Kohn et al., 2000), or dense-core vesicle mutants, such as *unc-31* (Speese et al., 2007). AFD activities could also be tested in an *in vitro* system to see if they behave normally in the absence of other cells.

AFD neurons can also influence locomotion through secreting neuromodulators, and thus affect other neurons' function indirectly. Among the neuromodulators involved in worm locomotion, PDF-1 may be expressed in AFD neurons (Barrios et al., 2012). AFD neurons also express the neuropeptides FLP-6, NLP-7, and NLP-21 (Li and Kim, 2008), but their function in locomotion and thermotaxis is unknown.

Finally, ciliary mutants with many affected neurons, the reason for reduced dispersal behaviors could be even more complicated. Locomotory behaviors seem to be controlled by many ciliated neurons, including those that share post-synaptic partners with AFD neurons (such as AWC neurons), and they modulate the activities of these interneurons in different ways. Other neurons can also interact directly or indirectly with AFD neurons and with each other through chemical synapses (with AFD neurons through AWA and AIN neurons), gap junctions (with AFD neurons through AIB neurons), or through neuropeptides modulating locomotory behaviors in worms (Barrios et al., 2012; Choi et al., 2013; Flavell et al., 2013). Therefore, the defects in these mutants would be the net outcome of the effects of ciliary disfunction in all of these neurons. Given the complex neuronal circuits of locomotory and thermotaxis behaviors, with the

function of many connections still unknown, it is hard to predict the effects of ciliary mutations on these behaviors. For both mutants and knockout strains of ciliary genes, a combination of measurements of behavioral parameters (using the MultiWorm tracker, for example) and neuronal activities (using calcium sensors or electrophysiology) will give better insights into the locomotory defects in these strains.

Potential uses of the cell-specific knockout method

Before this study, there have been several methods to disrupt gene function in a cell-specific manner for *C. elegans* neurons. This includes methods aiming to sensitize specific neurons to RNAi effects through the use of SID-1 over expression (Calixto et al., 2010), a method using dsRNA driven by specific promoters (Esposito et al. 2007), and a method to control temporal and spatial expression with the heatshock transcription factor HSF-1 (Bacaj and Shaham 2007). As described above, the promoter squelching problem seems to be an issue, which was demonstrated for the dsRNA method and is likely to present in the other methods because of the use of high copy numbers. The heatshock method may also interfere with the temperature sensing process, as HSF-1 also has a function in thermotaxis (Sugi et al., 2011).Therefore, a method using single copy insertion of cell-specific promoters in combination with the Q expression system and the FLP recombinase was developed in this study.

The data showed that AFD-specific knockout of *daf-19* resulted in thermotaxis defects. Preliminary data demonstrated that the deletion of DAF-19 DNA-binding domain happened in the tested strain but not the scramble control strain, but the frequency of deletion is currently unknown. This frequency is a function of the accessibility of the *daf-19* site by the FLP enzyme, and a large copy number of the *FLP* sequence was used in order to increase this frequency. However, the detection method for somatic deletions needs to be improved in order to measure the real frequency. The current estimation of 20-60% deletion is likely to be an underestimate. This is because there is a ~500 fold difference between the wild-type and the mutant copy numbers (*gcy-8* is expressed only in 2 out of 959 cells) and only ~3 fold difference in length (and thus ~20 fold difference in PCR efficiency, as estimated from data in McCulloch et al., 1995). Therefore, the wild-type band is ~20 times more likely to be amplified compared to the mutant band, thus animals with only the wild-type band may still have the deletion but the mutant band is

not amplified. The absence of the cilium in the deletion strain should be tested, for example by the use of the *gcy-8p::arl-13::gfp* construct, and the percentage of animals without cilia in AFD neurons would also give an indication of deletion frequency. RNA-mediated transcriptional interference using CRISPRs (clustered regularly interspaced short palindromic repeats) (CRISPR interference, CRISPRi - Marraffini and Sontheimer, 2010) is another potential way to control *daf-19* expression specific in AFD neurons. However, it is not known if CRISPRi constructs can gain better access to DNA compared to the FLP enzyme, and these constructs may still need to be amplified using the Q system. Moreover, the extent to which CRISPRi constructs can reduce transcription is harder to assess, compared to measuring somatic deletion frequency using the current FLP method.

There is a concern regarding the use of *unc-119* as the rescue marker, as this gene has been shown to affect ciliary localization of lipidated proteins (Wright et al., 2011). However, the genetic background of the resulting strains used for thermotaxis is such that MX1768 (the FRT strain) should carry 4 copies of *unc-119* in AFD neurons, and 6 copies in all other cells, whereas the control strain, MX1769 (the FRTsc strain) has 6 copies in all cells. If such increase in copy numbers of *unc-119* affects AFD ciliary function, I would expect MX1769 to be more affected, which is not the case. Indeed, MX1769 behaves like N2 wild-type strain under the dissecting microscope. Therefore, the defects seen in MX1768 are likely caused by loss of function of DAF-19 in AFD neurons. Another concern is the function of DAF-19 outside the cilium. It has been shown that DAF-19A and B isoforms have functions in synaptic maintenance (Senti and Swoboda, 2008), and the DNA binding domain deleted in the AFD neurons of MX1768 is common among all DAF-19 isoforms. However, these isoforms are only expressed in nonciliated cells in *C. elegans* (Senti and Swoboda, 2008), so the deletion in AFD neurons, a ciliated cell type, in MX1768 should not have any effect on the synaptic function in this strain. Thus, the behavioral defects in MX1768 are likely to be caused by the disruption of ciliary functions of DAF-19 in AFD neurons.

The cell-specific knockout method developed in this study can be further refined and improved in several ways in order to be used as a method of testing cell-specific functions of any gene of interest in general. First, in order to produce animals carrying FRT sites flanking the sequence of interest, the existence of strains carrying the desired

Mos1 insertions is important and may present a challenge as these lines may not be readily available. However, several methods can be used to produce such strains. One method is to carry out a Mos1 insertion screen to isolate strains carrying Mos1 around the region of interest (MosTIC - Robert and Bessereau, 2007). This method is more time consuming and requires more labour, but has the advantage of keeping the gene of interest in its original genomic context in other cells. In a second method, a construct carrying the gene of interest with the FRT sites already present at the desired place can be introduced into the strain mutated for that gene using MosSCI-related methods (Frøkjaer-Jensen et al., 2008, 2010). This method is relatively straight forward but has the disadvantage that the gene is likely to be in a different genomic context, which may affect its expression. Genome editing by CRISPR-targeted homologous recombination (Dickinson et al., 2013) can also be used to insert FRT sites into regions of interest. Second, the availability of cell-specific promoters to drive the QF expression in the cell of interest is crucial, but promoters driving genes in only one cell type seem to be rare and may not exist for some cells. The split Q system (Wei et al., 2012b) can help overcome this problem with the use of promoters with overlapping expression patterns. Finally, since the Q expression system can also be controlled with nontoxic chemicals, it also offers the potential for an inducible knockout option upon the addition of the drug (Wei et al., 2012b).

More specifically, in the study of *C. elegans* cilia, this conditional knockout method can be used in several ways. Firstly, with the available strains carrying FRT or FRTsc sites in the *daf-19* sequence (MX1768 and MX1769), the function of each cilium of the worm can be tested individually by driving the FLP in each ciliated cell. This method has an advantage over the single-cell rescue method to test for ciliary functions developed by (Senti et al., 2009). This is because the locomotory phenotype described in section 5.1 is caused by ciliary defects in multiple cells, so such single-cell rescued strains will likely have defects in locomotion, making them unsuitable for behavioral tests. Secondly, the function of different ciliary genes can be tested in a cell-specific manner to address the context-dependent function issue often observed in ciliary biology as described in Chapter 1.

In conclusion, the data in this chapter showed that the cilium in AFD neurons has a cell-autonomous function in thermotaxis behavior.

Conclusions and perspectives

To ensure faithful transmission of extracellular signals, signaling proteins are spatially arranged into domains where modulator proteins, and possibly lipid environments, can efficiently regulate signal strength. This has led to the evolution of signaling centers, including cilia. In this study, I have started to unravel how ciliary proteins help establish two sub-compartments which harbor different cGMP signaling components required for thermosensation in the *C. elegans* AFD neurons.

My research suggests that the sensory end of AFD neurons is a bipartite ciliary signaling compartment. The data support this conclusion include the presence of ciliary proteins in both compartments where cGMP proteins are found, the development of the two membranes, and the requirement of ciliary proteins for signaling components to localize there. I also identified a barrier between the finger and dendritic membranes, where transition zone proteins and BBS proteins are found. Interestingly, unlike in the canonical transition zone, there is no Y-link in this area, suggesting that this is not a cytoplasmic barrier. The phenotypes of *daf-25* and *bbs-8* mutants suggest that this barrier prevent mixing of membrane proteins, and that there is an active process to regulate the entry and exit of proteins through this gate. Finally, my data support a cell-autonomous function of the AFD cilium in thermotaxis behavior.

The ciliated end of the AFD neurons is a bipartite cGMP signaling compartment. The finger sub-compartment has a large membrane surface and a higher fluidity lipid environment, allowing quick changes in cGMP production in response to thermal stimuli. The ciliary sub-compartment has a lipid environment more suitable for ion channel conductance, and this could be the main reason for the segregation of signaling proteins into different domains.

Signaling protein localization patterns indicate that the role of the cilium in AFD neurons is not to act as the site of sensory perception per se. Instead, it may function as a calcium compartment, allowing short-term adaptation through the regulation of ion

channels. The long-term component of adaptation seems to be located in the finger sub-compartment, through the regulation of more upstream signaling proteins. Ciliary proteins can participate in the regulation of both components during adaptation, thanks to their roles in protein trafficking in both sub-compartments. The behavioral phenotypes of animals with disrupted ciliary functions in AFD neurons also suggest a regulatory role of ciliary proteins. Because the sensory end of AFD neurons can store memory of past culturing conditions, it is possible that ciliary proteins take part in this process. For example, culturing conditions can affect AFD neurons directly or through neuromodulators by changing the level of ciliary protein expression, or affect their function through post-translational modifications. This can set the baseline level of cGMP, which would affect the activation temperature, as well as regulate CNG channel opening through Ca^{2+}-regulated proteins.

Based on the developmental sequence of the two sub-compartments, I propose that another function of the cilium is to orient the growth of the fingers in a particular direction. Both of these two functions of the cilium could be the reason why some microvillar photoreceptor cells in the animal kingdom still retain a seemingly vestigial cilium.

Finally, the novel conditional knockout technique developed in this study can be widely used in *C. elegans* to test for gene function in a spatially and temporally controlled manner.

References

Adams, N.A., Awadein, A., and Toma, H.S. (2007). The retinal ciliopathies. Ophthalmic Genet. *28*, 113–125.

Arendt, D. (2003). Evolution of eyes and photoreceptor cell types. Int. J. Dev. Biol. *47*, 563–571.

Arnaiz, O., Malinowska, A., Klotz, C., Sperling, L., Dadlez, M., Koll, F., and Cohen, J. (2009). Cildb: a knowledgebase for centrosomes and cilia. Database J. Biol. Databases Curation *2009*, bap022.

Asano, A., Asano, K., Sasaki, H., Furuse, M., and Tsukita, S. (2003). Claudins in Caenorhabditis elegans: their distribution and barrier function in the epithelium. Curr. Biol. CB *13*, 1042–1046.

Bae, Y.-K., and Barr, M.M. (2008). Sensory roles of neuronal cilia: cilia development, morphogenesis, and function in C. elegans. Front. Biosci. J. Virtual Libr. *13*, 5959–5974.

Bae, Y.-K., Qin, H., Knobel, K.M., Hu, J., Rosenbaum, J.L., and Barr, M.M. (2006). General and cell-type specific mechanisms target TRPP2/PKD-2 to cilia. Dev. Camb. Engl. *133*, 3859–3870.

Bargmann, C.I. (1998). Neurobiology of the Caenorhabditis elegans genome. Science *282*, 2028–2033.

Bargmann, C.I. (2006). Chemosensation in C. elegans. WormBook Online Rev. C Elegans Biol. 1–29.

Barrios, A., Ghosh, R., Fang, C., Emmons, S.W., and Barr, M.M. (2012). PDF-1 neuropeptide signaling modulates a neural circuit for mate-searching behavior in C. elegans. Nat. Neurosci. *15*, 1675–1682.

Beales, P.L., Elcioglu, N., Woolf, A.S., Parker, D., and Flinter, F.A. (1999). New criteria for improved diagnosis of Bardet-Biedl syndrome: results of a population survey. J. Med. Genet. *36*, 437–446.

Bechstedt, S., Albert, J.T., Kreil, D.P., Müller-Reichert, T., Göpfert, M.C., and Howard, J. (2010). A doublecortin containing microtubule-associated protein is implicated in mechanotransduction in Drosophila sensory cilia. Nat. Commun. *1*, 11.

Beise, N., and Trimble, W. (2011). Septins at a glance. J. Cell Sci. *124*, 4141–4146.

Benton, R., Sachse, S., Michnick, S.W., and Vosshall, L.B. (2006). Atypical Membrane Topology and Heteromeric Function of Drosophila Odorant Receptors In Vivo. PLoS Biol. *4*.

Berbari, N.F., Johnson, A.D., Lewis, J.S., Askwith, C.C., and Mykytyn, K. (2008a). Identification of ciliary localization sequences within the third intracellular loop of G protein-coupled receptors. Mol. Biol. Cell *19*, 1540–1547.

Berbari, N.F., Lewis, J.S., Bishop, G.A., Askwith, C.C., and Mykytyn, K. (2008b). Bardet-Biedl syndrome proteins are required for the localization of G protein-coupled receptors to primary cilia. Proc. Natl. Acad. Sci. U. S. A. *105*, 4242–4246.

Beverly, M., Anbil, S., and Sengupta, P. (2011). Degeneracy and neuromodulation among thermosensory neurons contribute to robust thermosensory behaviors in Caenorhabditis elegans. J. Neurosci. Off. J. Soc. Neurosci. *31*, 11718–11727.

Bhogaraju, S., Engel, B.D., and Lorentzen, E. (2013). Intraflagellar transport complex structure and cargo interactions. Cilia *2*, 10.

Bhowmick, R., Li, M., Sun, J., Baker, S.A., Insinna, C., and Besharse, J.C. (2009). Photoreceptor IFT complexes containing chaperones, guanylyl cyclase 1 and rhodopsin. Traffic Cph. Den. *10*, 648–663.

Bielas, S.L., Silhavy, J.L., Brancati, F., Kisseleva, M.V., Al-Gazali, L., Sztriha, L., Bayoumi, R.A., Zaki, M.S., Abdel-Aleem, A., Rosti, R.O., et al. (2009). Mutations in INPP5E, encoding inositol polyphosphate-5-phosphatase E, link phosphatidyl inositol signaling to the ciliopathies. Nat. Genet. *41*, 1032–1036.

Biron, D., Shibuya, M., Gabel, C., Wasserman, S.M., Clark, D.A., Brown, A., Sengupta, P., and Samuel, A.D.T. (2006). A diacylglycerol kinase modulates long-term thermotactic behavioral plasticity in C. elegans. Nat. Neurosci. *9*, 1499–1505.

Biron, D., Wasserman, S., Thomas, J.H., Samuel, A.D.T., and Sengupta, P. (2008). An olfactory neuron responds stochastically to temperature and modulates Caenorhabditis elegans thermotactic behavior. Proc. Natl. Acad. Sci. U. S. A. *105*, 11002–11007.

Blacque, O.E., Reardon, M.J., Li, C., McCarthy, J., Mahjoub, M.R., Ansley, S.J., Badano, J.L., Mah, A.K., Beales, P.L., Davidson, W.S., et al. (2004). Loss of C. elegans BBS-7 and BBS-8 protein function results in cilia defects and compromised intraflagellar transport. Genes Dev. *18*, 1630–1642.

Boehlke, C., Kotsis, F., Patel, V., Braeg, S., Voelker, H., Bredt, S., Beyer, T., Janusch, H., Hamann, C., Gödel, M., et al. (2010). Primary cilia regulate mTORC1 activity and cell size through Lkb1. Nat. Cell Biol. *12*, 1115–1122.

Boesze-Battaglia, K., and Schimmel, R. (1997). Cell membrane lipid composition and distribution: implications for cell function and lessons learned from photoreceptors and platelets. J. Exp. Biol. *200*, 2927–2936.

Boldt, K., Mans, D.A., Won, J., van Reeuwijk, J., Vogt, A., Kinkl, N., Letteboer, S.J.F., Hicks, W.L., Hurd, R.E., Naggert, J.K., et al. (2011). Disruption of intraflagellar protein transport in photoreceptor cilia causes Leber congenital amaurosis in humans and mice. J. Clin. Invest. *121*, 2169–2180.

De Bono, M., and Maricq, A.V. (2005). Neuronal substrates of complex behaviors in C. elegans. Annu. Rev. Neurosci. *28*, 451–501.

Bradley, J., Reuter, D., and Frings, S. (2001). Facilitation of calmodulin-mediated odor adaptation by cAMP-gated channel subunits. Science *294*, 2176–2178.

Brenner, S. (1974). The genetics of Caenorhabditis elegans. Genetics *77*, 71–94.

Bretscher, A.J., Kodama-Namba, E., Busch, K.E., Murphy, R.J., Soltesz, Z., Laurent, P., and de Bono, M. (2011). Temperature, oxygen, and salt-sensing neurons in C. elegans are carbon dioxide sensors that control avoidance behavior. Neuron *69*, 1099–1113.

Calixto, A., Chelur, D., Topalidou, I., Chen, X., and Chalfie, M. (2010). Enhanced neuronal RNAi in C. elegans using SID-1. Nat. Methods *7*, 554–559.

Calvert, P.D., Strissel, K.J., Schiesser, W.E., Pugh, E.N., Jr, and Arshavsky, V.Y. (2006). Light-driven translocation of signaling proteins in vertebrate photoreceptors. Trends Cell Biol. *16*, 560–568.

Calvert, P.D., Schiesser, W.E., and Pugh, E.N., Jr (2010). Diffusion of a soluble protein, photoactivatable GFP, through a sensory cilium. J. Gen. Physiol. *135*, 173–196.

Cevik, S., Hori, Y., Kaplan, O.I., Kida, K., Toivenon, T., Foley-Fisher, C., Cottell, D., Katada, T., Kontani, K., and Blacque, O.E. (2010). Joubert syndrome Arl13b functions at ciliary membranes and stabilizes protein transport in Caenorhabditis elegans. J. Cell Biol. *188*, 953–969.

Cevik, S., Sanders, A.A.W.M., Van Wijk, E., Boldt, K., Clarke, L., van Reeuwijk, J., Hori, Y., Horn, N., Hetterschijt, L., Wdowicz, A., et al. (2013). Active Transport and Diffusion Barriers Restrict Joubert Syndrome-Associated ARL13B/ARL-13 to an Inv-like Ciliary Membrane Subdomain. PLoS Genet. *9*, e1003977.

Chalasani, S.H., Chronis, N., Tsunozaki, M., Gray, J.M., Ramot, D., Goodman, M.B., and Bargmann, C.I. (2007). Dissecting a circuit for olfactory behaviour in Caenorhabditis elegans. Nature *450*, 63–70.

Chen, T.Y., and Yau, K.W. (1994). Direct modulation by Ca(2+)-calmodulin of cyclic nucleotide-activated channel of rat olfactory receptor neurons. Nature *368*, 545–548.

Chen, T.Y., Illing, M., Molday, L.L., Hsu, Y.T., Yau, K.W., and Molday, R.S. (1994). Subunit 2 (or beta) of retinal rod cGMP-gated cation channel is a component of the 240-kDa channel-associated protein and mediates Ca(2+)-calmodulin modulation. Proc. Natl. Acad. Sci. U. S. A. *91*, 11757–11761.

Chen, Y., Hu, C., Hsu, C.-K., Zhang, Q., Bi, C., Asnicar, M., Hsiung, H.M., Fox, N., Slieker, L.J., Yang, D.D., et al. (2002). Targeted disruption of the melanin-concentrating hormone receptor-1 results in hyperphagia and resistance to diet-induced obesity. Endocrinology *143*, 2469–2477.

Chih, B., Liu, P., Chinn, Y., Chalouni, C., Komuves, L.G., Hass, P.E., Sandoval, W., and Peterson, A.S. (2012). A ciliopathy complex at the transition zone protects the cilia as a privileged membrane domain. Nat. Cell Biol. *14*, 61–72.

Choi, S., Chatzigeorgiou, M., Taylor, K.P., Schafer, W.R., and Kaplan, J.M. (2013). Analysis of NPR-1 reveals a circuit mechanism for behavioral quiescence in C. elegans. Neuron *78*, 869–880.

Christie, M.J. (1995). Molecular and functional diversity of K+ channels. Clin. Exp. Pharmacol. Physiol. *22*, 944–951.

Chuang, C.-F., Vanhoven, M.K., Fetter, R.D., Verselis, V.K., and Bargmann, C.I. (2007). An innexin-dependent cell network establishes left-right neuronal asymmetry in C. elegans. Cell *129*, 787–799.

Chung, S.H., Clark, D.A., Gabel, C.V., Mazur, E., and Samuel, A.D.T. (2006). The role of the AFD neuron in C. elegans thermotaxis analyzed using femtosecond laser ablation. BMC Neurosci. *7*, 30.

Clark, D.A., Biron, D., Sengupta, P., and Samuel, A.D.T. (2006). The AFD sensory neurons encode multiple functions underlying thermotactic behavior in Caenorhabditis elegans. J. Neurosci. Off. J. Soc. Neurosci. *26*, 7444–7451.

Clark, D.A., Gabel, C.V., Gabel, H., and Samuel, A.D.T. (2007). Temporal activity patterns in thermosensory neurons of freely moving Caenorhabditis elegans encode spatial thermal gradients. J. Neurosci. Off. J. Soc. Neurosci. *27*, 6083–6090.

Clarke, G., Goldberg, A.F., Vidgen, D., Collins, L., Ploder, L., Schwarz, L., Molday, L.L., Rossant, J., Szél, A., Molday, R.S., et al. (2000). Rom-1 is required for rod photoreceptor viability and the regulation of disk morphogenesis. Nat. Genet. *25*, 67–73.

Clement, C.A., Ajbro, K.D., Koefoed, K., Vestergaard, M.L., Veland, I.R., Henriques de Jesus, M.P.R., Pedersen, L.B., Benmerah, A., Andersen, C.Y., Larsen, L.A., et al. (2013). TGF-β signaling is associated with endocytosis at the pocket region of the primary cilium. Cell Rep. *3*, 1806–1814.

Coburn, C.M., and Bargmann, C.I. (1996). A putative cyclic nucleotide-gated channel is required for sensory development and function in C. elegans. Neuron *17*, 695–706.

Cole, D.G., Diener, D.R., Himelblau, A.L., Beech, P.L., Fuster, J.C., and Rosenbaum, J.L. (1998). Chlamydomonas kinesin-II-dependent intraflagellar transport (IFT): IFT particles contain proteins required for ciliary assembly in Caenorhabditis elegans sensory neurons. J. Cell Biol. *141*, 993–1008.

Collingridge, P., Brownlee, C., and Wheeler, G.L. (2013). Compartmentalized Calcium Signaling in Cilia Regulates Intraflagellar Transport. Curr. Biol. CB.

Colosimo, M.E., Brown, A., Mukhopadhyay, S., Gabel, C., Lanjuin, A.E., Samuel, A.D.T., and Sengupta, P. (2004). Identification of thermosensory and olfactory neuron-specific genes via expression profiling of single neuron types. Curr. Biol. CB *14*, 2245–2251.

Corbit, K.C., Aanstad, P., Singla, V., Norman, A.R., Stainier, D.Y.R., and Reiter, J.F. (2005). Vertebrate Smoothened functions at the primary cilium. Nature *437*, 1018–1021.

Corey, D.P., García-Añoveros, J., Holt, J.R., Kwan, K.Y., Lin, S.-Y., Vollrath, M.A., Amalfitano, A., Cheung, E.L.-M., Derfler, B.H., Duggan, A., et al. (2004). TRPA1 is a candidate for the mechanosensitive transduction channel of vertebrate hair cells. Nature *432*, 723–730.

Costa, M., Raich, W., Agbunag, C., Leung, B., Hardin, J., and Priess, J.R. (1998). A putative catenin-cadherin system mediates morphogenesis of the Caenorhabditis elegans embryo. J. Cell Biol. *141*, 297–308.

Craige, B., Tsao, C.-C., Diener, D.R., Hou, Y., Lechtreck, K.-F., Rosenbaum, J.L., and Witman, G.B. (2010). CEP290 tethers flagellar transition zone microtubules to the membrane and regulates flagellar protein content. J. Cell Biol. *190*, 927–940.

Cygnar, K.D., and Zhao, H. (2009). Phosphodiesterase 1C is dispensable for rapid response termination of olfactory sensory neurons. Nat. Neurosci. *12*, 454–462.

Dabdoub, A., and Kelley, M.W. (2005). Planar cell polarity and a potential role for a Wnt morphogen gradient in stereociliary bundle orientation in the mammalian inner ear. J. Neurobiol. *64*, 446–457.

daCosta, C.J.B., and Baenziger, J.E. (2009). A lipid-dependent uncoupled conformation of the acetylcholine receptor. J. Biol. Chem. *284*, 17819–17825.

Davis, E.E., and Katsanis, N. (2012). The ciliopathies: a transitional model into systems biology of human genetic disease. Curr. Opin. Genet. Dev. *22*, 290–303.

Deane, J.A., Cole, D.G., Seeley, E.S., Diener, D.R., and Rosenbaum, J.L. (2001). Localization of intraflagellar transport protein IFT52 identifies basal body transitional fibers as the docking site for IFT particles. Curr. Biol. CB *11*, 1586–1590.

DeCaen, P.G., Delling, M., Vien, T.N., and Clapham, D.E. (2013). Direct recording and molecular identification of the calcium channel of primary cilia. Nature *504*, 315–318.

Delling, M., DeCaen, P.G., Doerner, J.F., Febvay, S., and Clapham, D.E. (2013). Primary cilia are specialized calcium signalling organelles. Nature *504*, 311–314.

Denk, W., Holt, J.R., Shepherd, G.M., and Corey, D.P. (1995). Calcium imaging of single stereocilia in hair cells: localization of transduction channels at both ends of tip links. Neuron *15*, 1311–1321.

Deretic, D., Huber, L.A., Ransom, N., Mancini, M., Simons, K., and Papermaster, D.S. (1995). rab8 in retinal photoreceptors may participate in rhodopsin transport and in rod outer segment disk morphogenesis. J. Cell Sci. *108 (Pt 1)*, 215–224.

Dickinson, D.J., Ward, J.D., Reiner, D.J., and Goldstein, B. (2013). Engineering the Caenorhabditis elegans genome using Cas9-triggered homologous recombination. Nat. Methods *10*, 1028–1034.

Digel, I. (2011). Primary thermosensory events in cells. Adv. Exp. Med. Biol. *704*, 451–468.

Dishinger, J.F., Kee, H.L., Jenkins, P.M., Fan, S., Hurd, T.W., Hammond, J.W., Truong, Y.N.-T., Margolis, B., Martens, J.R., and Verhey, K.J. (2010). Ciliary entry of the kinesin-2 motor KIF17 is regulated by importin-beta2 and RanGTP. Nat. Cell Biol. *12*, 703–710.

Domire, J.S., Green, J.A., Lee, K.G., Johnson, A.D., Askwith, C.C., and Mykytyn, K. (2011). Dopamine receptor 1 localizes to neuronal cilia in a dynamic process that requires the Bardet-Biedl syndrome proteins. Cell. Mol. Life Sci. CMLS *68*, 2951–2960.

Donaldson, J.C., Dempsey, P.J., Reddy, S., Bouton, A.H., Coffey, R.J., and Hanks, S.K. (2000). Crk-associated substrate p130(Cas) interacts with nephrocystin and both proteins localize to cell-cell contacts of polarized epithelial cells. Exp. Cell Res. *256*, 168–178.

Dubin, A.E., Liles, M.M., and Harris, G.L. (1998). The K+ channel gene ether a go-go is required for the transduction of a subset of odorants in adult Drosophila melanogaster. J. Neurosci. Off. J. Soc. Neurosci. *18*, 5603–5613.

Dutcher, S.K. (2001). Motile organelles: the importance of specific tubulin isoforms. Curr. Biol. CB *11*, R419–422.

Dwyer, N.D., Adler, C.E., Crump, J.G., L'Etoile, N.D., and Bargmann, C.I. (2001). Polarized dendritic transport and the AP-1 mu1 clathrin adaptor UNC-101 localize odorant receptors to olfactory cilia. Neuron *31*, 277–287.

Ebrey, T., and Koutalos, Y. (2001). Vertebrate photoreceptors. Prog. Retin. Eye Res. *20*, 49–94.

Edgley, M., D'Souza, A., Moulder, G., McKay, S., Shen, B., Gilchrist, E., Moerman, D., and Barstead, R. (2002). Improved detection of small deletions in complex pools of DNA. Nucleic Acids Res. *30*, e52.

Elsaesser, R., and Paysan, J. (2007). The sense of smell, its signalling pathways, and the dichotomy of cilia and microvilli in olfactory sensory cells. BMC Neurosci. *8 Suppl 3*, S1.

Emmer, B.T., Maric, D., and Engman, D.M. (2010). Molecular mechanisms of protein and lipid targeting to ciliary membranes. J. Cell Sci. *123*, 529–536.

Engel, J.E., and Wu, C.F. (1998). Genetic dissection of functional contributions of specific potassium channel subunits in habituation of an escape circuit in Drosophila. J. Neurosci. Off. J. Soc. Neurosci. *18*, 2254–2267.

Engler, C., Kandzia, R., and Marillonnet, S. (2008). A one pot, one step, precision cloning method with high throughput capability. PloS One *3*, e3647.

Erclik, T., Hartenstein, V., McInnes, R.R., and Lipshitz, H.D. (2009). Eye evolution at high resolution: the neuron as a unit of homology. Dev. Biol. *332*, 70–79.

Esposito, G., Di Schiavi, E., Bergamasco, C., and Bazzicalupo, P. (2007). Efficient and cell specific knock-down of gene function in targeted C. elegans neurons. Gene *395*, 170–176.

Ezratty, E.J., Stokes, N., Chai, S., Shah, A.S., Williams, S.E., and Fuchs, E. (2011). A role for the primary cilium in Notch signaling and epidermal differentiation during skin development. Cell *145*, 1129–1141.

Fain, G.L. (2006). Why photoreceptors die (and why they don't). BioEssays News Rev. Mol. Cell. Dev. Biol. *28*, 344–354.

Félix, M.-A., and Braendle, C. (2010). The natural history of Caenorhabditis elegans. Curr. Biol. CB *20*, R965–969.

Fettiplace, R., and Ricci, A.J. (2003). Adaptation in auditory hair cells. Curr. Opin. Neurobiol. *13*, 446–451.

Fire, A., Xu, S., Montgomery, M.K., Kostas, S.A., Driver, S.E., and Mello, C.C. (1998). Potent and specific genetic interference by double-stranded RNA in Caenorhabditis elegans. Nature *391*, 806–811.

Fisch, C., and Dupuis-Williams, P. (2011). Ultrastructure of cilia and flagella - back to the future! Biol. Cell Auspices Eur. Cell Biol. Organ. *103*, 249–270.

Flavell, S.W., Pokala, N., Macosko, E.Z., Albrecht, D.R., Larsch, J., and Bargmann, C.I. (2013). Serotonin and the neuropeptide PDF initiate and extend opposing behavioral states in C. elegans. Cell *154*, 1023–1035.

Follit, J.A., Tuft, R.A., Fogarty, K.E., and Pazour, G.J. (2006). The intraflagellar transport protein IFT20 is associated with the Golgi complex and is required for cilia assembly. Mol. Biol. Cell *17*, 3781–3792.

Follit, J.A., San Agustin, J.T., Xu, F., Jonassen, J.A., Samtani, R., Lo, C.W., and Pazour, G.J. (2008). The Golgin GMAP210/TRIP11 anchors IFT20 to the Golgi complex. PLoS Genet. *4*, e1000315.

Follit, J.A., Li, L., Vucica, Y., and Pazour, G.J. (2010). The cytoplasmic tail of fibrocystin contains a ciliary targeting sequence. J. Cell Biol. *188*, 21–28.

Frøkjaer-Jensen, C., Davis, M.W., Hopkins, C.E., Newman, B.J., Thummel, J.M., Olesen, S.-P., Grunnet, M., and Jorgensen, E.M. (2008). Single-copy insertion of transgenes in Caenorhabditis elegans. Nat. Genet. *40*, 1375–1383.

Frøkjaer-Jensen, C., Davis, M.W., Hollopeter, G., Taylor, J., Harris, T.W., Nix, P., Lofgren, R., Prestgard-Duke, M., Bastiani, M., Moerman, D.G., et al. (2010). Targeted gene deletions in C. elegans using transposon excision. Nat. Methods *7*, 451–453.

Fujiwara, M., Sengupta, P., and McIntire, S.L. (2002). Regulation of body size and behavioral state of C. elegans by sensory perception and the EGL-4 cGMP-dependent protein kinase. Neuron *36*, 1091–1102.

Fujiwara, M., Teramoto, T., Ishihara, T., Ohshima, Y., and McIntire, S.L. (2010). A novel zf-MYND protein, CHB-3, mediates guanylyl cyclase localization to sensory cilia and controls body size of Caenorhabditis elegans. PLoS Genet. *6*, e1001211.

Gaertig, J., and Wloga, D. (2008). Ciliary tubulin and its post-translational modifications. Curr. Top. Dev. Biol. *85*, 83–113.

Gallio, M., Ofstad, T.A., Macpherson, L.J., Wang, J.W., and Zuker, C.S. (2011). The coding of temperature in the Drosophila brain. Cell *144*, 614–624.

Garcia-Gonzalo, F.R., Corbit, K.C., Sirerol-Piquer, M.S., Ramaswami, G., Otto, E.A., Noriega, T.R., Seol, A.D., Robinson, J.F., Bennett, C.L., Josifova, D.J., et al. (2011). A transition zone complex regulates mammalian ciliogenesis and ciliary membrane composition. Nat. Genet. *43*, 776–784.

Geng, L., Okuhara, D., Yu, Z., Tian, X., Cai, Y., Shibazaki, S., and Somlo, S. (2006). Polycystin-2 traffics to cilia independently of polycystin-1 by using an N-terminal RVxP motif. J. Cell Sci. *119*, 1383–1395.

Gerdes, J.M., Liu, Y., Zaghloul, N.A., Leitch, C.C., Lawson, S.S., Kato, M., Beachy, P.A., Beales, P.L., DeMartino, G.N., Fisher, S., et al. (2007). Disruption of the basal body compromises proteasomal function and perturbs intracellular Wnt response. Nat. Genet. *39*, 1350–1360.

Gerstein, M.B., Lu, Z.J., Van Nostrand, E.L., Cheng, C., Arshinoff, B.I., Liu, T., Yip, K.Y., Robilotto, R., Rechtsteiner, A., Ikegami, K., et al. (2010). Integrative analysis of the Caenorhabditis elegans genome by the modENCODE project. Science *330*, 1775–1787.

Gill, G., and Ptashne, M. (1988). Negative effect of the transcriptional activator GAL4. Nature *334*, 721–724.

Gillespie, P.G., and Walker, R.G. (2001). Molecular basis of mechanosensory transduction. Nature *413*, 194–202.

Gilula, N.B., and Satir, P. (1972). The ciliary necklace. A ciliary membrane specialization. J. Cell Biol. *53*, 494–509.

Gomez, M., De Castro, E., Guarin, E., Sasakura, H., Kuhara, A., Mori, I., Bartfai, T., Bargmann, C.I., and Nef, P. (2001). Ca2+ signaling via the neuronal calcium sensor-1 regulates associative learning and memory in C. elegans. Neuron *30*, 241–248.

Goodman, M.B. (2006). Mechanosensation. WormBook Online Rev. C Elegans Biol. 1–14.

Göpfert, M.C., Humphris, A.D.L., Albert, J.T., Robert, D., and Hendrich, O. (2005). Power gain exhibited by motile mechanosensory neurons in Drosophila ears. Proc. Natl. Acad. Sci. U. S. A. *102*, 325–330.

Gray, J.M., Hill, J.J., and Bargmann, C.I. (2005). A circuit for navigation in Caenorhabditis elegans. Proc. Natl. Acad. Sci. U. S. A. *102*, 3184–3191.

Hall, D.H., Hartwieg, E., and Nguyen, K.C.Q. (2012). Modern electron microscopy methods for C. elegans. Methods Cell Biol. *107*, 93–149.

Hamada, F.N., Rosenzweig, M., Kang, K., Pulver, S.R., Ghezzi, A., Jegla, T.J., and Garrity, P.A. (2008). An internal thermal sensor controlling temperature preference in Drosophila. Nature *454*, 217–220.

Hedgecock, E.M., and Russell, R.L. (1975). Normal and mutant thermotaxis in the nematode Caenorhabditis elegans. Proc. Natl. Acad. Sci. U. S. A. *72*, 4061–4065.

Hedgecock, E.M., Culotti, J.G., Thomson, J.N., and Perkins, L.A. (1985). Axonal guidance mutants of Caenorhabditis elegans identified by filling sensory neurons with fluorescein dyes. Dev Biol *111*.

Hobert, O. (2002). PCR fusion-based approach to create reporter gene constructs for expression analysis in transgenic C. elegans. BioTechniques *32*, 728–730.

Hobert, O. (2003). Behavioral plasticity in C. elegans: paradigms, circuits, genes. J. Neurobiol. *54*, 203–223.

Hsu, Y.T., and Molday, R.S. (1993). Modulation of the cGMP-gated channel of rod photoreceptor cells by calmodulin. Nature *361*, 76–79.

Hu, J., Wittekind, S.G., and Barr, M.M. (2007). STAM and Hrs down-regulate ciliary TRP receptors. Mol. Biol. Cell *18*, 3277–3289.

Hu, Q., Milenkovic, L., Jin, H., Scott, M.P., Nachury, M.V., Spiliotis, E.T., and Nelson, W.J. (2010). A septin diffusion barrier at the base of the primary cilium maintains ciliary membrane protein distribution. Science *329*, 436–439.

Huang, P., and Schier, A.F. (2009). Dampened Hedgehog signaling but normal Wnt signaling in zebrafish without cilia. Dev. Camb. Engl. *136*, 3089–3098.

Huang, K., Diener, D.R., Mitchell, A., Pazour, G.J., Witman, G.B., and Rosenbaum, J.L. (2007). Function and dynamics of PKD2 in Chlamydomonas reinhardtii flagella. J. Cell Biol. *179*, 501–514.

Huang, L., Szymanska, K., Jensen, V.L., Janecke, A.R., Innes, A.M., Davis, E.E., Frosk, P., Li, C., Willer, J.R., Chodirker, B.N., et al. (2011). TMEM237 is mutated in individuals with a Joubert syndrome related disorder and expands the role of the TMEM family at the ciliary transition zone. Am. J. Hum. Genet. *89*, 713–730.

Huangfu, D., and Anderson, K.V. (2005). Cilia and Hedgehog responsiveness in the mouse. Proc. Natl. Acad. Sci. U. S. A. *102*, 11325–11330.

Huangfu, D., Liu, A., Rakeman, A.S., Murcia, N.S., Niswander, L., and Anderson, K.V. (2003). Hedgehog signalling in the mouse requires intraflagellar transport proteins. Nature *426*, 83–87.

Hudspeth, A.J. (1989). How the ear's works work. Nature *341*, 397–404.

Humphries, M.M., Rancourt, D., Farrar, G.J., Kenna, P., Hazel, M., Bush, R.A., Sieving, P.A., Sheils, D.M., McNally, N., Creighton, P., et al. (1997). Retinopathy induced in mice by targeted disruption of the rhodopsin gene. Nat. Genet. *15*, 216–219.

Hunnicutt, G.R., Kosfiszer, M.G., and Snell, W.J. (1990). Cell body and flagellar agglutinins in Chlamydomonas reinhardtii: the cell body plasma membrane is a reservoir for agglutinins whose migration to the flagella is regulated by a functional barrier. J. Cell Biol. *111*, 1605–1616.

Iggo, A., and Andres, K.H. (1982). Morphology of cutaneous receptors. Annu. Rev. Neurosci. *5*, 1–31.

Inada, H., Ito, H., Satterlee, J., Sengupta, P., Matsumoto, K., and Mori, I. (2006). Identification of guanylyl cyclases that function in thermosensory neurons of Caenorhabditis elegans. Genetics *172*, 2239–2252.

Inglis, P.N., Boroevich, K.A., and Leroux, M.R. (2006). Piecing together a ciliome. Trends Genet. TIG *22*, 491–500.

Inglis, P.N., Ou, G., Leroux, M.R., and Scholey, J.M. (2007). The sensory cilia of Caenorhabditis elegans. WormBook Online Rev. C Elegans Biol. 1–22.

Inoue, H., Ha, V.L., Prekeris, R., and Randazzo, P.A. (2008). Arf GTPase-activating protein ASAP1 interacts with Rab11 effector FIP3 and regulates pericentrosomal localization of transferrin receptor-positive recycling endosome. Mol. Biol. Cell *19*, 4224–4237.

Insinna, C., and Besharse, J.C. (2008). Intraflagellar transport and the sensory outer segment of vertebrate photoreceptors. Dev. Dyn. Off. Publ. Am. Assoc. Anat. *237*, 1982–1992.

Jacoby, M., Cox, J.J., Gayral, S., Hampshire, D.J., Ayub, M., Blockmans, M., Pernot, E., Kisseleva, M.V., Compère, P., Schiffmann, S.N., et al. (2009). INPP5E mutations cause primary cilium signaling defects, ciliary instability and ciliopathies in human and mouse. Nat. Genet. *41*, 1027–1031.

Jarman, A.P. (2002). Studies of mechanosensation using the fly. Hum. Mol. Genet. *11*, 1215–1218.

Jékely, G., and Arendt, D. (2006). Evolution of intraflagellar transport from coated vesicles and autogenous origin of the eukaryotic cilium. BioEssays News Rev. Mol. Cell. Dev. Biol. *28*, 191–198.

Jenkins, P.M., Hurd, T.W., Zhang, L., McEwen, D.P., Brown, R.L., Margolis, B., Verhey, K.J., and Martens, J.R. (2006). Ciliary targeting of olfactory CNG channels requires the CNGB1b subunit and the kinesin-2 motor protein, KIF17. Curr. Biol. CB *16*, 1211–1216.

Jenkins, P.M., McEwen, D.P., and Martens, J.R. (2009). Olfactory cilia: linking sensory cilia function and human disease. Chem. Senses *34*, 451–464.

Jensen, V.L., Bialas, N.J., Bishop-Hurley, S.L., Molday, L.L., Kida, K., Nguyen, P.A.T., Blacque, O.E., Molday, R.S., Leroux, M.R., and Riddle, D.L. (2010). Localization of a guanylyl cyclase to chemosensory cilia requires the novel ciliary MYND domain protein DAF-25. PLoS Genet. *6*, e1001199.

Jiang, S.-T., Chiou, Y.-Y., Wang, E., Chien, Y.-L., Ho, H.-H., Tsai, F.-J., Lin, C.-Y., Tsai, S.-P., and Li, H. (2009). Essential role of nephrocystin in photoreceptor intraflagellar transport in mouse. Hum. Mol. Genet. *18*, 1566–1577.

Jin, H., White, S.R., Shida, T., Schulz, S., Aguiar, M., Gygi, S.P., Bazan, J.F., and Nachury, M.V. (2010). The conserved Bardet-Biedl syndrome proteins assemble a coat that traffics membrane proteins to cilia. Cell *141*, 1208–1219.

Jin, X., Mohieldin, A.M., Muntean, B.S., Green, J.A., Shah, J.V., Mykytyn, K., and Nauli, S.M. (2013). Cilioplasm is a cellular compartment for calcium signaling in response to mechanical and chemical stimuli. Cell. Mol. Life Sci. CMLS.

Johnson, J.-L.F., and Leroux, M.R. (2010). cAMP and cGMP signaling: sensory systems with prokaryotic roots adopted by eukaryotic cilia. Trends Cell Biol. *20*, 435–444.

Jones, C., Roper, V.C., Foucher, I., Qian, D., Banizs, B., Petit, C., Yoder, B.K., and Chen, P. (2008). Ciliary proteins link basal body polarization to planar cell polarity regulation. Nat. Genet. *40*, 69–77.

Kaneshiro, E.S. (1990). Lipids of Ciliary and Flagellar Membranes. In Ciliary and Flagellar Membranes, R.A. Bloodgood, ed. (Springer US), pp. 241–265.

Kaplan, M.R., Cho, M.H., Ullian, E.M., Isom, L.L., Levinson, S.R., and Barres, B.A. (2001). Differential control of clustering of the sodium channels Na(v)1.2 and Na(v)1.6 at developing CNS nodes of Ranvier. Neuron *30*, 105–119.

Kaplan, O.I., Doroquez, D.B., Cevik, S., Bowie, R.V., Clarke, L., Sanders, A.A.W.M., Kida, K., Rappoport, J.Z., Sengupta, P., and Blacque, O.E. (2012). Endocytosis genes facilitate protein and membrane transport in C. elegans sensory cilia. Curr. Biol. CB *22*, 451–460.

Karan, S., Tam, B.M., Moritz, O.L., and Baehr, W. (2011). Targeting of mouse guanylate cyclase 1 (Gucy2e) to Xenopus laevis rod outer segments. Vision Res. *51*, 2304–2311.

Kaupp, U.B. (2010). Olfactory signalling in vertebrates and insects: differences and commonalities. Nat. Rev. Neurosci. *11*, 188–200.

Kee, H.L., Dishinger, J.F., Blasius, T.L., Liu, C.-J., Margolis, B., and Verhey, K.J. (2012). A size-exclusion permeability barrier and nucleoporins characterize a ciliary pore complex that regulates transport into cilia. Nat. Cell Biol. *14*, 431–437.

Kimata, T., Sasakura, H., Ohnishi, N., Nishio, N., and Mori, I. (2012). Thermotaxis of C. elegans as a model for temperature perception, neural information processing and neural plasticity. Worm *1*, 31–41.

Kimura, K.D., Miyawaki, A., Matsumoto, K., and Mori, I. (2004). The C. elegans thermosensory neuron AFD responds to warming. Curr. Biol. CB *14*, 1291–1295.

Koga, M., and Ohshima, Y. (2004). The C. elegans ceh-36 gene encodes a putative homemodomain transcription factor involved in chemosensory functions of ASE and AWC neurons. J. Mol. Biol. *336*, 579–587.

Kohn, R.E., Duerr, J.S., McManus, J.R., Duke, A., Rakow, T.L., Maruyama, H., Moulder, G., Maruyama, I.N., Barstead, R.J., and Rand, J.B. (2000). Expression of multiple UNC-13 proteins in the Caenorhabditis elegans nervous system. Mol. Biol. Cell *11*, 3441–3452.

Komatsu, H., Mori, I., Rhee, J.S., Akaike, N., and Ohshima, Y. (1996). Mutations in a cyclic nucleotide-gated channel lead to abnormal thermosensation and chemosensation in C. elegans. Neuron *17*, 707–718.

Köppen, M., Simske, J.S., Sims, P.A., Firestein, B.L., Hall, D.H., Radice, A.D., Rongo, C., and Hardin, J.D. (2001). Cooperative regulation of AJM-1 controls junctional integrity in Caenorhabditis elegans epithelia. Nat. Cell Biol. *3*, 983–991.

Körschen, H.G., Beyermann, M., Müller, F., Heck, M., Vantler, M., Koch, K.W., Kellner, R., Wolfrum, U., Bode, C., Hofmann, K.P., et al. (1999). Interaction of glutamic-acid-rich proteins with the cGMP signalling pathway in rod photoreceptors. Nature *400*, 761–766.

Kovacs, J.J., Whalen, E.J., Liu, R., Xiao, K., Kim, J., Chen, M., Wang, J., Chen, W., and Lefkowitz, R.J. (2008). Beta-arrestin-mediated localization of smoothened to the primary cilium. Science *320*, 1777–1781.

Kozminski, K.G., Johnson, K.A., Forscher, P., and Rosenbaum, J.L. (1993). A motility in the eukaryotic flagellum unrelated to flagellar beating. Proc. Natl. Acad. Sci. U. S. A. *90*, 5519–5523.

Krzyzanowski, M.C., Brueggemann, C., Ezak, M.J., Wood, J.F., Michaels, K.L., Jackson, C.A., Juang, B.-T., Collins, K.D., Yu, M.C., L'etoile, N.D., et al. (2013). The C. elegans cGMP-dependent protein kinase EGL-4 regulates nociceptive behavioral sensitivity. PLoS Genet. *9*, e1003619.

Kuhara, A., Okumura, M., Kimata, T., Tanizawa, Y., Takano, R., Kimura, K.D., Inada, H., Matsumoto, K., and Mori, I. (2008). Temperature sensing by an olfactory neuron in a circuit controlling behavior of C. elegans. Science *320*, 803–807.

Kuhara, A., Ohnishi, N., Shimowada, T., and Mori, I. (2011). Neural coding in a single sensory neuron controlling opposite seeking behaviours in Caenorhabditis elegans. Nat. Commun. *2*, 355.

Kulaga, H.M., Leitch, C.C., Eichers, E.R., Badano, J.L., Lesemann, A., Hoskins, B.E., Lupski, J.R., Beales, P.L., Reed, R.R., and Katsanis, N. (2004). Loss of BBS proteins causes anosmia in humans and defects in olfactory cilia structure and function in the mouse. Nat. Genet. *36*, 994–998.

L'Etoile, N.D., Coburn, C.M., Eastham, J., Kistler, A., Gallegos, G., and Bargmann, C.I. (2002). The cyclic GMP-dependent protein kinase EGL-4 regulates olfactory adaptation in C. elegans. Neuron *36*, 1079–1089.

Lancaster, M.A., Louie, C.M., Silhavy, J.L., Sintasath, L., Decambre, M., Nigam, S.K., Willert, K., and Gleeson, J.G. (2009). Impaired Wnt-beta-catenin signaling disrupts adult renal homeostasis and leads to cystic kidney ciliopathy. Nat. Med. *15*, 1046–1054.

Lange, K. (1999). Microvillar Ca++ signaling: a new view of an old problem. J. Cell. Physiol. *180*, 19–34.

Larsson, M.C., Domingos, A.I., Jones, W.D., Chiappe, M.E., Amrein, H., and Vosshall, L.B. (2004). Or83b encodes a broadly expressed odorant receptor essential for Drosophila olfaction. Neuron *43*, 703–714.

Lechtreck, K.-F., Johnson, E.C., Sakai, T., Cochran, D., Ballif, B.A., Rush, J., Pazour, G.J., Ikebe, M., and Witman, G.B. (2009). The Chlamydomonas reinhardtii BBSome is an IFT cargo required for export of specific signaling proteins from flagella. J. Cell Biol. *187*, 1117–1132.

Leinders-Zufall, T., Ma, M., and Zufall, F. (1999). Impaired odor adaptation in olfactory receptor neurons after inhibition of Ca2+/calmodulin kinase II. J. Neurosci. Off. J. Soc. Neurosci. *19*, RC19.

Leinders-Zufall, T., Cockerham, R.E., Michalakis, S., Biel, M., Garbers, D.L., Reed, R.R., Zufall, F., and Munger, S.D. (2007). Contribution of the receptor guanylyl cyclase GC-D to chemosensory function in the olfactory epithelium. Proc. Natl. Acad. Sci. *104*, 14507–14512.

Lem, J., Krasnoperova, N.V., Calvert, P.D., Kosaras, B., Cameron, D.A., Nicolò, M., Makino, C.L., and Sidman, R.L. (1999). Morphological, physiological, and biochemical changes in rhodopsin knockout mice. Proc. Natl. Acad. Sci. U. S. A. *96*, 736–741.

Li, C., and Kim, K. (2008). Neuropeptides. WormBook Online Rev. C Elegans Biol. 1–36.

Li, Y., Zhao, Y., Huang, X., Lin, X., Guo, Y., Wang, D., Li, C., and Wang, D. (2013). Serotonin control of thermotaxis memory behavior in nematode Caenorhabditis elegans. PloS One *8*, e77779.

Lienkamp, S., Ganner, A., and Walz, G. (2012). Inversin, Wnt signaling and primary cilia. Differ. Res. Biol. Divers. *83*, S49–55.

Lin, Y.-C., Niewiadomski, P., Lin, B., Nakamura, H., Phua, S.C., Jiao, J., Levchenko, A., Inoue, T., Rohatgi, R., and Inoue, T. (2013). Chemically inducible diffusion trap at cilia reveals molecular sieve–like barrier. Nat. Chem. Biol. *9*, 437–443.

Liu, S., Schulze, E., and Baumeister, R. (2012). Temperature- and touch-sensitive neurons couple CNG and TRPV channel activities to control heat avoidance in Caenorhabditis elegans. PloS One *7*, e32360.

Loewen, C.J., and Molday, R.S. (2000). Disulfide-mediated oligomerization of Peripherin/Rds and Rom-1 in photoreceptor disk membranes. Implications for photoreceptor outer segment morphogenesis and degeneration. J. Biol. Chem. *275*, 5370–5378.

Lumpkin, E.A., and Hudspeth, A.J. (1995). Detection of Ca2+ entry through mechanosensitive channels localizes the site of mechanoelectrical transduction in hair cells. Proc. Natl. Acad. Sci. U. S. A. *92*, 10297–10301.

Luo, L., Cook, N., Venkatachalam, V., Martinez-Velazquez, L.A., Zhang, X., Calvo, A.C., Hawk, J., Macinnis, B.L., Frank, M., Ng, J.H.R., et al. (2014). Bidirectional thermotaxis in Caenorhabditis elegans is mediated by distinct sensorimotor strategies driven by the AFD thermosensory neurons. Proc. Natl. Acad. Sci. U. S. A. *111*, 2776–2781.

Mahjoub, M.R., Trapp, M.L., and Quarmby, L.M. (2005). NIMA-related kinases defective in murine models of polycystic kidney diseases localize to primary cilia and centrosomes. J. Am. Soc. Nephrol. JASN *16*, 3485–3489.

Marraffini, L.A., and Sontheimer, E.J. (2010). CRISPR interference: RNA-directed adaptive immunity in bacteria and archaea. Nat. Rev. Genet. *11*, 181–190.

Mashukova, A., Spehr, M., Hatt, H., and Neuhaus, E.M. (2006). Beta-arrestin2-mediated internalization of mammalian odorant receptors. J. Neurosci. Off. J. Soc. Neurosci. *26*, 9902–9912.

Mazelova, J., Astuto-Gribble, L., Inoue, H., Tam, B.M., Schonteich, E., Prekeris, R., Moritz, O.L., Randazzo, P.A., and Deretic, D. (2009a). Ciliary targeting motif VxPx directs assembly of a trafficking module through Arf4. EMBO J. *28*, 183–192.

Mazelova, J., Ransom, N., Astuto-Gribble, L., Wilson, M.C., and Deretic, D. (2009b). Syntaxin 3 and SNAP-25 pairing, regulated by omega-3 docosahexaenoic acid, controls the delivery of rhodopsin for the biogenesis of cilia-derived sensory organelles, the rod outer segments. J. Cell Sci. *122*, 2003–2013.

McCulloch, R.K., Choong, C.S., and Hurley, D.M. (1995). An evaluation of competitor type and size for use in the determination of mRNA by competitive PCR. PCR Methods Appl. *4*, 219–226.

McEwen, D.P., Koenekoop, R.K., Khanna, H., Jenkins, P.M., Lopez, I., Swaroop, A., and Martens, J.R. (2007). Hypomorphic CEP290/NPHP6 mutations result in anosmia caused by the selective loss of G proteins in cilia of olfactory sensory neurons. Proc. Natl. Acad. Sci. U. S. A. *104*, 15917–15922.

McKemy, D.D. (2007). Temperature sensing across species. Pflüg. Arch. Eur. J. Physiol. *454*, 777–791.

McMahon, L., Legouis, R., Vonesch, J.L., and Labouesse, M. (2001). Assembly of C. elegans apical junctions involves positioning and compaction by LET-413 and protein aggregation by the MAGUK protein DLG-1. J. Cell Sci. *114*, 2265–2277.

Menco, B.P. (1984). Ciliated and microvillous structures of rat olfactory and nasal respiratory epithelia. A study using ultra-rapid cryo-fixation followed by freeze-substitution or freeze-etching. Cell Tissue Res. *235*, 225–241.

Menco, B.P. (1997). Ultrastructural aspects of olfactory signaling. Chem. Senses *22*, 295–311.

Meyer, M.R., Angele, A., Kremmer, E., Kaupp, U.B., and Müller, F. (2000). A cGMP-signaling pathway in a subset of olfactory sensory neurons. Proc. Natl. Acad. Sci. *97*, 10595–10600.

Michael F., B. (1997). Chapter 8 Influence of Nonlamellar-Forming Lipids on Rhodopsin. In Lipid Polymorphism and Membrane Properties, (Academic Press), pp. 285–356.

Milenkovic, L., Scott, M.P., and Rohatgi, R. (2009). Lateral transport of Smoothened from the plasma membrane to the membrane of the cilium. J. Cell Biol. *187*, 365–374.

Mok, C.A., Healey, M.P., Shekhar, T., Leroux, M.R., Héon, E., and Zhen, M. (2011). Mutations in a guanylate cyclase GCY-35/GCY-36 modify Bardet-Biedl syndrome-associated phenotypes in Caenorhabditis elegans. PLoS Genet. *7*, e1002335.

Mollet, G., Silbermann, F., Delous, M., Salomon, R., Antignac, C., and Saunier, S. (2005). Characterization of the nephrocystin/nephrocystin-4 complex and subcellular localization of nephrocystin-4 to primary cilia and centrosomes. Hum. Mol. Genet. *14*, 645–656.

Mori, I., and Ohshima, Y. (1995). Neural regulation of thermotaxis in Caenorhabditis elegans. Nature *376*, 344–348.

Moritz, O.L., Tam, B.M., Hurd, L.L., Peränen, J., Deretic, D., and Papermaster, D.S. (2001). Mutant rab8 Impairs docking and fusion of rhodopsin-bearing post-Golgi membranes and causes cell death of transgenic Xenopus rods. Mol. Biol. Cell *12*, 2341–2351.

Mukhopadhyay, S., Lu, Y., Shaham, S., and Sengupta, P. (2008). Sensory signaling-dependent remodeling of olfactory cilia architecture in C. elegans. Dev. Cell *14*, 762–774.

Mukhopadhyay, S., Wen, X., Chih, B., Nelson, C.D., Lane, W.S., Scales, S.J., and Jackson, P.K. (2010). TULP3 bridges the IFT-A complex and membrane phosphoinositides to promote trafficking of G protein-coupled receptors into primary cilia. Genes Dev. *24*, 2180–2193.

Mukhopadhyay, S., Wen, X., Ratti, N., Loktev, A., Rangell, L., Scales, S.J., and Jackson, P.K. (2013). The ciliary G-protein-coupled receptor Gpr161 negatively regulates the Sonic hedgehog pathway via cAMP signaling. Cell *152*, 210–223.

Nachury, M.V., Loktev, A.V., Zhang, Q., Westlake, C.J., Peränen, J., Merdes, A., Slusarski, D.C., Scheller, R.H., Bazan, J.F., Sheffield, V.C., et al. (2007). A core complex of BBS proteins cooperates with the GTPase Rab8 to promote ciliary membrane biogenesis. Cell *129*, 1201–1213.

Nachury, M.V., Seeley, E.S., and Jin, H. (2010). Trafficking to the ciliary membrane: how to get across the periciliary diffusion barrier? Annu. Rev. Cell Dev. Biol. *26*, 59–87.

Najafi, M., Maza, N.A., and Calvert, P.D. (2012). Steric volume exclusion sets soluble protein concentrations in photoreceptor sensory cilia. Proc. Natl. Acad. Sci. U. S. A. *109*, 203–208.

Narayan, A., Laurent, G., and Sternberg, P.W. (2011). Transfer characteristics of a thermosensory synapse in Caenorhabditis elegans. Proc. Natl. Acad. Sci. U. S. A. *108*, 9667–9672.

Neugebauer, J.M., Amack, J.D., Peterson, A.G., Bisgrove, B.W., and Yost, H.J. (2009). FGF signalling during embryo development regulates cilia length in diverse epithelia. Nature *458*, 651–654.

Newton, F.G., zur Lage, P.I., Karak, S., Moore, D.J., Göpfert, M.C., and Jarman, A.P. (2012). Forkhead transcription factor Fd3F cooperates with Rfx to regulate a gene expression program for mechanosensory cilia specialization. Dev. Cell *22*, 1221–1233.

Ni, L., Bronk, P., Chang, E.C., Lowell, A.M., Flam, J.O., Panzano, V.C., Theobald, D.L., Griffith, L.C., and Garrity, P.A. (2013). A gustatory receptor paralogue controls rapid warmth avoidance in Drosophila. Nature *500*, 580–584.

Nishio, N., Mohri-Shiomi, A., Nishida, Y., Hiramatsu, N., Kodama-Namba, E., Kimura, K.D., Kuhara, A., and Mori, I. (2012). A novel and conserved protein AHO-3 is required for thermotactic plasticity associated with feeding states in Caenorhabditis elegans. Genes Cells Devoted Mol. Cell. Mech. *17*, 365–386.

Niven, J.E., and Laughlin, S.B. (2008). Energy limitation as a selective pressure on the evolution of sensory systems. J. Exp. Biol. *211*, 1792–1804.

Norman, R.X., Ko, H.W., Huang, V., Eun, C.M., Abler, L.L., Zhang, Z., Sun, X., and Eggenschwiler, J.T. (2009). Tubby-like protein 3 (TULP3) regulates patterning in the mouse embryo through inhibition of Hedgehog signaling. Hum. Mol. Genet. *18*, 1740–1754.

Ocbina, P.J.R., Tuson, M., and Anderson, K.V. (2009). Primary cilia are not required for normal canonical Wnt signaling in the mouse embryo. PloS One *4*, e6839.

Oh, E.C., and Katsanis, N. (2013). Context-dependent regulation of Wnt signaling through the primary cilium. J. Am. Soc. Nephrol. JASN *24*, 10–18.

Ohnishi, N., Kuhara, A., Nakamura, F., Okochi, Y., and Mori, I. (2011). Bidirectional regulation of thermotaxis by glutamate transmissions in Caenorhabditis elegans. EMBO J. *30*, 1376–1388.

Okawa, H., Sampath, A.P., Laughlin, S.B., and Fain, G.L. (2008). ATP consumption by mammalian rod photoreceptors in darkness and in light. Curr. Biol. CB *18*, 1917–1921.

Orozco, J.T., Wedaman, K.P., Signor, D., Brown, H., Rose, L., and Scholey, J.M. (1999). Movement of motor and cargo along cilia. Nature *398*, 674.

Ou, G., Blacque, O.E., Snow, J.J., Leroux, M.R., and Scholey, J.M. (2005). Functional coordination of intraflagellar transport motors. Nature *436*, 583–587.

Ou, G., Koga, M., Blacque, O.E., Murayama, T., Ohshima, Y., Schafer, J.C., Li, C., Yoder, B.K., Leroux, M.R., and Scholey, J.M. (2007). Sensory ciliogenesis in Caenorhabditis elegans: assignment of IFT components into distinct modules based on transport and phenotypic profiles. Mol. Biol. Cell *18*, 1554–1569.

Ovchinnikov YuA, Abdulaev, N.G., and Bogachuk, A.S. (1988). Two adjacent cysteine residues in the C-terminal cytoplasmic fragment of bovine rhodopsin are palmitylated. FEBS Lett. *230*, 1–5.

Papermaster, D.S., Schneider, B.G., and Besharse, J.C. (1985). Vesicular transport of newly synthesized opsin from the Golgi apparatus toward the rod outer segment. Ultrastructural immunocytochemical and autoradiographic evidence in Xenopus retinas. Invest. Ophthalmol. Vis. Sci. *26*, 1386–1404.

Pedersen, L.B., Geimer, S., Sloboda, R.D., and Rosenbaum, J.L. (2003). The Microtubule plus end-tracking protein EB1 is localized to the flagellar tip and basal bodies in Chlamydomonas reinhardtii. Curr. Biol. CB *13*, 1969–1974.

Perkins, L.A., Hedgecock, E.M., Thomson, J.N., and Culotti, J.G. (1986). Mutant sensory cilia in the nematode Caenorhabditis elegans. Dev. Biol. *117*, 456–487.

Pickles, J.O., Comis, S.D., and Osborne, M.P. (1984). Cross-links between stereocilia in the guinea pig organ of Corti, and their possible relation to sensory transduction. Hear. Res. *15*, 103–112.

Poetsch, A., Molday, L.L., and Molday, R.S. (2001). The cGMP-gated channel and related glutamic acid-rich proteins interact with peripherin-2 at the rim region of rod photoreceptor disc membranes. J. Biol. Chem. *276*, 48009–48016.

Poo, M., and Cone, R.A. (1974). Lateral diffusion of rhodopsin in the photoreceptor membrane. Nature *247*, 438–441.

Potokar, M., Kreft, M., Li, L., Daniel Andersson, J., Pangrsic, T., Chowdhury, H.H., Pekny, M., and Zorec, R. (2007). Cytoskeleton and vesicle mobility in astrocytes. Traffic Cph. Den. *8*, 12–20.

Qin, H., Burnette, D.T., Bae, Y.-K., Forscher, P., Barr, M.M., and Rosenbaum, J.L. (2005). Intraflagellar transport is required for the vectorial movement of TRPV channels in the ciliary membrane. Curr. Biol. CB *15*, 1695–1699.

Ramot, D., MacInnis, B.L., and Goodman, M.B. (2008). Bidirectional temperature-sensing by a single thermosensory neuron in C. elegans. Nat. Neurosci. *11*, 908–915.

Reiter, J.F., Blacque, O.E., and Leroux, M.R. (2012). The base of the cilium: roles for transition fibres and the transition zone in ciliary formation, maintenance and compartmentalization. EMBO Rep. *13*, 608–618.

Robert, V., and Bessereau, J.-L. (2007). Targeted engineering of the Caenorhabditis elegans genome following Mos1-triggered chromosomal breaks. EMBO J. *26*, 170–183.

Rogers, K.K., Wilson, P.D., Snyder, R.W., Zhang, X., Guo, W., Burrow, C.R., and Lipschutz, J.H. (2004). The exocyst localizes to the primary cilium in MDCK cells. Biochem. Biophys. Res. Commun. *319*, 138–143.

Rosenbaum, J.L., and Witman, G.B. (2002). Intraflagellar transport. Nat. Rev. Mol. Cell Biol. *3*, 813–825.

Ryu, W.S., and Samuel, A.D.T. (2002). Thermotaxis in Caenorhabditis elegans analyzed by measuring responses to defined Thermal stimuli. J. Neurosci. Off. J. Soc. Neurosci. *22*, 5727–5733.

Sang, L., Miller, J.J., Corbit, K.C., Giles, R.H., Brauer, M.J., Otto, E.A., Baye, L.M., Wen, X., Scales, S.J., Kwong, M., et al. (2011). Mapping the NPHP-JBTS-MKS protein network reveals ciliopathy disease genes and pathways. Cell *145*, 513–528.

Sato, K., Pellegrino, M., Nakagawa, T., Nakagawa, T., Vosshall, L.B., and Touhara, K. (2008). Insect olfactory receptors are heteromeric ligand-gated ion channels. Nature *452*, 1002–1006.

Satterlee, J.S., Sasakura, H., Kuhara, A., Berkeley, M., Mori, I., and Sengupta, P. (2001). Specification of thermosensory neuron fate in C. elegans requires ttx-1, a homolog of otd/Otx. Neuron *31*, 943–956.

Schafer, J.C., Haycraft, C.J., Thomas, J.H., Yoder, B.K., and Swoboda, P. (2003). XBX-1 encodes a dynein light intermediate chain required for retrograde intraflagellar transport and cilia assembly in Caenorhabditis elegans. Mol. Biol. Cell *14*, 2057–2070.

Schepers, R.J., and Ringkamp, M. (2010). Thermoreceptors and thermosensitive afferents. Neurosci. Biobehav. Rev. *34*, 177–184.

Schmidt, D., Jiang, Q.-X., and MacKinnon, R. (2006). Phospholipids and the origin of cationic gating charges in voltage sensors. Nature *444*, 775–779.

Schneider, L., Clement, C.A., Teilmann, S.C., Pazour, G.J., Hoffmann, E.K., Satir, P., and Christensen, S.T. (2005). PDGFRalphaalpha signaling is regulated through the primary cilium in fibroblasts. Curr. Biol. CB *15*, 1861–1866.

Scholey, J.M. (2003). Intraflagellar transport. Annu. Rev. Cell Dev. Biol. *19*, 423–443.

Sedmak, T., and Wolfrum, U. (2011). Intraflagellar transport proteins in ciliogenesis of photoreceptor cells. Biol. Cell Auspices Eur. Cell Biol. Organ. *103*, 449–466.

Senti, G., and Swoboda, P. (2008). Distinct isoforms of the RFX transcription factor DAF-19 regulate ciliogenesis and maintenance of synaptic activity. Mol. Biol. Cell *19*, 5517–5528.

Senti, G., Ezcurra, M., Löbner, J., Schafer, W.R., and Swoboda, P. (2009). Worms with a single functional sensory cilium generate proper neuron-specific behavioral output. Genetics *183*, 595–605, 1SI–3SI.

Shah, A.S., Ben-Shahar, Y., Moninger, T.O., Kline, J.N., and Welsh, M.J. (2009). Motile cilia of human airway epithelia are chemosensory. Science *325*, 1131–1134.

Shanbhag, S.R., Müller, B., and Steinbrecht, R.A. (1999). Atlas of olfactory organs of Drosophila melanogaster: 1. Types, external organization, innervation and distribution of olfactory sensilla. Int. J. Insect Morphol. Embryol. *28*, 377–397.

Shen, W.L., Kwon, Y., Adegbola, A.A., Luo, J., Chess, A., and Montell, C. (2011). Function of rhodopsin in temperature discrimination in Drosophila. Science *331*, 1333–1336.

Shiba, D., Yamaoka, Y., Hagiwara, H., Takamatsu, T., Hamada, H., and Yokoyama, T. (2009). Localization of Inv in a distinctive intraciliary compartment requires the C-terminal ninein-homolog-containing region. J. Cell Sci. *122*, 44–54.

Shiba, D., Manning, D.K., Koga, H., Beier, D.R., and Yokoyama, T. (2010). Inv acts as a molecular anchor for Nphp3 and Nek8 in the proximal segment of primary cilia. Cytoskelet. Hoboken NJ *67*, 112–119.

Sidi, S., Friedrich, R.W., and Nicolson, T. (2003). NompC TRP channel required for vertebrate sensory hair cell mechanotransduction. Science *301*, 96–99.

Silverman, M.A., and Leroux, M.R. (2009). Intraflagellar transport and the generation of dynamic, structurally and functionally diverse cilia. Trends Cell Biol. *19*, 306–316.

Simons, M., Gloy, J., Ganner, A., Bullerkotte, A., Bashkurov, M., Krönig, C., Schermer, B., Benzing, T., Cabello, O.A., Jenny, A., et al. (2005). Inversin, the gene product mutated in nephronophthisis type II, functions as a molecular switch between Wnt signaling pathways. Nat. Genet. *37*, 537–543.

Simske, J.S., and Hardin, J. (2011). Claudin family proteins in Caenorhabditis elegans. Methods Mol. Biol. Clifton NJ *762*, 147–169.

Sloboda, R.D., and Howard, L. (2007). Localization of EB1, IFT polypeptides, and kinesin-2 in Chlamydomonas flagellar axonemes via immunogold scanning electron microscopy. Cell Motil. Cytoskeleton *64*, 446–460.

Snow, J.J., Ou, G., Gunnarson, A.L., Walker, M.R.S., Zhou, H.M., Brust-Mascher, I., and Scholey, J.M. (2004). Two anterograde intraflagellar transport motors cooperate to build sensory cilia on C. elegans neurons. Nat. Cell Biol. *6*, 1109–1113.

Speese, S., Petrie, M., Schuske, K., Ailion, M., Ann, K., Iwasaki, K., Jorgensen, E.M., and Martin, T.F.J. (2007). UNC-31 (CAPS) is required for dense-core vesicle but not synaptic vesicle exocytosis in Caenorhabditis elegans. J. Neurosci. Off. J. Soc. Neurosci. *27*, 6150–6162.

Stinchcomb, D.T., Shaw, J.E., Carr, S.H., and Hirsh, D. (1985). Extrachromosomal DNA transformation of Caenorhabditis elegans. Mol. Cell. Biol. *5*, 3484–3496.

Styers, M.L., Kowalczyk, A.P., and Faundez, V. (2005). Intermediate filaments and vesicular membrane traffic: the odd couple's first dance? Traffic Cph. Den. *6*, 359–365.

Su, S., Phua, S.C., DeRose, R., Chiba, S., Narita, K., Kalugin, P.N., Katada, T., Kontani, K., Takeda, S., and Inoue, T. (2013). Genetically encoded calcium indicator illuminates calcium dynamics in primary cilia. Nat. Methods *10*, 1105–1107.

Sugi, T., Nishida, Y., and Mori, I. (2011). Regulation of behavioral plasticity by systemic temperature signaling in Caenorhabditis elegans. Nat. Neurosci. *14*, 984–992.

Svendsen, P.C., and McGhee, J.D. (1995). The C. elegans neuronally expressed homeobox gene ceh-10 is closely related to genes expressed in the vertebrate eye. Dev. Camb. Engl. *121*, 1253–1262.

Swierczek, N.A., Giles, A.C., Rankin, C.H., and Kerr, R.A. (2011). High-throughput behavioral analysis in C. elegans. Nat. Methods *8*, 592–598.

Swoboda, P., Adler, H.T., and Thomas, J.H. (2000). The RFX-type transcription factor DAF-19 regulates sensory neuron cilium formation in C. elegans. Mol. Cell *5*, 411–421.

Szymanska, K., and Johnson, C.A. (2012). The transition zone: an essential functional compartment of cilia. Cilia *1*, 10.

Tadenev, A.L.D., Kulaga, H.M., May-Simera, H.L., Kelley, M.W., Katsanis, N., and Reed, R.R. (2011). Loss of Bardet-Biedl syndrome protein-8 (BBS8) perturbs olfactory function, protein localization, and axon targeting. Proc. Natl. Acad. Sci. U. S. A. *108*, 10320–10325.

Takeuchi, H., and Kurahashi, T. (2002). Photolysis of caged cyclic AMP in the ciliary cytoplasm of the newt olfactory receptor cell. J. Physiol. *541*, 825–833.

Tan, P.L., Barr, T., Inglis, P.N., Mitsuma, N., Huang, S.M., Garcia-Gonzalez, M.A., Bradley, B.A., Coforio, S., Albrecht, P.J., Watnick, T., et al. (2007). Loss of Bardet Biedl syndrome proteins causes defects in peripheral sensory innervation and function. Proc. Natl. Acad. Sci. U. S. A. *104*, 17524–17529.

Tao, B., Bu, S., Yang, Z., Siroky, B., Kappes, J.C., Kispert, A., and Guay-Woodford, L.M. (2009). Cystin localizes to primary cilia via membrane microdomains and a targeting motif. J. Am. Soc. Nephrol. JASN *20*, 2570–2580.

Taschner, M., Bhogaraju, S., Vetter, M., Morawetz, M., and Lorentzen, E. (2011). Biochemical mapping of interactions within the intraflagellar transport (IFT) B core complex: IFT52 binds directly to four other IFT-B subunits. J. Biol. Chem. *286*, 26344–26352.

Thiele, J., Klumpp, S., Schultz, J.E., and Bardele, C.F. (1982). Differential distribution of voltage-dependent calcium channels and guanylate cyclase in the excitable ciliary membrane from Paramecium tetraurelia. Eur J Cell Biol *28*.

Tilney, L.G., Tilney, M.S., and DeRosier, D.J. (1992). Actin filaments, stereocilia, and hair cells: how cells count and measure. Annu. Rev. Cell Biol. *8*, 257–274.

Tobin, D., Madsen, D., Kahn-Kirby, A., Peckol, E., Moulder, G., Barstead, R., Maricq, A., and Bargmann, C. (2002). Combinatorial expression of TRPV channel proteins defines their sensory functions and subcellular localization in C. elegans neurons. Neuron *35*, 307–318.

Tong, J.X., Eichler, M.E., and Rich, K.M. (1996). Intracellular calcium levels influence apoptosis in mature sensory neurons after trophic factor deprivation. Exp. Neurol. *138*, 45–52.

Trivedi, D., Colin, E., Louie, C.M., and Williams, D.S. (2012). Live-cell imaging evidence for the ciliary transport of rod photoreceptor opsin by heterotrimeric kinesin-2. J. Neurosci. Off. J. Soc. Neurosci. *32*, 10587–10593.

Tsalik, E.L., and Hobert, O. (2003). Functional mapping of neurons that control locomotory behavior in Caenorhabditis elegans. J. Neurobiol. *56*, 178–197.

Tsujikawa, M., and Malicki, J. (2004). Intraflagellar Transport Genes Are Essential for Differentiation and Survival of Vertebrate Sensory Neurons. Neuron *42*, 703–716.

Tyler, K.M., Fridberg, A., Toriello, K.M., Olson, C.L., Cieslak, J.A., Hazlett, T.L., and Engman, D.M. (2009). Flagellar membrane localization via association with lipid rafts. J. Cell Sci. *122*, 859–866.

Valentine, M.S., Rajendran, A., Yano, J., Weeraratne, S.D., Beisson, J., Cohen, J., Koll, F., and Van Houten, J. (2012). Paramecium BBS genes are key to presence of channels in Cilia. Cilia *1*, 16.

Vieira, O.V., Gaus, K., Verkade, P., Fullekrug, J., Vaz, W.L.C., and Simons, K. (2006). FAPP2, cilium formation, and compartmentalization of the apical membrane in polarized Madin-Darby canine kidney (MDCK) cells. Proc. Natl. Acad. Sci. U. S. A. *103*, 18556–18561.

Voutev, R., and Hubbard, E.J.A. (2008). A “FLP-Out” system for controlled gene expression in Caenorhabditis elegans. Genetics *180*, 103–119.

Wakabayashi, T., Kitagawa, I., and Shingai, R. (2004). Neurons regulating the duration of forward locomotion in Caenorhabditis elegans. Neurosci. Res. *50*, 103–111.

Walker, R.G., Willingham, A.T., and Zuker, C.S. (2000). A Drosophila Mechanosensory Transduction Channel. Science *287*, 2229–2234.

Wallingford, J.B., and Mitchell, B. (2011). Strange as it may seem: the many links between Wnt signaling, planar cell polarity, and cilia. Genes Dev. *25*, 201–213.

Wang, D., O'Halloran, D., and Goodman, M.B. (2013). GCY-8, PDE-2, and NCS-1 are critical elements of the cGMP-dependent thermotransduction cascade in the AFD neurons responsible for C. elegans thermotaxis. J. Gen. Physiol. *142*, 437–449.

Wann, A.K.T., Chapple, J.P., and Knight, M.M. (2014). The primary cilium influences interleukin-1β-induced NFκB signalling by regulating IKK activity. Cell. Signal.

Warburton-Pitt, S.R.F., Jauregui, A.R., Li, C., Wang, J., Leroux, M.R., and Barr, M.M. (2012). Ciliogenesis in Caenorhabditis elegans requires genetic interactions between ciliary middle segment localized NPHP-2 (inversin) and transition zone-associated proteins. J. Cell Sci. *125*, 2592–2603.

Ward, A., Liu, J., Feng, Z., and Xu, X.Z.S. (2008). Light-sensitive neurons and channels mediate phototaxis in C. elegans. Nat. Neurosci. *11*, 916–922.

Ward, S., Thomson, N., White, J.G., and Brenner, S. (1975). Electron microscopical reconstruction of the anterior sensory anatomy of the nematode Caenorhabditis elegans.?2UU. J. Comp. Neurol. *160*, 313–337.

Wasserman, S.M., Beverly, M., Bell, H.W., and Sengupta, P. (2011). Regulation of response properties and operating range of the AFD thermosensory neurons by cGMP signaling. Curr. Biol. CB *21*, 353–362.

Wei, J., Zhao, A.Z., Chan, G.C., Baker, L.P., Impey, S., Beavo, J.A., and Storm, D.R. (1998). Phosphorylation and inhibition of olfactory adenylyl cyclase by CaM kinase II in Neurons: a mechanism for attenuation of olfactory signals. Neuron *21*, 495–504.

Wei, Q., Zhang, Y., Li, Y., Zhang, Q., Ling, K., and Hu, J. (2012a). The BBSome controls IFT assembly and turnaround in cilia. Nat. Cell Biol. *14*, 950–957.

Wei, X., Potter, C.J., Luo, L., and Shen, K. (2012b). Controlling gene expression with the Q repressible binary expression system in Caenorhabditis elegans. Nat. Methods *9*, 391–395.

Weinshenker, D., Wei, A., Salkoff, L., and Thomas, J.H. (1999). Block of an ether-a-go-go-like K(+) channel by imipramine rescues egl-2 excitation defects in Caenorhabditis elegans. J. Neurosci. Off. J. Soc. Neurosci. *19*, 9831–9840.

Wheway, G., Parry, D.A., and Johnson, C.A. (2013). The role of primary cilia in the development and disease of the retina. Organogenesis *10*.

White, J.G., Southgate, E., Thomson, J.N., and Brenner, S. (1986). The structure of the nervous system of the nematode Caenorhabditis elegans. Philos. Trans. R. Soc. Lond. B. Biol. Sci. *314*, 1–340.

Wicher, D., Schäfer, R., Bauernfeind, R., Stensmyr, M.C., Heller, R., Heinemann, S.H., and Hansson, B.S. (2008). Drosophila odorant receptors are both ligand-gated and cyclic-nucleotide-activated cation channels. Nature *452*, 1007–1011.

Wicks, S.R., de Vries, C.J., van Luenen, H.G., and Plasterk, R.H. (2000). CHE-3, a cytosolic dynein heavy chain, is required for sensory cilia structure and function in Caenorhabditis elegans. Dev. Biol. *221*, 295–307.

Williams, C.L., Li, C., Kida, K., Inglis, P.N., Mohan, S., Semenec, L., Bialas, N.J., Stupay, R.M., Chen, N., Blacque, O.E., et al. (2011). MKS and NPHP modules cooperate to establish basal body/transition zone membrane associations and ciliary gate function during ciliogenesis. J. Cell Biol. *192*, 1023–1041.

Wojtyniak, M., Brear, A.G., O'Halloran, D.M., and Sengupta, P. (2013). Cell- and subunit-specific mechanisms of CNG channel ciliary trafficking and localization in C. elegans. J. Cell Sci. *126*, 4381–4395.

Wright, K.J., Baye, L.M., Olivier-Mason, A., Mukhopadhyay, S., Sang, L., Kwong, M., Wang, W., Pretorius, P.R., Sheffield, V.C., Sengupta, P., et al. (2011). An ARL3-UNC119-RP2 GTPase cycle targets myristoylated NPHP3 to the primary cilium. Genes Dev. *25*, 2347–2360.

Yack, J.E. (2004). The structure and function of auditory chordotonal organs in insects. Microsc. Res. Tech. *63*, 315–337.

Yoshimura, S.-I., Egerer, J., Fuchs, E., Haas, A.K., and Barr, F.A. (2007). Functional dissection of Rab GTPases involved in primary cilium formation. J. Cell Biol. *178*, 363–369.

Zacharias, D.A., Violin, J.D., Newton, A.C., and Tsien, R.Y. (2002). Partitioning of lipid-modified monomeric GFPs into membrane microdomains of live cells. Science *296*, 913–916.

Zhao, C., and Malicki, J. (2011). Nephrocystins and MKS proteins interact with IFT particle and facilitate transport of selected ciliary cargos. EMBO J. *30*, 2532–2544.

Zhu, D., Shi, S., Wang, H., and Liao, K. (2009). Growth arrest induces primary-cilium formation and sensitizes IGF-1-receptor signaling during differentiation induction of 3T3-L1 preadipocytes. J. Cell Sci. *122*, 2760–2768.

Zuo, X., Guo, W., and Lipschutz, J.H. (2009). The exocyst protein Sec10 is necessary for primary ciliogenesis and cystogenesis in vitro. Mol. Biol. Cell *20*, 2522–2529.

(1997). C. elegans II (Cold Spring Harbor (NY): Cold Spring Harbor Laboratory Press).

Appendix A

Electron tomography data

The experiments were carried out by Hall lab at Albert Einstein College of Medicine. The following procedure was provided by Dr. Hall: Animals were prepared for electron microscopy by high pressure freezing, using a Bal-tech HM 010 High Pressure Freezer, followed by freeze substitution into osmium fixative in 100% acetone in an RMC Freeze Substitution Device (cf. Hall et al., 2012). After warming to 0^{o}C, samples were washed in 100% acetone and embedded into Embed 812 plastic resin. Serial thin sections were collected on an RMC Powertome XL for viewing on a Philiips CM10 electron microscope. For electron tomography, semi-thick serial sections were collected onto Pioloform-coated slot grids, and viewed on an FEI Technai F20 electron microscope. Tomograms were calculated using a back-projection method using internal reference points ("markerless alignment") with help from William Rice at the New York Structural Biology Center (Hall et al., 2012).

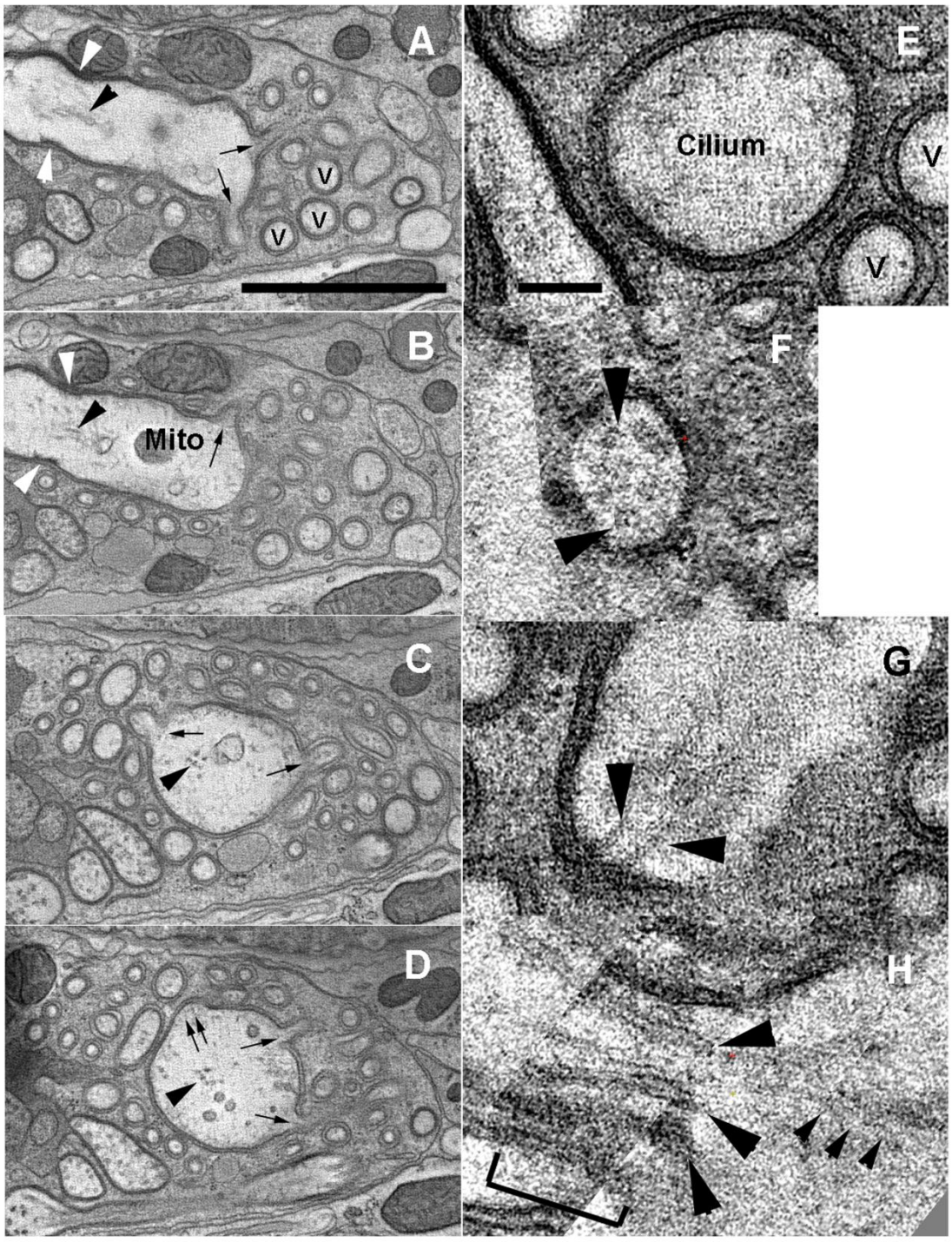
A
V
V
V
B
Mito
C
D
E
Cilium
V
V
F
G
H

Electron tomography reveals the structure of the AFD dendritic ending

The fine structure of the adult AFD dendritic ending was followed in serial thick section electron tomograms, after dual axis electron microscopy at high magnification. (A-D) illustrate one AFD(R) sensory ending at lower power to show features along the club ending at the distal end of the dendrite. (E-H) illustrate features of the AFD(R) cilium in a second animal, at higher power. Images (A) to (D) progress distally, as the club ending makes a sharp bend between (B) and (C). The club ending is sealed by ApJ (white arrowheads) as it penetrates into the amphid sheath. Intermediate filaments run inside the club ending as a tight bundle, seen lengthwise in (A) and (B), and crosswise in (C), (D) and (H) (small black arrowheads). Multiple thin microvilli emerge from the outer edge of the club ending (thin black arrows) in (A-D), and afterwards these villi (V) extend along the A/P axis surrounding the club ending. The cytoplasm near the base of each villus and the outer edge of the villar cytoplasm is more electron-dense, presumably due to its actin cytoskeleton. Larger channel cilia containing microtubules can be seen at the far left edge of panels (A-D). A possible base of the AFD cilium is indicated by double arrows in (D). The corresponding cilium base is shown in a second animal in panels (G,H) in lengthwise profiles, where singlet and doublet microtubules run in parallel (large arrowheads) as they traverse the axoneme (marked by black bracket in (H)). The axoneme is seen in cross-section in (F), with doublet microtubules marked by large arrowheads. Some microtubules extend for short range into the cilium beyond the axoneme in (H), but there are few microtubules evident at more distal portions of the cilium in (E). Intermediate filaments (small black arrowheads) extend from the base of the axoneme into the club ending in (H). Various vesicle cargoes and a mitochondrion (Mito) can be seen within the club ending, often in proximity to the intermediate filament bundle, but none are seen in the cilium or in the microvilli.
Scale bar in A is 1 µm, in E is 0.1 µm.

Appendix B

Calcium imaging data

The calcium imaging data were collected by Matthew Beverly at Sengupta lab (Brandeis University).

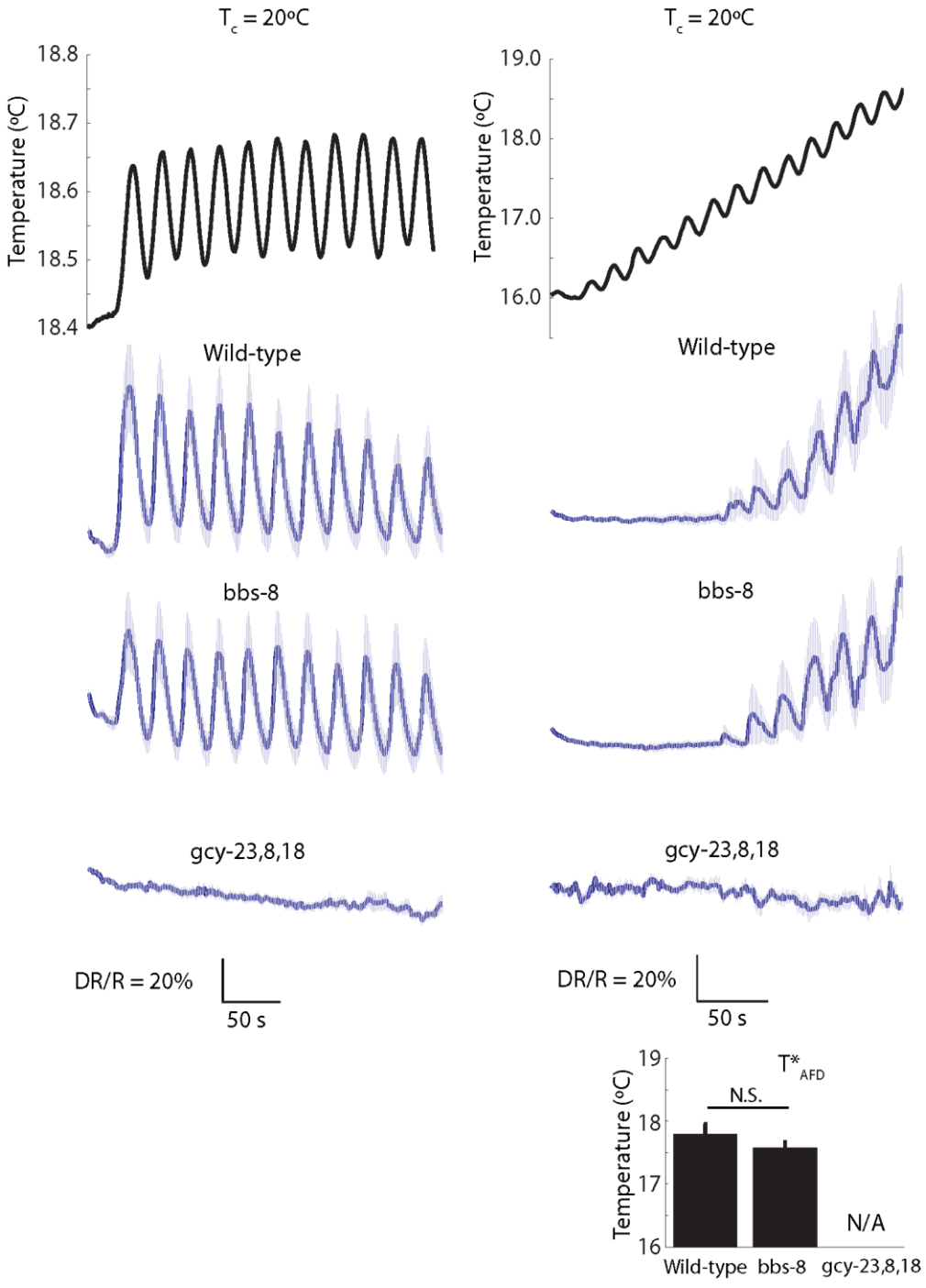
T_c = 20°C
Temperature (°C)
18.8
18.7
18.6
18.5
18.4
Wild-type
bbs-8
gcy-23,8,18
DR/R = 20%
50 s
T_c = 20°C
Temperature (°C)
19.0
18.0
17.0
16.0
Wild-type
bbs-8
gcy-23,8,18
DR/R = 20%
50 s
T*_AFD
N.S.
N/A
Temperature (°C)
19
18
17
16
Wild-type
bbs-8
gcy-23,8,18

The *bbs-8* mutant has normal AFD calcium influx in response to temperature changes.

Intracellular Ca^{2+} dynamics were measured in worms raised at 20°C and carrying the AFD-specific calcium sensor Cameleon YC2.12, as described in Wasserman et al., 2011. Top graphs: representative temperature stimuli used in oscillation (left) and ramp (right) conditions. For each genotype, the average percentage change is shown in dark blue ($DR = (R-R_0)/R_0$, where R is the fluorescence emission ratio and R_0 is the baseline). Grayed out bands indicate ±1 SEMs of the response (n=20). The bar graph represents the mean activation temperature (T*) as measured in the temperature ramp condition ('N.S.' indicates no significant).

Appendix C

Transgenic strain list

Name	Genotype
MX702	dpy-5(e907)I;nxEx2[p::tax-4::gfp + dpy-5(+)]
MX708	dpy-5(e907)I;nxEx1[p::tax-2::gfp + dpy-5(+)]
MX860	dpy-5(e907)I; nxEx5[p::gcy-8::gfp + dpy-5(+)]
MX861	dpy-5(e907)I; nxEx6[p::gcy-18::gfp + dpy-5(+)]
MX862	dpy-5(e907)I; nxEx7[p::gcy-23::gfp + dpy-5(+)]
MX863	dpy-5(e907)I;nxEx9[p::tax-6::gfp + dpy-5(+)]
MX900	dpy-5(e907)I; nxEx16[gcy-8p::bbs-8::gfp + p::strx-1::mCherry + dpy-5(+)]
MX939	dpy-5(e907)I; nxEx22[gcy-8p::xbx-1::tdTomato + p::srtx-1::gfp + dpy-5(+)]
MX940	dpy-5(e907)I; nxEx25[gcy-8p::arl-13::gfp + p::srtx-1::mCherry + dpy-5(+)]
MX953	dpy-5(e907)I; nxEx27[gcy-8p::mksr-2::gfp + p::srtx-1::mCherry + dpy-5(+)]
MX955	nxEx28[p::tax-4::gfp + p::mksr-2::tomatoes + rol-6(su1006)]
MX978	nxEx24[p::srtx-1::gfp + unc-122:gfp]
MX1006	nxEx41[gcy-8p::nphp-1::tdTomato + p::srtx-1::gfp + unc-122::gfp]
MX1036	dpy-5(e907)I; nxEx60[gcy-8p::MyrPalmGFP + p::srtx-1::mCherry + dpy-5 (+)]
MX1037	dpy-5(e907)I; nxEx52[gcy-8p::GerGerGFP + p::srtx-1::mCherry + dpy-5(+)]
MX1038	dpy-5(e907)I; nxEx58[gcy-8p::PalmPalmGFP; p::srtx-1::mCherry + dpy-5(+)]
MX1042	dpy-5(e907)I; nxEx49[gcy-8p::mks-6::gfp + p::srtx-1::mCherry + dpy-5(+)]
MX1057	nxEx62[gcy-8p::tram-1::gfp + p::srtx-1::mCherry + unc-122:gfp]
MX1079	dpy-5(e907)I; nxEx69[p::tax-4::mCherry + gcy-8p::arl-13::gfp + dpy-5(+)]
MX1164	dpy-5(e907)I; nxEx80[p::tax-4:mCherry + p:: nphp-2::gfp + dpy-5(+)]
MX1170	nxEx81[gcy-8p::arl-13::gfp + p::gcy-18::mCherry + unc-122::gfp]
MX1204	nxIs4[gcy-8p::bbs-8(sas) + unc-122:gfp]
MX1248	nxIs10[gcy-8p::daf-19(sas) + unc-122::gfp]
MX1249	nxIs14[gcy-8p::daf-25(sas) + unc-122::gfp]
MX1291	dpy-5(e907)I; nxEx42[osm-5p::xbx-1::tdTomato + unc-122::gfp]; nxEx73[p::tax-4::gfp + gcy-8p::odr-1::mCherry + dpy-5(+)]
MX1343	dpy-5(e907)I; nxEx73[p::tax-4::gfp + gcy-8p::odr-1::mCherry + dpy-5(+)]
MX1482	nxIs22[gcy-8p:unc-122(sas) + unc-122:gfp]
MX1689	daf-19(ttTi36198)II; unc-119(ed3)III
MX1768	daf-19(nx112-FRT)II
MX1769	daf-19(nx113-FRTsc)II
MX1772	nxSi1[gcy-8p:QF:unc-54 3'UTR + 5xQUAS/dpes-10p:FLP:let-858 3'UTR + unc-119(+)]IV
MX1776	daf-19(nx112-FRT)II; nxSi1[gcy-8p:QF:unc-54 3'UTR + 5xQUAS/dpes-10p:FLP:let-858

	3'UTR + unc-119(+)]IV
MX1778	daf-19(nx113-FRTsc)II; nxSi1[gcy-8p:QF:unc-54 3'UTR + 5xQUAS/dpes-10p:FLP:let-858 3'UTR + unc-119(+)]IV
MX1827	nxEx113[gcy-8p::gfp::gasr-8 + p::srtx-1::mCherry + rol-6(su1006)]
MX1828	nxEx114[gcy-8p::mks-5::gfp + p::srtx-1::mCherry + rol-6(su1006)]
MX1850	unc-119(ed4) III; syIs78 [ajm-1::GFP + unc-119(+)]; nxEx116[p::srtx-1::mCherry + rol-6(su1006)]
MX1852	nxEx118[gcy-8p::egl-2::gfp + p::srtx-1::mCherry + rol-6(su1006)]
MX1868	nxEx120[gcy-8p::ajm-1(e4-9)::mCherry + gcy-8p::mks-6::gfp + unc-122::gfp]
MX1884	nxIs29[5xQUAS/dpes-10p:FLP:let-858 3'UTR + dpy-5(+)]
MX2141	daf-19(nx112-FRT); nxSi1[gcy-8p:QF:unc-54 3'UTR + 5xQUAS/dpes-10p:FLP:let-858 3'UTR + unc-119(+)] IV; nxIs29[5xQUAS/dpes-10p:FLP:let-858 3'UTR + dpy-5(+)]
MX2142	daf-19(nx113-FRTsc); nxSi1[gcy-8p:QF:unc-54 3'UTR + 5xQUAS/dpes-10p:FLP:let-858 3'UTR + unc-119(+)] IV; nxIs29[5xQUAS/dpes-10p:FLP:let-858 3'UTR + dpy-5(+)]